PROPERTIES OF GASIFICATION-DERIVED CHAR AND ITS UTILIZATION FOR CATALYTIC TAR REFORMING

By

KEZHEN QIAN

Bachelor of Engineering in Thermal and Power Engineering
Chongqing University
Chongqing, China
2009

Master of Engineering in Thermal and Power Engineering
Huazhong University of Science and Technology
Wuhan, China
2012

Submitted to the Faculty of the
Graduate College of the
Oklahoma State University
in partial fulfillment of
the requirements for
the Degree of
DOCTOR OF PHILOSOPHY
May, 2015

PROPERTIES OF GASIFICATION-DERIVED CHAR AND ITS UTILIZATION FOR CATALYTIC TAR REFORMING

Dissertation Approved:

Dr. Ajay Kumar

Dissertation Adviser

Dr. Danielle Bellmer

Dr. Mark Wilkins

Dr. Hailin Zhang

ACKNOWLEDGEMENTS

The accomplishment of this dissertation would not have been done without help from many wonderful people at Oklahoma State University. Here, I would like to express my deepest gratitude to all individuals.

I would like to express the deepest appreciation to my research advisor, Dr. Ajay Kumar. Without his enthusiasm in mentorship and academic support over the past several years, I would not be able to finish this dissertation. His unwavering guidance helps improve my academic performance, especially on academic writing and research skills. I would like thank my research advisory committee members, Dr. Krushna N. Patil, Dr. Mark Wilkins, Dr. Danielle Bellmer and Dr. Hailin Zhang. They provided excellent suggestions for improving my research work.

I acknowledge Mr. Mark Gilstrap for sharing his immense knowledge of lab skills and lab safety and for assistance with all the analytical equipment. I also appreciate the support of research BAE workshop team, Mr. Wayne R. Kiner, Mr. Mike Veldman, and Mr. Jason Walker for developing and building the necessary experimental facilities for this research.

I would like to take this opportunity to thank graduate students Madhura Sarkar, Cody Collins, Zixu Yang, Shaswat Dixit, Deepak Padaliy, Mohit Dobhal and Karthikragunath Mariyappan, for their help in conducting experiments. This work would not have been done without their hard work and continuous involvement. I appreciate the support of Pushpak Bhandari, Dr. Prakash Bhoi and Dr. Ashokkumar M Sharmar for sharing their knowledge regarding experiment design and technical details.

I am deeply indebted to my parents for their support and love. I also appreciate my whole family for their blessings and support during my graduate school period.

I also want to give my thanks to Nancy Rogers and BAE administrative staff for their support and services. To all these people and many more whom I may have missed out, my thanks goes out to you:

Acknowledgements reflect the views of the author and are not endorsed by committee members or Oklahoma State University.

Name: KEZHEN QIAN

Date of Degree: MAY, 2015

Title of Study: PROPERTIES OF GASIFICATION-DERIVED CHAR AND ITS UTILIZATION FOR CATALYTIC TAR REFORMING

Major Field: BIOSYSTEMS AND AGRICULTURAL ENGINEERING

Abstract: Char is a low-value byproduct of biomass gasification and pyrolysis with many potential applications, such as soil amendment and the synthesis of activated carbon. The overall goal of the proposed research was to develop novel methods to use char derived from gasification for high-value applications in syngas conditioning. The first objective was to investigate effects of gasification condition and feedstock on properties of char derived from fluidized bed gasification. Results show that the surface areas of most of the char were 1–10 m^2/g and increased as the equivalence ratio increased. Char moisture and fixed carbon contents decreased while ash content increased as equivalence ratio increased. The next objective was to study the properties of sorghum and red cedar char derived from downdraft gasifier. Red cedar char contained more aliphatic carbon and o-alkyl carbon than sorghum char. Char derived from downdraft gasification had higher heating values and lower ash contents than char derived from fluidized bed gasification. The gasification reactivity of red cedar char was higher than that of sorghum char. Then, red cedar char based catalysts were developed with different preparation method to reform toluene and naphthalene as model tars. The catalyst prepared with nickel nitrate was found to be better than that with nickel acetate. The nickel particle size of catalyst impregnated with nickel nitrate was smaller than that of catalyst impregnated with nickel acetate. The particle size of catalyst impregnated with nickel acetate decreased by hydrazine reduction. The catalyst impregnated with nickel nitrate had the highest toluene removal efficiency, which was 70%-100% at 600-800 °C. The presence of naphthalene in tar reduced the catalyst efficiency. The toluene conversion was 36-99% and the naphthalene conversion was 37%-93% at 700-900 °C. Finally, effects of atmosphere and pressure on catalytic reforming of lignin-derived tars over the developed catalyst were investigated. An increase in reaction temperature led to an increase in removal of most tar components except naphthalene. High pressure promoted the catalytic conditioning of lignin tar. Hydrogen promoted the conversion of lignin into non-condensable gas.

TABLE OF CONTENTS

Chapter Page

Chapter Page

Chapter Page

LIST OF TABLES

Table Page

LIST OF FIGURES

Figure Page

Figure Page

CHAPTER I

INTRODUCTION AND LITERATURE REVIEW: RECENT ADVANCES IN UTILIZATION OF BIOCHAR

This review paper was published as "K. Qian, A. Kumar, H. Zhang, D. Bellmer, R. Huhnke, Recent advances in utilization of biochar, Renewable and Sustainable Energy Reviews, 42 (2015) 1055-1064".

Abstract: Biomass thermochemical processes result in a common byproduct char. The char is also called biochar particularly when it is used as a soil amendment for soil health improvement. Effective utilization of biochar is critical for improving economic viability and environmental sustainability of biomass thermochemical technologies. Application of biochar for both agricultural and environmental benefits has been studied and reviewed extensively. However, there are limited reviews on other biochar applications, such as for catalysis and adsorption. This paper provides an overview of recent advances in several biochar utilizations including its use as catalyst, soil amendment, fuel cell, contaminant adsorbent, gas storage and activated carbon. Discussions on biochar production methods, properties and advanced characterization techniques are also provided. Biochar is a valuable resource, however, its effective utilization require further investigation of its structure and properties, and methods to modify those.

Keywords: biochar; char; biochar application; biochar-based catalyst; adsorbent

1.1. Introduction

Biomass can be converted to biofuels and bioproducts via thermochemical processes, such as pyrolysis and gasification. The net carbon dioxide emissions from biofuel use are considered zero or negative because the released CO_2 was recycled from the atmosphere captured during photosynthesis [1]. In addition, since biomass contains a low amount of sulphur and nitrogen, combustion of biofuels leads to lower emissions of harmful gas, such as nitrous oxides (NO_x) and sulphur dioxide (SO_2), than most of fossil fuels [2]. Such advantages of biomass make it a promising renewable energy resource.

The major products from biomass thermochemical processes are syngas, bio-oil, biochar and tar with yields that depend on the process. Syngas and bio-oil are considered as major intermediate products that can be used to create fuels alternative to conventional fuels. Numerous studies have been conducted involving upgrading and utilization of syngas and bio-oil for various applications [3-6]. Recently, biochar, a product from biomass thermochemical conversion, has received increasing attention for use in several applications. The most common biochar application is soil amendment to mitigate greenhouse gas emission and improve soil health. Other applications include using biochar as a precursor for making catalysts and contaminant adsorbents. These new high-value applications are still in their infancy, and further research and development is needed to reach commercialization. Even though, charcoal, a carbon material similar to biochar, has been used for centuries, using biochar as a sustainable material for these applications (precursor of catalyst and contaminant adsorbents, and soil amendment) has only been studied in last few years.

The potential to utilize biochar for various applications depends on its properties. For example, biochar with high electrical conductivity, porosity and stability at lower temperatures is preferred as electrodes material in microbial fuel cells [7]. Biochar containing relatively high structural bound oxygen groups is preferred in direct carbon fuel cells [8]. Biochar with high porosity and structural bound nitrogen groups is preferred in the development of supercapacitors

[9]. Furthermore, the high surface area, low ash content of biochar may be preferred as soil amendments, although the relationship between biochar properties and its applicability as a soil amendment is still not conclusive [10].

Reviews on biochar production, properties and use, especially as a soil amendment, can be found in other works [10-15]. Meyer et al. [15] reviewed production methods, properties, economics and environmental aspects of using biochar as soil amendment. Laird et al. [16] reviewed pyrolysis reactors for producing biochar used as a soil amendment. Several others extensively reviewed effects of different pyrolysis methods on properties of biocharand its impacts on soil [10, 12, 13]. Although, review on biochar properties and its specific application as soil amendment is available in literature, review on new state of the art applications of biochar is limited. This paper provides an overview of recent advances in utilization of biochar, especially for applications other than soil amendment. This paper also discusses production methods, properties and new characterization techniques that are used to solve underlying problems in identifying novel applications of biochar.

1.2. Biochar Production

Biochar is charred organic matter. The International Biochar Initiative defines biochar as ‘‘a solid material obtained from the thermochemical conversion of biomass in an oxygen-limited environment’’ [17]. Biochar is produced in solid form by dry carbonization, pyrolysis or gasification of biomass, and in slurry form by hydrothermal carbonization of biomass under pressure [11]. Typical operating conditions and char yields of different thermochemical processes are shown in Table 1.1.

Table 1.1. Typical char yield from thermochemical processes

Process	Temperature (ºC)	Residence time (s/h/min/days)	Char yield (% of biomass)	Ref.
Slow pyrolysis	400-600	min to days	20-40	[18-20]
Fast pyrolysis	400-600	~1 s	10-20	[21, 22]
Gasification	800-1000	5-20 s	~10	[15]
Hydrothermal carbonization	180-250	1-12 h	30-60	[23, 24]

1.2.1. Pyrolysis

The most common method to produce biochar is pyrolysis. Pyrolysis can be categorized into slow pyrolysis and fast pyrolysis depending on the heating rate and residence time. Slow pyrolysis, also called conventional carbonization, produces biochar by heating biomass at a low heating rate for a relatively long residence time (up to several days). This method has been used to generate charcoal for centuries. On the other hand, fast pyrolysis produces biochar at a high heating rate (above 200 K/min) and short residence time (less than 10 s). The major differences between the two pyrolysis methods are the yields of biochar and bio-oil: fast pyrolysis favors high yield of bio-oil while slow pyrolysis favors high yield of biochar.

1.2.2. Gasification

Gasification transforms biomass into primarily a gaseous mixture (syngas containing CO, H_2, CO_2, CH_4, and smaller quantities of higher hydrocarbons) by supplying a controlled amount of oxidizing agent under high temperature (greater than 700 °C). The typical biochar yield of gasification averages about 10 wt.% of biomass [15, 25]. The oxidizing agent used in gasification can be oxygen, air, steam or mixtures of these gases. Air gasification produces syngas with low heating values of 4–7 MJ/Nm^3, while gasification with steam produces syngas with high heating values of 10–14 MJ/Nm^3 [5].

1.2.3. Hydrothermal Carbonization

Hydrothermal carbonization (HTC) of biomass takes place in water at elevated temperatures (160-800 °C). Since the water temperature is above 100 °C, the reaction pressure also must be elevated (more than 1 atm) to maintain the water in liquid form. Based on reaction temperature, hydrothermal carbonization can be divided into high-temperature HTC (between 300 and 800 °C and low-temperature HTC (below 300 °C) [26]. Since the reaction conditions of high-temperature HTC (above 300 °C) are beyond the stability condition of most organic compounds, the dominant reaction during high-temperature HTC is hydrothermal gasification and the dominant products are gases, such as methane and hydrogen [24]. Below 300 °C, gasification is limited and carbonization of biomass to char dominates the reaction. Low-temperature HTC can mimic the natural coalification of biomass, although the reaction rate is higher and reaction time is shorter compared to the hundreds of years of slow natural coalification of biomass. Char yield of low-temperature biomass HTC varies from 30 to 60 % depending on the feedstock properties, reaction temperature and pressure. Since HTC requires water, this may be a cost-effective biochar production method for feedstocks with high moisture content [9].

1.3. Applications of Biochar

The most appealing feature of biochar is the fact that it represents an inexpensive, sustainable and easy-produced process allowing the production of materials with extensive applications at a lower cost compared to materials from petrochemical or other chemical processes. Even though most of the applications are still in their infancy, biochar can already be used in many applications with extraordinary effects. Those applications include soil amendment, catalysis, water purification, and energy and gas storage. Table 1.2 summarizes the primary advantages and disadvantages for each biochar application.

Table 1.2. Primary advantages and disadvantages of various biochar applications

Application	Purpose	Advantage	Disadvantage	References
Catalyst	Syngas cleaning, biodiesel production, Fischer-Tropsch synthesis	Easy to recycle supported metal, co-catalyst, low cost	Relative low efficiency and low abrasive resistance compared with commercial catalyst	[27-30]
Soil amendment	Carbon sequestration, soil quality improvement	Low cost, sustainable resource, retain water and nutrient, reduce fertilizer consumption, reduce greenhouse gas emission and nutrient losses	Possible heavy metal and PAHs contaminant	[12, 31, 32]
Fuel cell	Fuel for fuel cell	Renewable fuel compared with coal	High ash content, relative low voltage and power output	[33]
Sorbent of contaminant	Adsorption of organic contaminants and heavy metals present in soil and water	Low cost, abundant and sustainable resource, and oxygenated groups on biochar surface facilitate adsorption	Effectiveness of organic/inorganic contaminants remediation is still uncertain, and persistence of heavy metals	[11, 34, 35]
Storage material	CO_2 sequestration, H_2 storage	Low cost, abundant and sustainable resource, high recyclability	Require surface treatment	[36-39]
Activated carbon	Precursor for making activated carbon	Low cost, abundant and sustainable resource	Properties vary with different precursors, may not produce desired granular or spherical activated carbon	[39, 40]

1.3.1. Biochar as A Precursor for Making Catalyst

1.3.1.1. Catalyst for Syngas Cleaning

Syngas produced from gasification of biomass contains a considerable amount of tar that is detrimental to downstream processes [41]. The tar components are categorized into four groups as follows [42]:

- Primary tar is released from pyrolysis of biomass (same oxygenated compounds as found in bio-oil).
- Secondary tars are phenolic and olefin made from decomposition of primary tar.
- Alkyl tertiary tar is aromatic hydrocarbons.
- Condensed tertiary tar is poly aromatic hydrocarbons.

Several methods are available to remove syngas tars: water or oil scrubbing, thermal cracking (decompose tars at sufficiently high temperatures, typically greater than 1000 °C) and catalytic cracking [42]. Water and Oil scrubbing result in waste water and oil that require appropriate treatment. Thermal cracking is energy-intensive, unable to crack refractory tars and may encourage formation of carcinogenic polyaromatic hydrocarbons. Catalytic cracking of tar is considered to be the most promising technology for syngas cleaning. Catalytic cracking can be achieved at low temperatures (less than 700 °C) and thus requiring less energy and can achieve high tar removal efficiency (more than 90%) by using appropriate catalysts.

Traditionally, dolomite and metal-based catalysts are used for syngas cleaning. Use of biochar for tar removing also appears promising in recent studies [43-46]. Biochar can be used for syngas cleaning as a catalyst directly with no active metal loading or as a support for active metal [47]. The catalytic activity of biochar for tar elimination is related to its pore size, surface area, and mineral content. Mani et al. [29] used pine bark biochar as a catalyst in catalytic decomposition of model tar (toluene). Using raw pine bark biochar, generated by slow pyrolysis (950 °C), to decompose toluene over a temperature range of 600-900 °C in the presence of steam, researchers showed that the fractional toluene conversion increased from 13 to 94% when temperature was increased from 600 to 900 °C. The activation energy (91 kJ/mol) and removal efficiencies of pine bark biochar were comparable to that of synthetic catalysts (e.g., 80.24kJ/mol for Ni/Mayenite and 196 kJ/mol for olivine). El-Rub et al. [43] compared biochar to other catalysts such as dolomite, olivine, nickel, FCC catalysts, and ash using the model tar compounds

phenol and naphthalene in a fixed bed reactor. Biochar performed satisfactorily (with conversion efficiencies of biochar and dolomite at 90 and 60%, respectively) for naphthalene conversion among the low-cost catalysts.

Shen et al. [48] used Ni-Fe catalyst supported on rice husk biochar as an in-bed catalyst for in-situ catalytic conversion of tars during biomass gasification. The biochar-supported Ni-Fe catalyst was prepared by incipient wetness impregnation of Ni and Fe on biochar using $Fe(NO_3)_3 \cdot 9H_2O$ and $Ni(NO_3)_2 \cdot 6H_2O$. The biochar was produced by slow pyrolysis of rice husk at 700 °C in a N_2 atmosphere. After impregnation, the biochar-supported catalyst was dried and calcined in air at 600 ºC for 1 h. Volatile gas was produced and in-situ reformed in a two-stage pyrolyzer with a sintered quartz porous plate fixed inside to support the catalyst under 800 °C. Shen et al. [36] proposed that biomass tar could be removed effectively in this set up by mixing with the char-supported catalysts. The condensable tar could be catalytically reformed into the non-condensable tars and permanent gases. Among four types of catalysts studied (Ni/char, Fe/char, Ni-Fe/char with calcination and Ni-Fe/char without calcination), Ni-Fe/char without calcination and Ni-Fe/char with calcination showed highest removal of condensable tar (about 92.3% and 93%, respectively).

Biochar plays multiple roles in functioning of biochar-supported metal catalysts. Firstly, biochar acts as a reduction media converting metal oxides into metallic state, thus enhancing the catalytic performance. Secondly, biochar has co-catalyst and adsorbents effects to adsorb metal ions and tar for enhancing the tar reforming process.

1.3.1.2. Catalyst for Conversion of Syngas into Liquid Hydrocarbons

Fischer–Tropsch synthesis of biomass-derived syngas to liquid hydrocarbons is one of feasible ways to produce liquid fuel from biomass. Using efficient catalyst is critical for Fischer–Tropsch synthesis process. Yan et al. [49] developed carbon-encapsulated iron nanoparticles catalyst for the Fischer–Tropsch synthesis of biomass-derived syngas to liquid hydrocarbons. The

catalyst was synthesized by thermal treatment of iron-impregnated pine biochar at 1000 °C for 1 h. Biochar was obtained from a typical fast pyrolysis of pine wood and treated with HNO_3 to remove intrinsic ash and tar before impregnation. The Fischer–Tropsch synthesis results showed that the biochar-based iron nanoparticles catalyst had an efficiency of converting syngas into liquid hydrocarbons (CO conversion rate over 90% and liquid hydrocarbon selectivity as high as 70%), which is higher than other reported carbon supported iron catalysts for Fischer-Tropsch synthesis of syngas (2 to 88% CO conversion and 5 to 60% liquid hydrocarbon selectivity) [49]. This catalyst also had a very high deactivating ability (maintained CO conversion over 90% and liquid hydrocarbon selectivity at about 68% over a 1500 h testing period). The author postulated that the high deactivating ability and conversion rate for catalytic conversion of this biochar-based iron encapsuled catalyst is related to the strong metal–carbon support interaction between the biochar support and the supported metals. This interaction, which was occurred during the thermal treatment of catalyst at 1000 °C, created C–Fe chemical bonds, and cementing (Fe_3C) and $CFe_{15.1}$ formed between the graphite shell and the iron core. Finally, a highly stable core-shell nanocomposites composed of an α-iron core, a carbide interface layer and an outer graphite layer were formed, which make metal iron active sites fully packed and prevents active sites from sintering.

1.3.1.3. Solid Acid Catalyst for Biodiesel Production

Heterogeneous and homogenous acid catalysts are commonly used for esterification and transesterification of vegetable oil or animal fat for biodiesel production [50]. With appropriate treatment, biochar has proven to be a good precursor for producing heterogeneous acid catalysts (also called solid acid catalyst) [28, 50, 51]. The biochar-derived acid catalyst can be prepared by sulfonating biochar with concentrated sulfuric acid. Dehkhoda et al. [28, 50] successfully prepared a biochar-based solid acid catalyst for transesterification of canola oil with alcohol and oleic acid. The catalyst was prepared by first chemically treating the biochar with 7M KOH and

then sulfonating the biochar with concentrated sulfuric acid. The use of KOH increased porosity and surface area of the biochar. The catalyst yield was up to 48.1% at high temperature (150 °C) and pressure (1.52 MPa) for alkali-ester formation with a mixture of canola oil and oleic acid. The reusability of the catalyst was also high (reaction yield decreased only about 8% upon reusing the catalyst).

Kastner el al. [30] prepared three biochar based solid acid catalysts made from peanut hulls, pine residues and wood chips and one activated carbon based solid acid catalysts using a method similar to Dehkhoda et al. [28]. The sulfonated carbons were tested for their ability to esterify free fatty acids of vegetable oil and animal fat with methanol. All catalysts showed high efficiencies in esterification of fatty acids (90-100% in conversion within 30-60 minutes) and high reusability (can be reused for up to 7 cycles with no significant loss in esterification). Results by Kastner et al. [30] and Dehkhoda et al. [28] showed that biochar based solid acid catalysts with high surface area and acid density had high catalytic activity and reusability for the biodiesel production. The high esterification activity and reuse capability of biochar-based solid acid catalysts is related to their particle strength, hydrophobicity, high surface area (1137 m^2/g) and sulfonic acid group density [28, 30].

1.3.2. Biochar as Soil Amendment

Several recent studies have highlighted the multiple benefits of applying biochar in soil including mitigation of global warming by carbon sequestration and improvement of soil health and productivity [1, 12]. The benefits of using biochar as a soil amendment are summarized below.

1.3.2.1. Mitigate Greenhouse Gas Emission

Use of biochar as a soil amendment results in mitigation of greenhouse gas emissions directly by sequestering solid carbon in the ground for hundreds or even thousands of years, and indirectly by improving soil fertility and overall soil health. Improvement in soil fertility stimulates plant growth which leads to additional CO_2 consumption. Improvement in soil fertility

also reduces the need for fertilizer input and thus reducing carbon emissions during fertilizer production, transporting and application. In addition, biochar additions to soil may also reduce emissions of other greenhouse gases, such as N_2O and CH_4, whose greenhouse effects are even higher than that of CO_2. Carbon emissions can be reduced by about 0.9 Gt each year if 50% of global crop residues and 67% of global forestry residues are used as pyrolysis feedstocks for producing biochar as soil amendments [16]. Up to 12% of the total anthropogenic carbon emissions could be off-set annually if crop residues were converted into biochar through pyrolysis, instead of direct burning, and used as a soil amendment [13].

1.3.2.2. Increase Soil Quality

Increase in agricultural productivity with the use of biochar as a soil amendment can be attributed to an increase in soil fertility pH in acidic soils [52], soil cation exchange capacity (CEC) [52] and improved soil microbial activity and nutrient retention [12]. Increase in soil CEC increases soil fertility by preventing soil nutrients from leaching through water movement and by providing a nutrient reserve available to plant roots. Liang et al. [53] studied the effects of black carbon (similar carbon based material like biochar) on the CEC of Anthrosols (a type of soil formed with long-term human activity impact) and found that CEC was up to 1.9 times higher in Anthrosols with high black carbon than in the adjacent soils without the black carbon. The underlying reason for impact of black carbon on CEC is not well understood. However, Liang et al. [53] speculated that improvement in CEC is related to the oxidation of aromatic carbon and formation of carboxyl groups or other functional groups with a net negative charge. This is thought to take place through two mechanisms: surface oxidation of black carbon particles and adsorption of highly oxidized organic matter onto carbon surfaces [53]. Since biochar contains nutrients, such as N, P, K, it can supply nutrients to the soil directly. Moreover, biochar increases soil fertility indirectly by increasing ability of soil to retain nutrients [31]. Biochar also reduces eutrophication potential of surface water bodies by minimizing nutrient losses from soil. Laird et al. [54] studied the impact of biochar on nutrient leaching in a Midwestern agricultural soil and

found that the addition of biochar substantially reduced nutrient leaching [23]. Increase in nutrient uptake by crops on biochar-amended soil in the Amazon region was due to improvement in soil nitrogen retention capability [55]. Microbial communities, especially mycorrhizal fungi, are considered to be critically important for nutrient cycling. Biochar appears to stimulate soil microbial activity [56] and increase fungi abundance and functioning. Warnock et al. [57] proposed the following hypothesis to explain influence on fungi activity: "…biochar used as soil amendment can alter soil physico-chemical properties, indirectly affect mycorrhizae through influence on other soil microbes, alter plant–mycorrhizal fungi signaling processes or detoxifies allelochemicals leading to altered root colonization by mycorrhizal fungi, and provide refugia from fungal grazers". Zhang et al. [58] incorporated a small amount of char into soils to study the biodegradation of benzonitrile and found that biochar could stimulate biodegradation of benzonitrile. Yu et al. [59] found that biochar applications in agricultural soils suppress plant uptake of pesticides from soils, suggesting biochar's ability to retain organic compounds.

1.3.3. Biochar as A Sorbent for Contaminant Reduction in Soil and Water

Biochar can help mitigate environmental issues by removing pollutants from soil and water. Biochar has been proven to be an effective sorbent for some contaminants in soils [11]. Contrary to activated carbons, the surface area of most biochar is not high (less than 200 m^2/g) that may limit its use as a sorbent in removing contaminants. This is counterbalanced by the high number of oxygenated groups, such as carboxyl, hydroxyl, and phenolic surface function groups, on the biochar surface. These oxygenated groups have proven to be binding sites for soil contaminants [19]. Sorption of organic contaminants from water onto biochar occurs due to its high surface area and microporosity; therefore, biochar produced at temperatures above 400 ºC (with higher surface area) is more effective than biochar produced below 400 ºC in adsorbing contaminants from water. Sorption with natural sorbents, such as soil organic matter, occurs in two major adsorbing domains (rubbery and glassy). The sorption behavior in the rubbery domain is partitioning, which is linear and noncompetitive, whereas the sorption behavior in the glassy

domain is dominated by adsorption with pore-filling mechanism and is nonlinear and solute-solute competitive [60]. Biochar is, generally, not a product of complete carbonization [61]. Carbonized fraction of biochar behaves as an adsorption phase the glassy domain and noncarbonized fraction behaves as partition phase like in the rubbery domain. Since the carbonized fraction in biochar is increased with the increased pyrolysis temperature, partitioning of organic contaminants into non-carbonized fraction of biochar is the major sorption mechanism for biochar produced at low pyrolysis temperatures (less than 300 ºC), whereas adsorption onto porous carbonized fractions is dominant in biochar produced at high temperatures (higher than 400 °C) [61].

Retention of heavy metals in soils in the presence of biochar has also been reported [34]. High surface area and microporosity of biochar play important roles in sequestration of these toxic chemicals by altering their bioavailability and eco-toxicological impacts. The mechanism of adsorbing metal contaminants by biochar is also related to oxygenated groups on the biochar surface [19]. Uchimiya et al. [19] reported high uptake of heavy metals (Cu, Ni, Cd, and Pb) from soil with biochar of high oxygen content made from cottonseed hulls.

1.3.4. Biochar as Gas Adsorbents

The capture and storage of CO_2 is one of the promising strategies to reduce CO_2 emissions. González et al. [62] produced biomass-based carbon adsorbents by a single-step activation with CO_2 from olive stones and almond shells for post-combustion CO_2 capture. The main challenges of capturing post-combustion CO_2 are the high flow rate of flue gases and low partial pressure of CO_2. For effective CO_2 capture and removal, high CO_2 selectivity and adsorption capacity are required. Additional desired properties include long life, ease of regeneration, and low cost. Biochar-based activated carbon has shown high CO_2 adsorption capacity (up to 4.8 mmol/g at 1 atm and 0 ºC) [62]. With CO_2 partial pressure close to the pressure of real flue gas (15 kPa), CO_2 adsorption capacity was found to be 0.6–0.7 mmol/g at 50 °C (a typical temperature for flue gas after desulfurization) [62]. This adsorption capacity was

similar to the highest adsorption capacity reported for carbon materials. Experiments conducted in a fixed bed reactor showed that biomass-based activated carbon adsorbents were capable of separating CO_2 from a CO_2-N_2 mixture (containing 14% CO_2) at 50 ºC. The adsorption capacity for N_2 was significantly lower than that for CO_2 which implies that CO_2 adsorption is not significantly influenced by the presence of N_2 [62].

Hydrogen is considered a promising clean energy carrier, and has the potential to play a major role in transportation. One of the technical obstacles encountered in deploying hydrogen-based technologies is the difficulty in storing hydrogen. To overcome this obstacle, physisorption of hydrogen on sorbents, such as carbon nanotubes [63] has gained attention due to its high sorption rate, reversibility, and storage capacity. Physisorption employs high surface area sorption materials that can effectively adsorb hydrogen. By optimizing preparation conditions, Zhang et al. [38] developed a corncob biochar based activated carbon using KOH chemical activation. The activated carbons showed high surface area (up to 3500 m^2/g) and large pore volume (1.3-1.94 cm^3/g). Researchers concluded that surface area and micropore volumes (with desired diameters of 0.65 nm and 1.5 nm) play an important role in adsorbing hydrogen. The activated carbon with small pore size exhibited the highest hydrogen uptake capacities of over 2.85 wt.% at 1.0 bar and 196 °C, although its BET surface area (2988 m^2/g) was not the highest among all produced activated carbon (the highest was 3500 m^2/g). Loading biochar with nickel without using sensitization or activation pretreatments can also produce sorbents for hydrogen. Figueroa-Torres et al. [64] dispersed an even layer of Ni nanoparticles on Quercus agrifolia (coast live oak) biochar-derived activated carbon using a hydrazine based bath at 50 °C. Results indicated that hydrogen storage capacity of the nickel loaded activated carbon was 1.6 wt. %, which was two times higher than that of activated carbon without the nickel layer. The higher hydrogen storage capacity was high due to the hydrogen spillover mechanism with Ni nanoparticles.

1.3.5. Biochar in Fuel Cell Systems

As compared to traditional power generation facilities, fuel cells show high efficiencies and relatively low greenhouse gas emissions when a compatible fuel source, such as hydrogen, is available. Recently, a direct carbon fuel cell (DCFC) was developed to convert molten carbonaceous solid fuel directly into electricity without the need of converting the solid into gaseous fuels. When comparing performances of DCFC systems using biochar and coal as fuel sources, Ahn et al. [33] found that fuel cell power density with biochar as fuel was 60-70% of the coal-based fuel and was further improved by stirring the char bed. Their results showed the possibility of using biochar as a renewable, low cost fuel for DCFC despite its relatively low carbon and higher ash contents.

Other researchers [8, 65] also found that biochar is a promising DCFC fuel alternative to coal. Kacprzak et al. [8] studied the effects of nine carbonaceous fuels (commercial graphite, a carbon black, two types of commercial hard coal, four biochars produced by the authors in the laboratory and one commercial biochar) on DCFC performance. Among the fuels, the commercial biochar had the second highest current (64.2 mA/cm^2) and power density (32.8 mW/cm^2) at 0.5 V. The laboratory-produced biochars also had high current (36-44.6 mA/cm^2) and power density (18-22.4 mW/cm^2). Elleuch et al. [65] tested the performance of a DCFC based on ceria-carbonate composite electrolyte fueled by almond shell biochar. The almond shell biochar provided a current density of about 480 mA/cm^2 and maximum power output of 127 mW/cm^2 at 750 °C. Current density delivered by the almond shell biochar was double that delivered by commercial activated carbon. Performance of almond shell biochar fueled DCFC could be further improved by modifying the anode composition [66]. Later, Ellenuch et al. [66] fabricated a three layer DCFC pellet by adding a NiO-Samaria-Doped-Ceria (NiO-SDC) anode layer to the original bi-layer DCFC pellet (containing only cathode and electrolyte) using a die-pressing, screen printing and sintering method. In the modified DCFC, peak power density of

DCFC increased from 127 to 150 mW/cm^{2}and stability of DCFC improved (stable current lasted about 130 min).

Biochar can also be used as a low-cost anode material on microbial fuel cell (MFC). MFC is a new technology that can simultaneously remove organic and inorganic contaminant from soil or wastewater and generate electricity [67]. The exoelectrogenic bacteria in MFC oxidize fuel on the anode, generating electrons and protons. The electrons flow through an external circuit to reach a cathode and thus generating a current. The most promising application of MFC is for wastewater treatment. However, high cost and the non-renewable nature of electrode materials in MFC limit its commercialization. Most electrode materials used in MFCs are granular activated carbon or graphite granules. The average cost of granular activated carbon and graphite granule is $500 to $2500 per ton, which is cost prohibitive at large scale [7]. Biochar was found to be a promising cheap alternative material for MFC [7, 68]. By comparing the cost and power output of a wood-based biochar electrodes with activated carbon and graphite electrodes, Huggins et al [7] found that power output of biochar (532-457 mW/m^2) was comparable to activated carbon (674 mW/m^2) and graphite (566 mW/m^2). However, the power output cost of biochar ($17–$35 /W) was 90% lower than that of activated carbon ($402 /W) and graphite ($392 /W).

Biochar has also been used as a catalyst in MFC. Yuan et al. [69] built an air cathode with a catalytic layer that coated both sides of a wet-proofed carbon cloth for a microbial fuel cell. The catalytic layer was comprised of sewage sludge-derived biochar or Pt/C (as comparison). Power density of the cathode coated by the biochar catalyst layer reached 500 ±17 mW/m^2, which was comparable to that of cathode coated by the Pt/C. This result illustrated that sewage sludge biochar was active in catalyzing the oxygen reduction reaction in microbial fuel cells and can be an alternative to Pt catalyst. In addition, stability of biochar-coated cathode is even better than that of Pt/C cathode. For over two months of operation with 1kΩ external loading, there was little

change in voltage generation that occurred in MFC with biochar-coated cathode while a significant decrease of voltage output was observed in MFC with Pt/C cathode. Another stability test by the addition of methanol showed that the biochar-coated cathode has better anti-depolarization ability. While the methanol concentration in MFC suddenly increased, current on the biochar-coated electrode did not change; however, the current on the Pt/C electrode decreased significantly.

1.3.6. Biochar Based Supercapacitor

Supercapacitor, an energy storage device, has received attention to harvest energy due to its high-power density, long cycle life, and quick charge/discharge capability [70]. Supercapacitor can be used as uninterruptible power sources in electric vehicles, digital communications system, etc. The microstructure of supercapacitor electrodes has a great influence on supercapacitor performance. Carbon material with high surface area and rich porous structure are the primary raw materials for making supercapacitors due to its wide availability and low environmental impacts [71]. Producing attractive, high quality carbon material at low cost is critical for development of the supercapacitor industry. Recently, several researchers used biochar originated from different biomass (such as paper cardboard and woody biomass) as raw material for fabricating a supercapacitor [71-74]. Results indicated that the use of biochar is promising as an electrode due to its low cost and satisfactory performance. The supercapacitor electrodes, made from biochar (derived from woody biomass) had a potential window of about 1.3 V and fast charging-discharging behavior with a gravimetric capacitance of about 14 F/g [75]. Authors also improved the performance of woody biochar by activating the biochar with nitric acid. Results showed that nitric acid treatment increased the capacitance from 14 to 115 F/g. The capacitance increase after nitric acid treatment was most likely due to the increase in surface oxygen groups, especially the formation of surface carboxyl groups and hydroxyl groups. The surface oxygen groups increase the pseudo-capacitance arising through redox reactions of carbonyl-type surface oxygen groups. Stability tests showed that both biochar supercapacitors, with and without HNO_3

treatment, were stable over 5000 cycles without performance decays. Liu et al. [71] also synthesized a high performance supercapacitor from biochar-derived carbon monolith that was made from pyrolysis of poplar wood at 900 °C for 6 hours followed by surface modification with nitric acid. The supercapacitor was found to have highly consistent structure and high porosity. The maximum specific capacitance was high (234 F/g) with excellent cyclic stability.

1.3.7. Biochar as A Raw Material for Making Activated Carbon

The two main steps for the preparation of activated carbon from char are (a) carbonization of the raw material (such as agriculture residue) under inert atmosphere or limited oxygen atmosphere to produce char and (b) activation of the char through chemical or physical activation [76, 77]. The activation temperature usually ranges between 600 and 1200 °C. Physical activation occurs at high temperature (600 to 1200 °C) in the presence of oxidizing gases, such as carbon dioxide, steam and air. Physical activation method does not involve any chemicals to activate char. Chemical activation uses chemicals as activating agent. Chemical activation can be categorized into one-step activation and two-step activation. In the one-step chemical activation, the carbonization and activation steps are carried out simultaneously with an activating chemical agent. Two-step chemical activation involves carbonization of raw material followed by activation of the product by mixing with a chemical agent. Most common chemical activation agents are $ZnCl_2$, KOH, H_3PO_4 and K_2CO_3 [40]. The one-step chemical activation is less time-intensive. However, environmental concerns of using chemical agents for activation in both one and two-step processes must be taken into consideration. Physical activation offers advantages over chemical activation since physical activation agents are clean and easy to control. Compared with one step chemical activation and physical activation, two-step chemical activation has advantage of producing highly microporous activated carbon with high surface area.

1.4. Biochar Properties and Advanced Characterization Techniques

Surface morphology, such as pore distribution, surface area and surface functionality, are key properties to effectively utilize biochar as catalysts and absorbents. The intrinsic ash content

of biochar, such as alkaline and alkali metal, may also affect the catalyst performance. For biochar as a soil amendment, mineral content and surface area of biochar may play important role in improving soil quality. However, the relationships between biochar properties and their effects on enhancing performance in various applications are still not well-understood. Although many papers have reported relationships between biochar properties and its respective production conditions, no universal relationship between the properties and process conditions has been well established. Hence, research on characterizations of biochar properties and its relationship to reaction conditions used for its production are critical to optimizing and tailoring of biochar properties for its effectiveness in any application.

Biochar properties can be divided into physical (such as specific surface area, morphology) and chemical (such as proximate and ultimate analyses, and heating value) properties. The proximate analysis includes contents of volatile, moisture, ash and fixed carbon. The volatile content can be determined following ASTM D3175-11 [78]. Moisture content is determined by drying the samples at 105°C according to ASTM D4442-07 [79]. Ash content is determined by combusting the biochar at 600 °C, based on ASTM E1755 [80] and fixed carbon content is determined following ASTM D3172 [81] as the difference. Energy content or higher heating value (HHV) is determined using a bomb calorimeter. The biochar pH is determined following ASTM D4972−01 [82]. The concentrations of P, Al, Ca, Cr, Ni, Cu, Fe, K, Mg, Mn, and Na are determined using an inductively coupled plasma (ICP) spectrometer or X-ray fluorescence (XRF) by ashing the biochar at 600 °C or low-temperature oxygen plasma ashing. Surface area is typically measured via N_2 adsorption using the Brunauer–Emmett–Teller (BET) theory. If the biochar contains a large amount of micropores, the surface area is estimated using CO_2 isothermal adsorption method at 0 °C. These methods are well-developed and used routinely for biochar characterization. However, molecular-level analysis on chemical structure of biochar organic matters is very limited. Most information on biochar organic structure is acquired by

Fourier transform infrared (FT-IR) and Raman spectroscopy. FT-IR analyzes the chemical properties of biochar by assigning peaks of interest to functional groups based on characteristic absorption regions (as in Table 1.3).

Table 1.3. FT-IR characteristic absorption of biochar. Adapted from reference[25]

Functional Group	Absorption, cm^{-1}
Alkyl C-H Stretch	2950–2850
Aromatic C-H Bending	860–680
Aromatic C=C Bending	1600–1500
Aromatic C, indicative of lignin C=C	1440, 1510
Alcohol/Phenol O-H Stretch	3550–3200
Aldehyde, Ketone, Ester, Carboxylic Acid	1780–1700
Phenol O-H bending	1375
C-O stretching C-O-C groups and aryl ethers; phenolic C-O associated with lignin	1270–1250
Phosphines and phosphine oxides, Silican oxid, C-O-C stretching	1100–950

Raman spectroscopy can identify structural features of highly disordered carbonaceous materials, such as chars [83-85]. Raman spectral characteristics of the G (graphite band) and D (disordered structure) bands are usually used to investigate coal structure. However, Li et al. [83] found that Raman spectra of coal chars differ from that of ordered carbon materials because coal char is not highly ordered. Researchers divided the Raman spectra (from 800–1800 cm^{-1}) in 10 bands and correlated these bands with aromatic structures in the char. They also correlated the ratio of small to larger aromatic rings (ratio of respective peak areas) with char reactivity. Advanced solid state ^{13}C nuclear magnetic resonance (NMR) experiments can be used to study the chemical structure of biochar [86-88]. While FT-IR and Raman identify surface functionality of biochar quantitatively, solid state ^{13}C NMR spectroscopy reveals the biochar bulk structure exposing more species that are present inside biochar [88]. Furthermore, advanced solid state ^{13}C NMR techniques were recently developed by Mao et al. [86, 87] and Brewer et al. [88] using a

combination of selective pulse sequences to reliably quantify the carbon species and estimating the size of fused aromatic rings. A series of cross-polarization spin-lattice relaxation time (CP/T_1) experiments with total sideband suppression (TOSS) (CP/T_1–TOSS) were firstly conducted to measure relaxation time and correction factor [86, 87]. Direct-polarization with magic-angle spinning (DP/MAS) with recoupled dipolar dephasing (DP/MAS/DD) technique was then applied to quantify the nonprotonated carbons and mobile carbon fractions using recycle delay time obtained from CP/T_1–TOSS. Because NMR signals of O−C−O carbon and aromatic carbon overlap, a chemical-shift-anisotropy (CSA) filter was used to suppress the aromatic carbon signals to obtain the O−C−O carbon spectra. The fused aromatic ring size was estimated by measuring distances of the aromatic carbons from hydrogen at the edge of the fused ring using the long-range ^{1}H-^{13}C dipolar dephasing technique. The strongly distance-dependent ^{1}H-^{13}C dipolar couplings slow dephasing of the ^{13}C signal for large fused aromatic rings. The obtained carbon signals were then assigned to different functional groups according to chemical shifts. By using these methods, quantitative information on structural changes of woody chars with different pyrolysis temperatures were obtained [86]. They also showed that the fraction of aromatic C−O groups decreased from 17 to 9% and nonprotonated aromatic carbons increased from 2.2 to 66% with an increase in temperature from 300 to 700 °C. The cluster size of aromatic rings increased with an increase in temperature (cluster size of 27 and 1-2 rings in biochar treated at 700 and 300 °C, respectively).

The stability of biochar applied to soil is thought to be related to the structure of biochar. The biochar leachable aromatic compounds, such as polyaromatic hydrocarbons (PAHs), are one of the environmental concerns in using biochar as a soil amendment. However, there is no agreement on analytical methods to quantify leachable PAHs in biochar [89]. The entrapped organic matters in biochar can be determined via extraction procedures. Extraction dissolves the trapped organic matter in solvents, such as toluene, methanol, cyclohexane, acetone using soxhlet,

accelerated solvent extraction and reflux extraction methods. Soxhlet extraction was approved to be the best extraction method to determine leachable PAHs in biochar [89, 90]. Toluene and acetone/cyclohexane are two of the best solvents for the extraction [89].

Due to the complexity in extraction of chemicals from biochar, regular GC-mass spectrometry may not identify all the compounds. An ultrahigh-resolution mass spectrometry, Fourier-transform ion cyclotron-mass spectrometry (FT-ICR-MS) has been used to analyze the composition and structure of biochar compounds with higher reliability [91]. Three ionization methods (atmospheric desorption, pressurized photoionization and electrospray ionization) were compared and the ionized biochar extracts were analyzed using mass spectrometry. The results found significant differences between biochar produced from gasification and pyrolysis. The MS spectra of pyrolysis biochar were consistent with those of bio-oil compounds (phenolic and carbohydrate-derived compounds) and gasification biochar extracts were mainly composed of polyaromatic hydrocarbon.

Kinetic properties of biochar are critical in the design and optimization of the operation if biochar is used for gasification and combustion purposes. A number of the theoretical or semi-empirical kinetic models have been proposed to describe reactivity profiles of the chars and carbons. Among these, a typical theoretical model is the random pore model [92] that considers the effects of pore growth and coalescence during reaction and fits the reactivity profile of char that has a maximum reaction rate at char conversion levels below 0.39 [93]. The model has been successfully used in modeling gasification reactions of coal chars and carbons. Another widely used kinetic model is the shrinking core model [92], which is based on the assumption that biochar gasification reaction initiates at the external surface of char particles and gradually proceeds inside the pores. However, any of these models cannot fit all applications; the model should be evaluated before applying and modified based on the application. For example, the random pore model is not adequate to represent systems if char reactivity rate increases with increase in conversion or if char reactivity rate reaches a maximum conversion (above 0.393),

like some of biomass char or alkali catalyzed carbons [94]. For these reasons and for more extensive applications, new models, such as extended random pore model (ERPM), were developed by adding new conversion terms into the original random pore model [95].

1.5. Perspectives on Biochar Applications

As discussed above, biochar has been successfully used in many applications, such as soil amendment and fuel cells. For use as soil amendment, although biochar offers several benefits, there are concerns. Toxic organic compounds, such as polycyclic aromatic hydrocarbons, chlorinated hydrocarbons, and dioxins can be present in biochar to a varying degree depending on the process and feedstocks. Heavy metal, inherently available in biochar, can also increase its availability in soil. Biochar can also deteriorate eco-toxicological effects on soil organisms [43]. Understanding biochar properties is critical in mitigating its undesired impacts while harnessing its benefits as soil amendment.

For use as a catalyst, biochar has a potential role in different reactions, such as reforming and conditioning of syngas, upgrading of bio-oil or biodiesel. Use of biochar-based catalyst for applications such as syngas cleaning will increase the net sustainability of bioenergy refinery system by reducing the need for external material and processing. For use in fuel cells and supercapacitors, biochar offers economic and environmental benefits as well. However, properties of biochar-based functional materials highly depend on the waste biomass precursors. In addition, performance of biochar-based fuel cells or supercapacitors is still low, e.g. the capacitance of Co_3O_4 nanotube based supercapacitor can reach 500 F/g at 4 A/g [70] while the reported maximum capacitance of biochar-based supercapacitor was only 250 F/g [71]. Post treatment of biochar with nitric acid or KOH has shown improved structure and performance. Biomass type and biochar production method also affect the quality of functional biochar. Woody biomass with high lignin content and porosity is preferred over grassy biomass for production of high quality biochar because woody biomass can result in higher porosity and electrical conductivity. High carbonization temperatures are also preferred for increased surface area,

electrical conductivity, recalcitrance, and tensile strength. Investigation on optimizing carbonization method, biomass selection and post treatment is critically needed to produce biochar with the necessary properties for specific applications. For DCFC applications, experiments demonstrated that DCFC polarization is dominated by anode polarization [66]. Improving the material structure of the anode can improve the power output and durability of DCFC. An ideal anode should have high porosity and large surface area to provide sufficient active site for the electrochemical oxidation of fuel and a continuous framework to maintain sufficient mechanical strength. Developing advanced anode material will play a key role in improving DCFC performance.

In addition, life-cycle analysis of all biochar applications is needed to identify potential benefits and concerns for specific applications. However, optimum reaction conditions for producing biochar and biofuels are not always the same; hence, the conditions must be optimized based on the target products for specific applications. For example, high carbonization temperatures (>700 °C) [67] is preferred for biochar production for MFC application, while 400–600 °C carbonization temperature is preferred for bio-oil production with high bio-oil yield. Thus, life-cycle analysis of manufacturing biobased products (bio-oil and syngas) and byproducts (biochar) would guide biomass selection to minimize environmental impacts and costs.

1.6. Conclusions

Recent advances in biochar utilization, production methods, properties and characterization techniques, are discussed. The potential biochar applications include its use as precursor for catalyst, soil amendment for improving soil quality and carbon sequestration, sorbent for removing contaminants from soil and water, storage material for CO2 and H2, and as fuel for fuel cells. Overall, use of char as sustainable high-value products seems to have a very promising future. However, in order to successfully utilize for various purposes, biochar properties need further improvement and tailoring for the appropriate applications. Standards and methods used

to determine structure and properties of biochar need further development so that its effectiveness as soil amendment, catalyst and sorbents can be realized.

1.7. Objectives

The overall goal of the proposed research is to develop novel methods to use biochar derived from gasification for high-value applications. Although several studies are reported on using pyrolysis-based biochar, study on gasification-derived biochar and its utilization are limited. The specific objectives of each chapter are as follows:

- The objective of chapter 2 was to investigate effects of gasification condition and feedstock on properties of char derived from fluidized bed gasification.
- The objective of chapter 3 was to investigate properties of char derived from downdraft gasifier and its kinetic performance in CO_2 gasification. The correlation between structure of biochar and kinetic performance of gasification- derived char were explored.
- The objective of chapter 4 was to develop an effective catalyst using gasification derived char as precursor for steam reforming of toluene as model tar.
- The objective of chapter 5 was to test the catalyst produced in study 3 in reforming of condensed tertiary tar using naphthalene as model tar.
- The objective of chapter 6 was to investigate effects of atmosphere and pressure on catalytic reforming of lignin-derived tars using biochar-based catalyst developed.

1.8. References

[1] J. Routa, S. Kellomaki, H. Strandman, Effects of forest management on total biomass production and CO_2 emissions from use of energy biomass of norway spruce and scots pine, Bioenerg Res, 5 (2012) 733-747.

[2] S.V. Vassilev, D. Baxter, L.K. Andersen, C.G. Vassileva, An overview of the chemical composition of biomass, Fuel, 89 (2010) 913-933.

[3] P.M. Mortensen, J.D. Grunwaldt, P.A. Jensen, K.G. Knudsen, A.D. Jensen, A review of catalytic upgrading of bio-oil to engine fuels, Applied Catalysis A: General, 407 (2011) 1-19.

[4] P.K. Swain, L.M. Das, S.N. Naik, Biomass to liquid: A prospective challenge to research and development in 21st century, Renewable and Sustainable Energy Reviews, 15 (2011) 4917-4933.

[5] A. Kumar, D. Jones, M. Hanna, Thermochemical biomass gasification: A review of the current status of the technology, Energies, 2 (2009) 556-581.

[6] M.A. Noordermeer, L. Petrus, Biomass to biofuels, a chemical perspective, Green Chem, 8 (2006) 861-867.

[7] T. Huggins, H. Wang, J. Kearns, P. Jenkins, Z.J. Ren, Biochar as a sustainable electrode material for electricity production in microbial fuel cells, Bioresour. Technol., 157 (2014) 114-119.

[8] A. Kacprzak, R. Kobyłecki, R. Włodarczyk, Z. Bis, The effect of fuel type on the performance of a direct carbon fuel cell with molten alkaline electrolyte, J Power Sources, 255 (2014) 179-186.

[9] M.-M. Titirici, R.J. White, C. Falco, M. Sevilla, Black perspectives for a green future: hydrothermal carbons for environment protection and energy storage, Energ Environ Sci, 5 (2012) 6796-6822.

[10] J.J. Manyà, Pyrolysis for Biochar Purposes: A Review to Establish Current Knowledge Gaps and Research Needs, Environmental Science & Technology, 46 (2012) 7939-7954.

[11] M. Ahmad, A.U. Rajapaksha, J.E. Lim, M. Zhang, N. Bolan, D. Mohan, M. Vithanage, S.S. Lee, Y.S. Ok, Biochar as a sorbent for contaminant management in soil and water: A review, Chemosphere, 99 (2014) 19-33.

[12] J. Lehmann, M.C. Rillig, J. Thies, C.A. Masiello, W.C. Hockaday, D. Crowley, Biochar effects on soil biota – A review, Soil Biology and Biochemistry, 43 (2011) 1812-1836.

[13] J. Lehmann, J. Gaunt, M. Rondon, Bio-char Sequestration in Terrestrial Ecosystems – A Review, Mitig Adapt Strat Glob Change, 11 (2006) 395-419.

[14] Y. Shen, K. Yoshikawa, Recent progresses in catalytic tar elimination during biomass gasification or pyrolysis—A review, Renewable and Sustainable Energy Reviews, 21 (2013) 371-392.

[15] S. Meyer, B. Glaser, P. Quicker, Technical, Economical, and Climate-Related Aspects of Biochar Production Technologies: A Literature Review, Environmental Science & Technology, 45 (2011) 9473-9483.

[16] D.A. Laird, R.C. Brown, J.E. Amonette, J. Lehmann, Review of the pyrolysis platform for coproducing bio-oil and biochar, Biofuels, Bioproducts and Biorefining, 3 (2009) 547-562.

[17] I.B. Initiate, Standardized product definition and product testing guidelines for biochar that is used in soi, in, International Biochar Initiate, 2012.

[18] J.F. González, S. Román, J.M. Encinar, G. Martínez, Pyrolysis of various biomass residues and char utilization for the production of activated carbons, J Anal Appl Pyrol, 85 (2009) 134-141.

[19] M. Uchimiya, L.H. Wartelle, K.T. Klasson, C.A. Fortier, I.M. Lima, Influence of pyrolysis temperature on biochar property and function as a heavy metal sorbent in soil, J Agr Food Chem, 59 (2011) 2501-2510.

[20] M.J. Antal, S.G. Allen, X.F. Dai, B. Shimizu, M.S. Tam, M. Gronli, Attainment of the theoretical yield of carbon from biomass, Industrial & Engineering Chemistry Research, 39 (2000) 4024-4031.

[21] L. Wei, S. Xu, L. Zhang, H. Zhang, C. Liu, H. Zhu, S. Liu, Characteristics of fast pyrolysis of biomass in a free fall reactor, Fuel Processing Technology, 87 (2006) 863-871.

[22] W.J. DeSisto, N. Hill, S.H. Beis, S. Mukkamala, J. Joseph, C. Baker, T.H. Ong, E.A. Stemmler, M.C. Wheeler, B.G. Frederick, A. van Heiningen, Fast pyrolysis of pine sawdust in a fluidized-bed reactor, Energy Fuels, 24 (2010) 2642-2651.

[23] J. Poerschmann, I. Baskyr, B. Weiner, R. Koehler, H. Wedwitschka, F.D. Kopinke, Hydrothermal carbonization of olive mill wastewater, Bioresour. Technol., 133 (2013) 581-588.

[24] A. Kruse, A. Funke, M.M. Titirici, Hydrothermal conversion of biomass to fuels and energetic materials, Curr. Opin. Chem. Biol., 17 (2013) 515-521.

[25] K. Qian, A. Kumar, K. Patil, D. Bellmer, D. Wang, W. Yuan, R. Huhnke, Effects of biomass feedstocks and gasification conditions on the physiochemical properties of char, Energies, 6 (2013) 3972-3986.

[26] B. Hu, K. Wang, L. Wu, S.-H. Yu, M. Antonietti, M.-M. Titirici, Engineering carbon materials from the hydrothermal carbonization process of biomass, Adv Mater, 22 (2010) 813-828.

[27] S. Zhang, M. Asadullah, L. Dong, H.-L. Tay, C.-Z. Li, An advanced biomass gasification technology with integrated catalytic hot gas cleaning. Part II: Tar reforming using char as a catalyst or as a catalyst support, Fuel, 112 (2013) 646-653.

[28] A.M. Dehkhoda, A.H. West, N. Ellis, Biochar based solid acid catalyst for biodiesel production, Applied Catalysis A: General, 382 (2010) 197-204.

[29] S. Mani, J.R. Kastner, A. Juneja, Catalytic decomposition of toluene using a biomass derived catalyst, Fuel Processing Technology, 114 (2013) 118-125.

[30] J.R. Kastner, J. Miller, D.P. Geller, J. Locklin, L.H. Keith, T. Johnson, Catalytic esterification of fatty acids using solid acid catalysts generated from biochar and activated carbon, Catal. Today, 190 (2012) 122-132.

[31] S.P. Sohi, E. Krull, E. Lopez-Capel, R. Bol, Chapter 2 - A review of biochar and its use and function in soil, in: L.S. Donald (Ed.) Advances in Agronomy, Academic Press, 2010, pp. 47-82.

[32] A. Zhang, R. Bian, G. Pan, L. Cui, Q. Hussain, L. Li, J. Zheng, J. Zheng, X. Zhang, X. Han, X. Yu, Effects of biochar amendment on soil quality, crop yield and greenhouse gas emission in a Chinese rice paddy: A field study of 2 consecutive rice growing cycles, Field Crops Research, 127 (2012) 153-160.

[33] S.Y. Ahn, S.Y. Eom, Y.H. Rhie, Y.M. Sung, C.E. Moon, G.M. Choi, D.J. Kim, Utilization of wood biomass char in a direct carbon fuel cell (DCFC) system, Appl. Energy, 105 (2013) 207-216.

[34] D. Houben, L. Evrard, P. Sonnet, Mobility, bioavailability and pH-dependent leaching of cadmium, zinc and lead in a contaminated soil amended with biochar, Chemosphere.

[35] P. Oleszczuk, S.E. Hale, J. Lehmann, G. Cornelissen, Activated carbon and biochar amendments decrease pore-water concentrations of polycyclic aromatic hydrocarbons (PAHs) in sewage sludge, Bioresource Technology, 111 (2012) 84-91.

[36] W. Hao, E. Björkman, M. Lilliestråle, N. Hedin, Activated carbons prepared from hydrothermally carbonized waste biomass used as adsorbents for CO_2, Applied Energy, 112 (2013) 526-532.

[37] X.B. Zhao, B. Xiao, A.J. Fletcher, K.M. Thomas, Hydrogen adsorption on functionalized nanoporous activated carbons, The Journal of Physical Chemistry B, 109 (2005) 8880-8888.

[38] C. Zhang, Z. Geng, M. Cai, J. Zhang, X. Liu, H. Xin, J. Ma, Microstructure regulation of super activated carbon from biomass source corncob with enhanced hydrogen uptake, Int J Hydrogen Energ, 38 (2013) 9243-9250.

[39] M.V. Gil, M. Martínez, S. García, F. Rubiera, J.J. Pis, C. Pevida, Response surface methodology as an efficient tool for optimizing carbon adsorbents for CO_2 capture, Fuel Processing Technology, 106 (2013) 55-61.

[40] O. Ioannidou, A. Zabaniotou, Agricultural residues as precursors for activated carbon production—A review, Renewable and Sustainable Energy Reviews, 11 (2007) 1966-2005.

[41] A. Mudinoor, D. Bellmer, L. Marin, A. Kumar, R. Huhnke, Conversion of Toluene(Model Tar) Using Selected Steam Reforming Catalysts, Transactions of the ASABE, 54 (2011) 1819-1827.

[42] S. Anis, Z.A. Zainal, Tar reduction in biomass producer gas via mechanical, catalytic and thermal methods: A review, Renewable and Sustainable Energy Reviews, 15 (2011) 2355-2377.

[43] Z. Abu El-Rub, E.A. Bramer, G. Brem, Experimental comparison of biomass chars with other catalysts for tar reduction, Fuel, 87 (2008) 2243-2252.

[44] D. Wang, W. Yuan, W. Ji, Char and char-supported nickel catalysts for secondary syngas cleanup and conditioning, Applied Energy, 88 (2011) 1656-1663.

[45] P.N. Bhandari, A. Kumar, R.L. Huhnke, Simultaneous Removal of Toluene (Model Tar), NH3, and H2S, from Biomass-Generated Producer Gas Using Biochar-Based and Mixed-Metal Oxide Catalysts, Energy Fuels, 28 (2013) 1918-1925.

[46] P.N. Bhandari, A. Kumar, D.D. Bellmer, R.L. Huhnke, Synthesis and evaluation of biochar-derived catalysts for removal of toluene (model tar) from biomass-generated producer gas, Renew Energ, 66 (2014) 346-353.

[47] L.S. Marin, Treatment of biomass-derived synthesis gas using commercial steam reforming catalysts and biochar, in: Biosystems engineering, Oklahoma state university, Stillwater, 2011.

[48] Y. Shen, P. Zhao, Q. Shao, D. Ma, F. Takahashi, K. Yoshikawa, In-situ catalytic conversion of tar using rice husk char-supported nickel-iron catalysts for biomass pyrolysis/gasification, Applied Catalysis B: Environmental, 152–153 (2014) 140-151.

[49] Q. Yan, C. Wan, J. Liu, J. Gao, F. Yu, J. Zhang, Z. Cai, Iron nanoparticles in situ encapsulated in biochar-based carbon as an effective catalyst for the conversion of biomass-derived syngas to liquid hydrocarbons, Green Chem, 15 (2013) 1631-1640.

[50] A.M. Dehkhoda, N. Ellis, Biochar-based catalyst for simultaneous reactions of esterification and transesterification, Catal. Today, 207 (2013) 86-92.

[51] M. Li, Y. Zheng, Y. Chen, X. Zhu, Biodiesel production from waste cooking oil using a heterogeneous catalyst from pyrolyzed rice husk, Bioresour. Technol., 154 (2014) 345-348.

[52] R.S. Kookana, A.K. Sarmah, L. Van Zwieten, E. Krull, B. Singh, Chapter three - Biochar application to soil: Agronomic and environmental benefits and unintended consequences, in: L.S. Donald (Ed.) Advances in Agronomy, Academic Press, 2011, pp. 103-143.

[53] B. Liang, J. Lehmann, D. Solomon, J. Kinyangi, J. Grossman, B. O'Neill, J.O. Skjemstad, J. Thies, F.J. Luizão, J. Petersen, E.G. Neves, Black carbon increases cation exchange capacity in soils, Soil Sci. Soc. Am. J., 70 (2006) 1719-1730.

[54] D. Laird, P. Fleming, B. Wang, R. Horton, D. Karlen, Biochar impact on nutrient leaching from a Midwestern agricultural soil, Geoderma, 158 (2010) 436-442.

[55] C. Steiner, B. Glaser, W. Geraldes Teixeira, J. Lehmann, W.E.H. Blum, W. Zech, Nitrogen retention and plant uptake on a highly weathered central Amazonian Ferralsol amended with compost and charcoal, Journal of Plant Nutrition and Soil Science, 171 (2008) 893-899.

[56] C. Steiner, M.R. de Arruda, W.G. Teixeira, W. Zech, Soil respiration curves as soil fertility indicators in perennial central Amazonian plantations treated with charcoal, and mineral or organic fertilisers, Tropical Science, 47 (2007) 218-230.

[57] D. Warnock, J. Lehmann, T. Kuyper, M. Rillig, Mycorrhizal responses to biochar in soil – concepts and mechanisms, Plant Soil, 300 (2007) 9-20.

[58] P. Zhang, G. Sheng, Y. Feng, D.M. Miller, Role of Wheat-Residue-Derived Char in the Biodegradation of Benzonitrile in Soil: Nutritional Stimulation versus Adsorptive Inhibition, Environ. Sci. Technol., 39 (2005) 5442-5448.

[59] X.-Y. Yu, C.-L. Mu, C. Gu, C. Liu, X.-J. Liu, Impact of woodchip biochar amendment on the sorption and dissipation of pesticide acetamiprid in agricultural soils, Chemosphere, 85 (2011) 1284-1289.

[60] W. Zheng, M. Guo, T. Chow, D.N. Bennett, N. Rajagopalan, Sorption properties of greenwaste biochar for two triazine pesticides, J Hazard Mater, 181 (2010) 121-126.

[61] B. Chen, D. Zhou, L. Zhu, Transitional Adsorption and Partition of Nonpolar and Polar Aromatic Contaminants by Biochars of Pine Needles with Different Pyrolytic Temperatures, Environ. Sci. Technol., 42 (2008) 5137-5143.

[62] A.S. González, M.G. Plaza, F. Rubiera, C. Pevida, Sustainable biomass-based carbon adsorbents for post-combustion CO2 capture, Chemical Engineering Journal, 230 (2013) 456-465.

[63] S.M. Lee, K.S. Park, Y.C. Choi, Y.S. Park, J.M. Bok, D.J. Bae, K.S. Nahm, Y.G. Choi, S.C. Yu, N.-g. Kim, T. Frauenheim, Y.H. Lee, Hydrogen adsorption and storage in carbon nanotubes, Synthetic Metals, 113 (2000) 209-216.

[64] M.Z. Figueroa-Torres, C. Domínguez-Ríos, J.G. Cabañas-Moreno, O. Vega-Becerra, A. Aguilar-Elguézabal, The synthesis of Ni-activated carbon nanocomposites via electroless deposition without a surface pretreatment as potential hydrogen storage materials, Int J Hydrogen Energ, 37 (2012) 10743-10749.

[65] A. Elleuch, A. Boussetta, J.S. Yu, K. Halouani, Y.D. Li, Experimental investigation of direct carbon fuel cell fueled by almond shell biochar: Part I. Physicochemical characterization of the biochar fuel and cell performance examination, Int J Hydrogen Energ, 38 (2013) 16590-16604.

[66] A. Elleuch, A. Boussetta, K. Halouani, Y. Li, Experimental investigation of Direct Carbon Fuel Cell fueled by almond shell biochar: Part II. Improvement of cell stability and performance by a three-layer planar configuration, Int J Hydrogen Energ, 38 (2013) 16605-16614.

[67] K. Ganesh, J.R. Jambeck, Treatment of landfill leachate using microbial fuel cells: Alternative anodes and semi-continuous operation, Bioresour. Technol., 139 (2013) 383-387.

[68] S. Chen, G. He, Q. Liu, F. Harnisch, Y. Zhou, Y. Chen, M. Hanif, S. Wang, X. Peng, H. Hou, U. Schroder, Layered corrugated electrode macrostructures boost microbial bioelectrocatalysis, Energ Environ Sci, 5 (2012) 9769-9772.

[69] Y. Yuan, T. Yuan, D. Wang, J. Tang, S. Zhou, Sewage sludge biochar as an efficient catalyst for oxygen reduction reaction in an microbial fuel cell, Bioresource Technol, 144 (2013) 115-120.

[70] Y.H. Xiao, A.Q. Zhang, S.J. Liu, J.H. Zhao, S.M. Fang, D.Z. Jia, F. Li, Free-standing and porous hierarchical nanoarchitectures constructed with cobalt cobaltite nanowalls for supercapacitors with high specific capacitances, J Power Sources, 219 (2012) 140-146.

[71] M.-C. Liu, L.-B. Kong, P. Zhang, Y.-C. Luo, L. Kang, Porous wood carbon monolith for high-performance supercapacitors, Electrochim Acta, 60 (2012) 443-448.

[72] N.H. Basri, M. Deraman, S. Kanwal, I.A. Talib, J.G. Manjunatha, A.A. Aziz, R. Farma, Supercapacitors using binderless composite monolith electrodes from carbon nanotubes and pre-carbonized biomass residues, Biomass and Bioenergy, 59 (2013) 370-379.

[73] R. Farma, M. Deraman, A. Awitdrus, I.A. Talib, E. Taer, N.H. Basri, J.G. Manjunatha, M.M. Ishak, B.N.M. Dollah, S.A. Hashmi, Preparation of highly porous binderless activated carbon electrodes from fibres of oil palm empty fruit bunches for application in supercapacitors, Bioresour. Technol., 132 (2013) 254-261.

[74] P.A. Goodman, H. Li, Y. Gao, Y.F. Lu, J.D. Stenger-Smith, J. Redepenning, Preparation and characterization of high surface area, high porosity carbon monoliths from pyrolyzed bovine bone and their performance as supercapacitor electrodes, Carbon, 55 (2013) 291-298.

[75] J. Jiang, L. Zhang, X. Wang, N. Holm, K. Rajagopalan, F. Chen, S. Ma, Highly ordered macroporous woody biochar with ultra-high carbon content as supercapacitor electrodes, Electrochim Acta, 113 (2013) 481-489.

[76] R. Azargohar, A.K. Dalai, Steam and KOH activation of biochar: Experimental and modeling studies, Micropor Mesopor Mat, 110 (2008) 413-421.

[77] A. Dąbrowski, P. Podkościelny, Z. Hubicki, M. Barczak, Adsorption of phenolic compounds by activated carbon—a critical review, Chemosphere, 58 (2005) 1049-1070.

[78] ASTM, D3175-11 Standard Test Method for Volatile Matter in the Analysis Sample of Coal and Coke, in, 2011.

[79] ASTM, D4442-07 Standard Test Methods for Direct Moisture Content Measurement of Wood and Wood-Base Materials, in, 2007.

[80] ASTM, E1755-01(2007) Standard Test Method for Ash in Biomass, in, 2007.

[81] ASTM Standard D3172- 07a "Standard Practice for Proximate Analysis of Coal and Coke", in, ASTM International, West Conshohocken, PA, 2007.

[82] ASTM, ASTM Standard E1755-01(2007) "Standard Test Method for pH of Soils", in, ASTM International, West Conshohocken, PA, 2007.

[83] X. Li, J.-i. Hayashi, C.-Z. Li, FT-Raman spectroscopic study of the evolution of char structure during the pyrolysis of a Victorian brown coal, Fuel, 85 (2006) 1700-1707.

[84] C.-Z. Li, Some recent advances in the understanding of the pyrolysis and gasification behaviour of Victorian brown coal, Fuel, 86 (2007) 1664-1683.

[85] S. Potgieter-Vermaak, N. Maledi, N. Wagner, J.H.P. Van Heerden, R. Van Grieken, J.H. Potgieter, Raman spectroscopy for the analysis of coal: a review, Journal of Raman Spectroscopy, 42 (2011) 123-129.

[86] X. Cao, J.J. Pignatello, Y. Li, C. Lattao, M.A. Chappell, N. Chen, L.F. Miller, J. Mao, Characterization of wood chars produced at different temperatures using advanced solid-state ^{13}C NMR spectroscopic techniques, Energy Fuels, 26 (2012) 5983-5991.

[87] J.D. Mao, N. Chen, X.Y. Cao, Characterization of humic substances by advanced solid state NMR spectroscopy: Demonstration of a systematic approach, Organic Geochemistry, 42 (2011) 891-902.

[88] C.E. Brewer, K. Schmidt-Rohr, J.A. Satrio, R.C. Brown, Characterization of biochar from fast pyrolysis and gasification systems, Environ. Prog. Sustain. Energy, 28 (2009) 386-396.

[89] D. Fabbri, A.G. Rombolà, C. Torri, K.A. Spokas, Determination of polycyclic aromatic hydrocarbons in biochar and biochar amended soil, J Anal Appl Pyrol, 103 (2013) 60-67.

[90] I. Hilber, F. Blum, J. Leifeld, H.-P. Schmidt, T.D. Bucheli, Quantitative determination of PAHs in biochar: A prerequisite to ensure its quality and safe application, J Agr Food Chem, 60 (2012) 3042-3050.

[91] D.P. Cole, E.A. Smith, Y.J. Lee, High-resolution mass spectrometric characterization of molecules on biochar from pyrolysis and gasification of switchgrass, Energy Fuels, 26 (2012) 3803-3809.

[92] P. Lahijani, Z.A. Zainal, A.R. Mohamed, M. Mohammadi, CO_2 gasification reactivity of biomass char: Catalytic influence of alkali, alkaline earth and transition metal salts, Bioresour. Technol., 144 (2013) 288-295.

[93] S.K. Bhatia, D.D. Perlmutter, A random pore model for fluid-solid reactions: II. Diffusion and transport effects, AIChE Journal, 27 (1981) 247-254.

[94] Y. Zhang, M. Ashizawa, S. Kajitani, K. Miura, Proposal of a semi-empirical kinetic model to reconcile with gasification reactivity profiles of biomass chars, Fuel, 87 (2008) 475-481.

[95] M.F. Irfan, M.R. Usman, K. Kusakabe, Coal gasification in CO_2 atmosphere and its kinetics since 1948: A brief review, Energy, 36 (2011) 12-40.

CHAPTER II

EFFECTS OF BIOMASS FEEDSTOCKS AND GASIFICATION CONDITIONS ON THE PHYSIOCHEMICAL PROPERTIES OF CHAR

This research paper was published as “Kezhen Qian, Ajay Kumar, Krushna Patil, Danielle Bellme, Donghai Wang, Wenqiao Yuan and Raymond L. Huhnke. Effects of Biomass Feedstocks and Gasification Conditions on the Physiochemical Properties of Char, Energies, 2013”

Abstract: Char is a low-value byproduct of biomass gasification and pyrolysis with many potential applications, such as soil amendment and the synthesis of activated carbon and carbon-based catalysts. Considering these high-value applications, char could provide economic benefits to a biorefinery utilizing gasification or pyrolysis technologies. However, the properties of char depend heavily on biomass feedstock, gasifier design and operating conditions. This paper reports the effects of biomass type (switchgrass, sorghum straw and red cedar) and equivalence ratio (0.20, 0.25 and 0.28), i.e., the ratio of air supply relative to the air that is required for stoichiometric combustion of biomass, on the physiochemical properties of char derived from gasification. Results show that the Brunauer-Emmett-Teller (BET) surface areas of most of the char were 1–10 m^2/g and increased as the equivalence ratio increased. Char moisture and fixed carbon contents decreased while ash content increased as equivalence ratio increased. The corresponding Fourier Transform Infrared spectra showed that the surface functional groups of char differed between biomass types but remained similar with change in equivalence ratio.Keywords: biochar; gasification; fluidized bed

Keywords: char; gasification; fluidized bed

2.1. Introduction

Char (or charcoal) has been used in human history for thousands of years. Char was used as an energy resource for heating and cooking in households and for heating in the iron industry because of reduced smoke release and high temperatures reached during its combustion. Currently, char is being used in several new high-value applications, besides as an energy source. A typical utilization of char (also called char) is as a soil amendment [1], which increases soil fertility and agricultural productivity [2] through increasing soil organic matter, utilizing high carbon (C) recalcitrance against microbial decay and providing habitat for microbes and inorganic matter for crops [3]. Making activated carbon from char is another potential application of char[4]. Activated carbon is a form of carbon with a high surface area (larger than 300 m^2 /g) and a high degree of microporosity [5], which make it suitable for chemical catalysis or physical sorption e.g. purification of waste wate [6]. Recently, raw char has been suggested as a promising catalyst for syngas cleaning [7, 8].

Char can be produced through several technologies: slow pyrolysis, fast pyrolysis, gasification, or conventional and flash carbonization [9]. Among these technologies, slow pyrolysis has been shown to retain the highest biomass carbon content in the char. Gasification, which is used for syngas production, provides a modest amount of char as a byproduct (about 10%). Generally, the char obtained in gasification is either disposed as waste or recycled to the gasifier for supplying heat; these applications provide little economic benefit to the industry. Therefore, finding a cost-effective approach that can convert the char to a value-added product will greatly benefit the biorefinery and contribute to the commercialization of bioproducts.

The properties of char generated from biomass gasification processes vary widely based on the feedstocks, reactor design, and the operating conditions. Agricultural residues, forestry residues, wood, municipal solid waste and animal manures are all potential feedstocks for gasification [10]. The properties of these feedstocks vary significantly in terms of mineral content, elemental composition and fiber structure, and variation of these properties further impact properties of the

char derived. In addition, different reactor designs, such as fluidized beds and fixed beds and their operating conditions (e.g. reaction temperature, equivalence ratio, feeding rate of biomass, flow rate of carrier gas or oxidizing agents and residence time), impact conversion efficiencies of biomass and properties of char [11]. Unfortunately, the gasification derived char has some undesired qualities that may also adversely affect its applications. For example, char with high ash concentration and low porosity may not be suitable for producing activated carbon [12]. Numerous researchers have reported the properties of char obtained from thermochemical conversions of biomass [9, 10, 13, 14]. However, the impacts of feedstock properties and operating conditions on char properties are not well understood. Earlier studies have focused primarily on the char derived from biomass pyrolysis with limited information available on gasification-based char. The objective of this research was to investigate the effects of biomass feedstocks and gasification operating conditions on the properties of char derived from gasification. Three biomass species—switchgrass, forage sorghum and red cedar—representing herbaceous plants, agricultural straw and woody biomass, respectively, were selected as the feedstocks in this study. The physiochemical properties of gasification-derived char were analyzed. Results of this study will provide valuable information on how gasification conditions can be manipulated to produce char with wanted properties, adding value to this bioproduct.

2.2. Materials and Methods

2.2.1. Material

The Kanlow variety of switchgrass (*Panicum virgatum*) and forage sorghum (*Sorghum spp*.) were obtained from the Oklahoma State University Agronomy Research Station. Large round bales of switchgrass and sorghum were chopped by a Haybuster tub grinder (H1000, Duratech Industries International, Inc., Jamestown, N.D.) with a screen size of 1.25 cm. Red cedar (eastern red cedar) was obtained locally and chopped with a screen size of 1.25 cm by a local company (Bliss Industries, Ponca City, Oklahoma).

2.2.2. Fluidized Bed Gasification

The gasification experiments were carried out in a lab-scale fluidized bed gasifier at three equivalence ratios (ERs): 0.20, 0.25 and 0.28. ER is defined as the ratio of air supplied into the gasifier to the air required for complete combustion. The gasifier, with designed feedstocks throughput of 2 to 5 kg/h, had dimensions of 102 mm i.d. × 1118 mm height and 250 mm i.d. × 310 mm height in the reactor and disengagement zones, respectively. The gasification bed temperature stabilized at average temperatures was around 700, 780 and 800 °C at ERs of 0.2, 0.25 and 0.28, respectively. The residence time ranged from 5 to 7 s. Biomass feeding rate was 3.9 to 4.2 kg/h. A screw feeder continuously injected the biomass into the gasifier. Silica sand with particle size ranging from 106 to 850 μm was used as the fluidizing agent. The ER was varied by adjusting the air flow rate and biomass feeding rate. The biomass feeding rate was controlled by adjusting the rotational speed of the screw feeder. The relationship between biomass feeding rate and rotational speed of the screw feeder was calibrated before each run. The gasification reactor temperature profile, pressure drop along the gasifier and air flow rate were closely monitored using a LabVIEW system (National instruments, Austin, TX, USA). Every run lasted approximately 4 h, including preheating. At the conclusion of each run, char was collected from two cyclones. Each experiment has been repeated twice. Detailed information on the configuration of the experimental-setup and procedures for running the gasifier was previously reported[15].

2.2.3. Property Analysis of Biomass and Biochar

Biomass feedstocks and resultant char were analyzed for proximate and elemental analyses, BET surface area and FT-IR spectrum. Ultimate analysis (contents of carbon, hydrogen, oxygen, nitrogen and sulfur) was measured using an elemental analyzer (Perkin Elmer 2400 Series 2, PerkinElmer Inc., Waltham, MA) at Kansas State University. Oxygen content was not determined in char samples due to presence of oxygen in its high ash content. For the proximate

analysis, volatile content was determined following ASTM D3175-11[16]. Char（1 g） was kept in a crucile with lid and heated in oven with temperature of 950 °C for 7 minutes. Then calculate the valtaile matters by difference. Moisture content was analyzed by drying the samples at 105 °C according to ASTM D4442-07 [17]. Ash content was determined by combusting the char at 600 °C, based on ASTM E1755 [18]. Fixed carbon content was determined following ASTM D3172 as the difference between 100 and the sum of percentage contents of volatile matter, moisture and ash[19]. Energy content or higher heating value (HHV) was determined using a bomb calorimeter (Parr 6300 Automatic Isoperibol Calorimete, Parr Instrument Co, Moline, Illinois). Energy content or higher heating value (HHV) was determined using a bomb calorimeter (Parr 6300 Automatic Isoperibol Calorimete, Parr Instrument Co., Moline, IL, USA). Mineral and heavy metal contents of char are important property for soil amendment as minerals are required for plant growth and heavy metal is not desired. Mineral and heavy metal content was determined using an inductively coupled plasma (ICP) analyzer (Spectro Ciros, Kleve, Germany) to determine the concentrations of P, Al, Ca, Cr, Ni, Cu, Fe, K, Mg, Mn, and Na. Surface areas and pore properties were measured via isothermal N_2 adsorption at 77 K using a surface area analyzer (Autosorb-1C, Quantachrome, Boynton Beach, FL, USA). Data were analyzed using the Brunauer-Emmett-Teller (BET) theory. The surface area was determined using multilayer adsorption model by measuring the quantity of nitrogen adsorbed onto or desorbed from char sample at different equilibrium vapor pressures. Samples were degassed at 300 °C for 12 h. Char structure and surface morphology were analyzed by a field-Emission Environmental Scanning Electron Microscope (SEM) (FEI Quanta 600, FEI company, Hillsboro, OR, USA). In order to obtain a clear image, the char particles were coated with gold.

Surface functional groups of char were analyzed using Fourier transform infrared spectroscopy (FTIR) (Nicolet FT-IR 6700, Thermo Electron Corporation, Madison, WI) with attenuated total reflectance (ATR) accessory. The crystal used on ATR accessory is diamond.

Compared with the traditional infrared techniques, the ART-FTIR technique not only shortens the analysis time but also improves the spectra quality of char. The 256 scans of spectra of samples were obtained at 8 cm^{-1} resolution from 4000 to 650 cm^{-1}. Ambient air was scanned as background signal before scanning samples. All samples were scanned without pretreatments. The FTIR spectral peaks were analyzed by comparing the peak position with known peaks.

All data were analyzed statistically using Statistical Analysis System (Version 9.2, SAS Institute Inc., Cary, NC). Significant differences between treatments were analyzed using a F-test (p-value < 0.05). Correlations were also developed using the Pearson's correlation test at a p-value of 0.05. The experiment design used is a factorial design with complete random design. Interaction between biomass type and equivalence ratio was also included in the model. However, the interaction was not found based on the data.

2.3. Results and Discussion

2.3.1. Physical and Chemical Properties

2.3.1.1. Proximate Analysis

The char yield could not be determined in this study because the cyclones were not able to capture all the char. Some char remained in the pipes connecting the cyclones and the reactor, and some char was entrained with the syngas. The char yield was estimated to be approximately 12% based on the mass balance of fluidized bed gasification (by subtracting tar and syngas percentage yields from 100).

The proximate analyses of raw biomass feedstocks and char are shown in Table 2.1 and Table 2.2. As the reaction temperature of gasification reached above 700 °C, free moisture should be released during gasification. However, chars did contain some moisture, which could be adsorbed from the atmosphere between gasification and sample analyzing.

The volatile contents of switchgrass char and sorghum chars increased with an increase in ER from 0.2 to 0.25 and decreased with further increase in ER to 0.28. However, the volatile contents of red cedar-derived char at the three ERs were not statistically different. The char ash

content derived from switchgrass and red cedar increased from 51.61 wt.% to 64.07 wt.% and from 40.41 wt.% to 47.52 wt.%, respectively, with an increase in ER from 0.20 to 0.28. Gasification with increasing ER also decreased the fixed carbon content of each char. The fixed carbon content of switchgrass, sorghum and red cedar decreased from 34.99 wt.% to 21.98 wt.%, 33.76 wt.% to 32.67 wt.% and 40.49 wt.% to 35.66 wt.%, respectively, with increase in ER from 0.20 to 0.28. The variation of ash content and fixed carbon in char can be explained by the variation in carbon conversion during the gasification. When ER was increased, more organic content of the biomass oxidized and converted into the gaseous phase, which lead to the reduction in unconverted carbon that remained in the solid phase. Since most of the minerals (except chemically reactive alkali and alkali earth elements such as potassium and calcium) remained stable during gasification, the total quantity of ash in the solid phase did not change; however, the ash content in char still increased due to mass loss of other solid residues due to carbon conversion.

Table 2.1. Proximate analysis and ultimate analysis of feedstocks

Content	Switchgrass	Sorghum	Red cedar
Moisture (w.b.)	9.70	9.39	8.50
Volatile matter (w.b.)	70.36	68.1	71.79
Ash (w.b.)	4.62	5.05	4.09
Fixed carbon (w.b.)	15.02	17.46	15.62
Nitrogen (d.b.)	0.57	0.51	0.37
Hydrogen (d.b.)	5.74	6.4	6.27
Sulfur (d.b.)	0.30	0.20	1.07
Carbon (d.b.)	43.19	40.68	47.51
Oxygen (d.b.)	50.20	52.2	44.79

w.b represents wet basis and d.b represents dry basis.
Oxygen content was determined by difference.

Table 2.2. Proximate analysis, higher heating value (HHV) and BET surface area of biochar derived from switchgrass, sorghum and red cedar at three equivalence ratios (ER)

Feedstock	ER	Moisture (wt% on w.b.)	Volatile (wt% on w.b.)	Ash (wt% on w.b.)	Fixed carbon (wt% on w.b.)	HHV (MJ/Kg)	S_{BET} (m^2/g)	V_{mic} (10^{-3} mL/g)
Switchgrass	0.20	0.69±0.09	12.69±1.48	51.61±2.21	34.99±0.57	7.40	1.3	0.63
	0.25	2.01±0.18	16.86±0.89	57.70±2.67	23.42±1.39	4.03	5.2	2.84
	0.28	1.83±0.37	12.11±0.71	64.07±1.29	21.98±0.67	6.70	20.8	11.88
Sorghum	0.20	1.99±0.20	14.24±0.71	50.89±0.59	33.76±0.34	4.18	1.0	0.45
	0.25	1.94±0.13	20.01±2.12	45.94±2.49	32.10±0.35	9.42	0.7	0.44
	0.28	1.1±0.11	11.36±1.06	54.87±1.17	32.67±0.16	4.63	5.6	2.14
Red cedar	0.20	3.4±0.27	15.72±1.41	40.41±1.00	40.49±0.10	9.09	2.1	1.57
	0.25	3.1±0.17	15.68±0.81	43.89±3.65	37.33±2.13	5.87	60.8	31.33
	0.28	2.7±0.14	14.14±1.70	47.52±0.81	35.66±0.89	4.07	30.6	16.34

V_{mic} represented micropore volume, S_{BET} represented BET Surface area

As expected, the gasification process led to significant differences between compositions of raw biomass feedstocks and resulted char. Moisture content of the raw biomass feedstocks was 8.5 wt.%–9.7 wt.%, while that of the char was all 0.7 wt.%–3.4 wt.%. The volatile contents of chars (10 wt.%–20 wt.%) were much lower than those of the raw biomass the char was derived from (68 wt.%–72 wt.%). Ash contents of chars were higher (40 wt.%–64 wt.%) than those of raw biomass the char was derived from (less than 5 wt.%), which implied that most of the ash in biomass remained in the char during gasification. On the contrary, fixed carbon content of char was higher than that of raw biomass. Average fixed carbon contents of chars ranged from 22 wt.% to 41 wt%, while those of biomass feedstocks ranged from 15 wt.% to17 wt.%.

2.3.1.2. Heating Value and BET Surface Area

The main effect of biomass type on the higher heating value (HHV) of char was not significant (data shown in Table 2.2). The heating value of the char ranged from 4 to10 MJ/Kg, which was lower than that of raw biomass (typically 15-20 MJ/Kg) or other combustible fuels such as coal (25-35 MJ/Kg). Surface area and microporosity are two of the most relevant properties to evaluate char absorption capacity of minerals and organic matter [20]. ER had a significant effect on the BET surface area of the char. At 0.20 ER, all char had surface areas of 1 to 2 m^2/g, while at 0.28 ER, the BET surface areas of char derived from switchgrass and red cedar increased to 20 and 30 m^2/g, respectively. Among all char, the red cedar-derived char had the highest BET surface area at each ER. These observations conclude that chars derived from woody biomass tend to have larger surface areas compared to chars derived from herbaceous biomass. Similar observations have been reported by Bruun [20]. This suggests that red cedar may be a better feedstock than switchgrass and sorghum to produce high surface area char. The micropore volume (calculated by Dubinin-Radushkevich method) of char are listed in Table 2.2. As shown in Figure 2.1, the micropore volume and surface area of our char samples were linearly correlated with $R^2 = 0.99$. This correlation is supported by earlier study done by Lehmann et al. [21], who

compiled surface area data and micropore volume data of chars available in literatures and concluded that micropore volume had a strongly positive correlation with BET surface area.

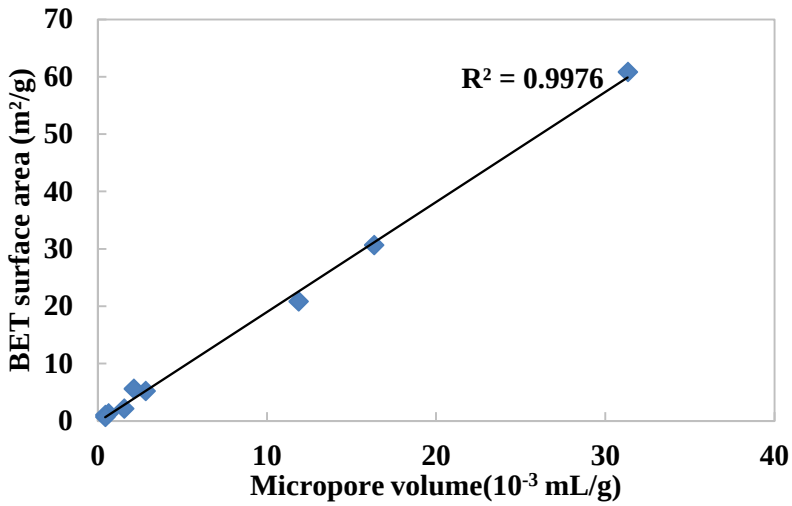

Figure 2.1. BET surface areas versus micropore volume of biochar

2.3.1.3. SEM Morphology

Surface morphology of chars obtained from gasification of switchgrass, sorghum and red cedar char at ER 0.28 were studied by SEM (see Figure 2.2). It can be observed that the chars maintained part of the biomass fibrous structure. Char also is clearly seen to be porous in all of the SEM images. The porous structure of char could be derived from the porous structure existing in raw biomass or was formed during the devolatilization process of gasification [13].

The surface of the char derived from switchgrass and red cedar showed more pores with regular geometrical morphology. The surface of the char obtained from sorghum, however, exhibited less developed pores. The difference in char porosity can also be related to the BET surface area as high BET surface is indicative of high porosity. BET surface areas of char derived from switchgrass and red cedar at ER 0.28 were 20.1 and 30.6 m^2/g, respectively; which were much higher than the surface area of char derived from sorghum (5.6 m^2/g).

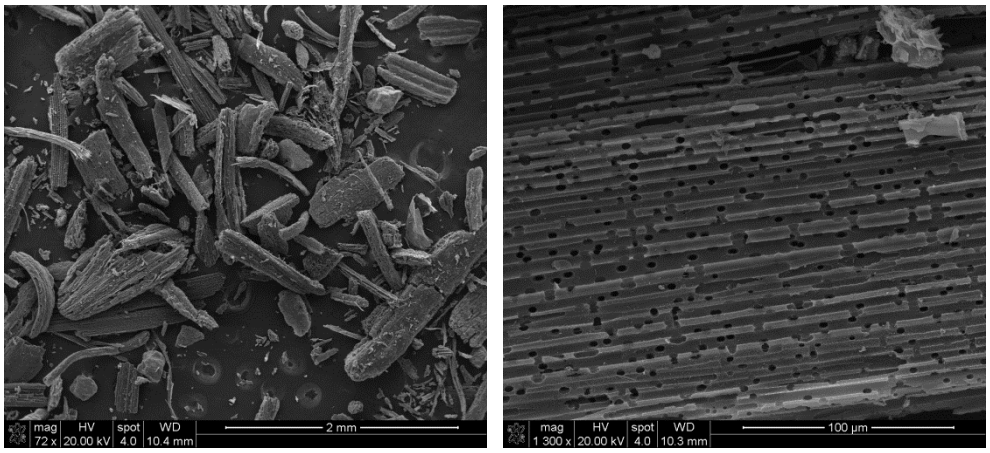

(A)

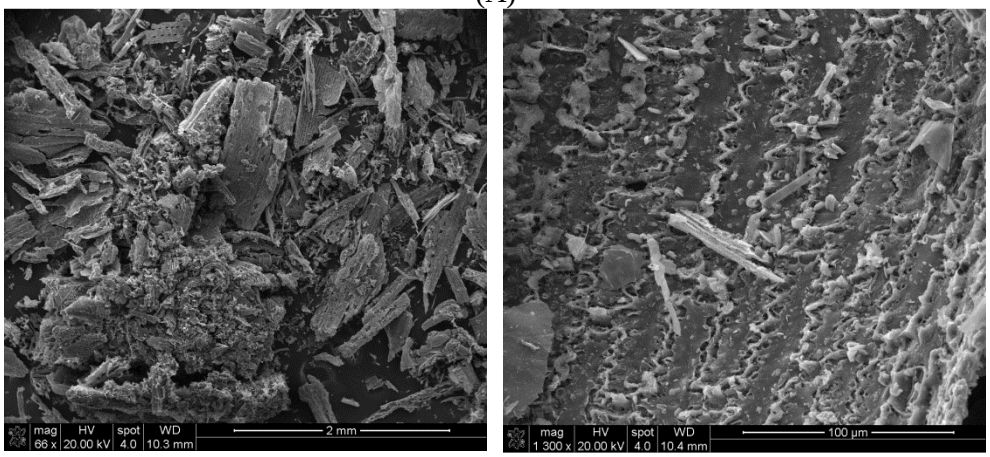

(B)

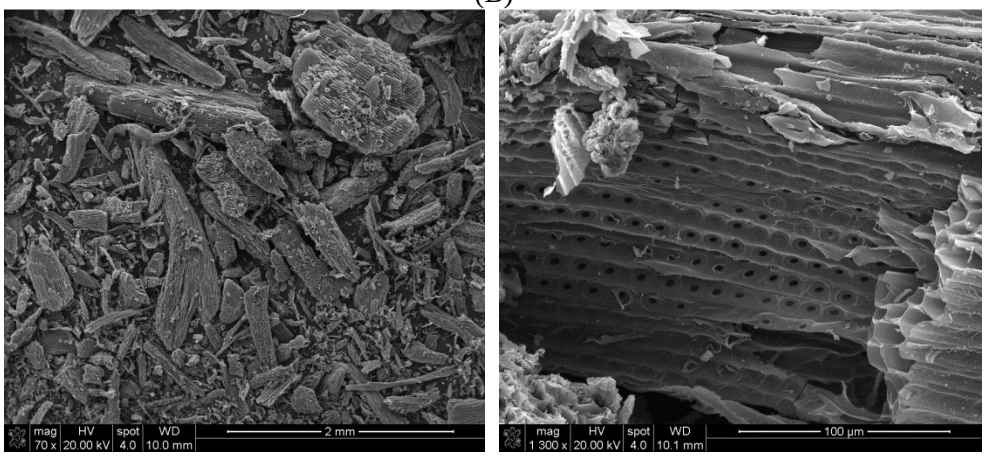

(C)

Figure 2.2. Scanning electron graphs of biochar at 0.28 equivalence ratio. From top to bottom is (A) switchgrass biochar, (B) sorghum biochar and (C) red cedar biochar. Magnifications of 72 and 1300 are shown on left and right, respectively.

2.3.2. Elemental Analysis

The elemental compositions of chars are presented in Table 2.3. Brewer et al. [13] observed that oxygen content could not be determined in their char samples using this method due to high oxygen content in the ash that decomposes during analysis. Our samples also contained high ash and the oxygen present in ash may decompose during analysis. Thus, oxygen contents of chars were not reported in this paper. As expected, the carbon content of gasification-based char (34%–48%) was much lower than pyrolysis-based char (typically > 60%) reported in literature [21]. The carbon content of switchgrass-derived char varied from 35 wt% to 48 wt% (d.b.) and decreased with increase in ER. No significant variation in carbon content was found in sorghum and red cedar char with change in ER. The order of average char carbon content from highest to lowest was red cedar > switchgrass > sorghum. This order was consistent with the order of carbon content in raw biomass. The hydrogen content of char was significantly lower (average of 85%) than that of the raw biomass due to gasification. The N content of raw biomass ranged from 0.37%–0.57%, which increased to 0.26%–1.48% of the char due to gasification. The sorghum-derived char had the highest N content (1.48%) among all chars. The increase in N content of char as compared to the raw biomass may be explained by the stability of N-containing compounds such as heterocyclic aromatic compounds during thermal conversion [10]. The char sulfur content was not affected significantly by the equivalence ratio. The sulfur content of char directly corresponded to that of the raw biomass. The order of average sulfur content of char from highest to lowest was the same as that of the raw biomass, i.e. red cedar>switchgrass>sorghum. Generally, during gasification, the biomass sulfur is released in the form of H_2S and a small amount of COS, SO_2 and thiols, while the remaining sulfur solidifies with the alkali metals in ash [22].

Table 2.3. Elemental composition for biochar derived from switchgrass, sorghum and red cedar at three equivalence ratios (ER)

Feedstock	ER	Carbon (%, d.b)	Hydrogen (%, d.b)	Nitrogen (%, d.b)	Sulfur (%, d.b)
Switchgrass	0.20	48.29±0.80	1.21±0.30	0.67±0.06	0.22±0.09
	0.25	34.73±2.35	0.65±0.01	0.65±0.05	0.07±0.01
	0.28	38.55±1.59	0.82±0.04	0.66±0.08	0.12±0.01
Sorghum	0.20	38.5±13.13	0.80±0.05	1.46±0.17	0.14±0.01
	0.25	40.11±0.16	0.94±0.02	1.48±0.04	0.13±0.00
	0.28	40.69±1.23	0.79±0.03	0.38±0.04	0.10±0.01
Red cedar	0.20	45.14±0.83	1.12±0.06	0.26±0.08	0.13±0.01
	0.25	44.89±0.76	1.05±0.07	0.51±0.03	0.20±0.02
	0.28	43.71±2.40	0.99±0.42	0.61±0.15	0.19±0.07

The atomic H/C ratio is usually used to distinguish fuels (e.g. coals, biomass), or fuel related compounds such as soot [23]. The typical atomic H/C ratio of fuel material composed of lignin and cellulose, such as biomass, is approximately 1.5 [21]. Kuhlbusch et al. observed that the atomic H/C ratio of black carbon was less than 0.2 [24]. The soot and lignite often had H/C values less than 0.1. The atomic H/C ratio of most pyrolysis-based char was below 0.5, which depends on feedstock variety and reaction conditions. Normally, H/C ratio of char obtained from high temperature pyrolysis (above 500^{o} C) is below 0.3[10, 25]. The H/C ratio of gasification-derived char in this study varied from 0.2-0.3, which was close to that of high temperature pyrolysis char (<0.3) but higher than soot and lignite. The atomic H/C ratio of raw biomass in this study ranged from 1.5-1.8, which was consistent with Lehmann's conclusion.

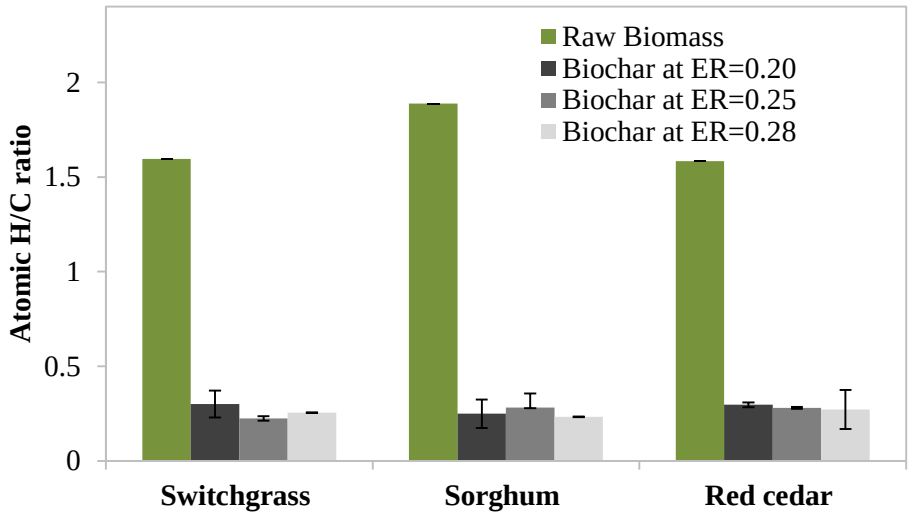

Figure 2.3. Atomic H/C of raw biomass and biochar obtained at equivalent ratios of 0.2, 0.25 and 0.28.

As shown in Table 2.3, atomic H/C ratios of chars were lower than those of the raw biomass. The decrease in atomic H/C ratio of char during biomass gasification can be attributed to loss of hydrogen caused by dehydration and dehydrogenation reactions, and the cleavage and cracking of weak hydrogen bonds within the char structure, similar to the observations in pyrolysis char [25]. The H/C ratio has also been used to estimate the possibility of bond arrangement [21]. Prior research has confirmed that low H/C ratio in char reflect high contents of aromatic compounds by NMR tests [13]. The low H/C ratio in char and high H/C ratio in the raw biomass suggests that the aliphatic carbon containing compounds decrease and aromatic compounds increase during gasification. The atomic H/C of char derived from switchgrass and red cedar decreased slightly with increase in ER and sorghum-derived char did not show any trend in the atomic H/C with change in ER. Statistical analysis of the data showed that main effect of ER on atomic H/C was not significant. These observations conclude that ER was not the primary factor controlling atomic H/C of char.

2.3.3. Mineral Content

The mineral contents of the raw biomass and biochar, as determined by ICP analysis, are shown in Table 2.4. The major minerals included P, Ca, K, and Mg (>0.1 wt. %) while the minor

(<0.1 wt. %) minerals included Na, Fe, Zn, Cu and other heavy metals. Among the major minerals, K was the most abundant component in switchgrass (0.89%) and sorghum (0.42%), while Ca was the highest (0.65%) in red cedar. The order of trace mineral contents in the three feedstocks were the same; Fe was the highest followed by Mn and Zn.

When comparing the mineral contents of char and raw feedstocks, it is clear that the concentrations of all mineral in char were higher than that of raw biomass. The contents of K and Ca increased from less than 1 % in the raw biomass to 1-6 % in the char. Among the heavy metals, Mn content increased from less than 80 ppm in the raw biomass to 200-700 ppm in the char, indicating that the gasification process enhanced the aggregation of mineral contents in the char. However, the increase in concentration also depended on the biomass variety. For example, Mg content in sorghum-derived char was 10 times higher than that of sorghum, while Mg content in switchgrass-derived char was only 3 times higher than that of the switchgrass. The K content of sorghum-derived char increased by 10 to 20 times as compared that of the raw sorghum, while K content of switchgrass-derived char only doubled as compared to that of the raw switchgrass. The gasification process also did not change the order of individual mineral concentration in char as compared to that in the raw biomass.

Table 2.4. Mineral content of biochar based on ICP results

Feedstock	ER	P (%)	Ca (%)	K (%)	Mg (%)	Na (%)	S (%)	Fe (ppm)	Zn (ppm)	Cu (ppm)	Mn (ppm)	Ni (ppm)
Switchgrass	0*	0.10	0.25	0.89	0.26	0.002	0.05	134	25	2	38	3
	0.20	0.53	1.70	1.52	0.82	0.05	0.08	10692	184	15	602	51
	0.25	0.68	1.90	2.08	1.05	0.06	0.10	24292	180	33	785	56
	0.28	0.29	0.77	0.75	0.40	0.03	0.04	6838	78	9	248	27
Sorghum	0*	0.04	0.22	0.42	0.09	0.04	0.05	640	10	2	38	1
	0.20	0.47	1.08	4.12	0.81	0.02	0.11	3191	73	10	161	8
	0.25	0.71	1.63	6.25	1.34	0.02	0.13	8207	90	17	278	11
	0.28	0.56	1.75	3.87	0.69	0.15	0.09	2249	52	6.2	107	7
Red Cedar	0*	0.02	0.65	0.12	0.04	0.002	0.03	294	9	1	87	1
	0.20	0.04	0.91	0.22	0.08	0.005	0.02	2552	40	3	161	8
	0.25	0.12	2.64	0.71	0.26	0.018	0.07	35592	59	35	278	11
	0.28	0.15	2.46	1.36	0.33	0.025	0.07	30610	63	21	107	7

* Equivalent ratio of zero represents raw biomass. All values are on dry weight basis.

The distribution of char mineral content, such as Ca and K, is considered an important characteristic when used as a soil amendment, as they are nutrient elements for plant growth. On the other hand, heavy metals in char are considered hazardous for the environment [26]. Since the gasification process accumulated Ca and K content as well as the heavy metals, use of biomass-based char as a soil amendment may need to be further investigated. Contents of K and Ca in char was the highest at 0.25 ER (as shown in Table 2.4), although ash content of the char obtained at this ER was not the highest. A higher ER usually leads to a higher gasification temperature due to more heat generated from intensified oxidation. The increases in gasification temperature and amount of oxygen in turn increase volatilization of the minerals (K and Ca) [27] and reaction with the carbon during gasification. The intensified oxidation with increase in ER would also consume more biomass carbon, reducing the carbon content of char and thus increasing the mineral contents in the char. For instance, char obtained at 0.20 ER had high carbon content and low K and Ca contents because of low gasification temperature (Table 2.3).

2.3.4. ATR FT-IR Analysis

The FTIR spectra of biomass and char are illustrated in Figure 2.2. Table 2.5 lists the typical identified FTIR spectrum adsorptions reported in literature [10, 28, 29]. A broad band was found (see Figure 2.4) at 3400-3200cm^{-1} (O-H stretching) in all the biomass and sorghum-derived char, but not in the char derived from switchgrass and red cedar. This O-H stretching may be attributed to the moisture content, or presence of hydroxyl or phenol groups. The disappearance of the O-H group in char derived from red cedar and switchgrass could be attributed to the removal of moisture and dehydration processes. The peaks in the 2950-2800 cm^{-1} range, corresponding to aliphatic C-H stretching, were found in all three types of biomass. However, only char derived from sorghum showed a small peak in the 2950-2800 cm^{-1} region, suggesting that the gasification process might have destroyed aliphatic structure in the biomass. The remaining small peak observed from sorghum-derived char may be due to the existence of a heat-resistant aliphatic structure in sorghum. The peaks around 780 cm^{-1}, corresponding to aromatic C-

H bending, were clearly visible in all biomass and char. This implied that aromatic structure existed in both the raw biomass and char. The peaks around 1375 cm^{-1}, corresponding to O–H bending of phenols, were found in all the raw biomass and chars derived from red cedar and sorghum, but were not found in switchgrass-derived char. This suggests that the char derived from red cedar and sorghum contained more phenol groups than the char derived from switchgrass. Phenolic group are usually considered to be related with the lignin content in feedstock. The more phenol groups in char derived from red cedar and sorghum may result from the higher lignin content in raw biomass. Pasangulapati et al. [31] tested the the switchgrass and red cedar lignin content and proved that the lignin content in red cedar are more than switchgrass. All of the biomass and char samples showed a strong and broad band at 1000 cm^{-1}, which may represent phosphines, phosphine oxides or silicon oxides [10]. Keiluweit et al. [29] also observed the broad peak at around 1000 cm^{-1} in char obtained at low temperature (less than 500 °C) and they associated this peak to C-O-C stretching in cellulose and hemicellulose. It was observed that this peak disappears in char obtained at higher temperature (greater than 700 °C), which they attributed to the degradation of cellulose and hemicellulose. In our study, all three biomass showed broad and strong peak at around 1000 cm^{-1}. On the other hand, all biomass-derived char showed much weaker peaks indicating that cellulose and hemicellulose of biomass decomposed during gasification. All biomass also showed peaks near 1250 cm^{-1}, which corresponded to the C-O stretching of aryl ethers and phenolics of lignin-derived compounds, and C-O stretching of pyranone rings and guaiacyl monomers related to cellulose-derived compounds [29]. However, these peaks were not seen in the char indicating the breakage of methoxyl groups during decomposition of lignin and cellulose during biomass gasification.

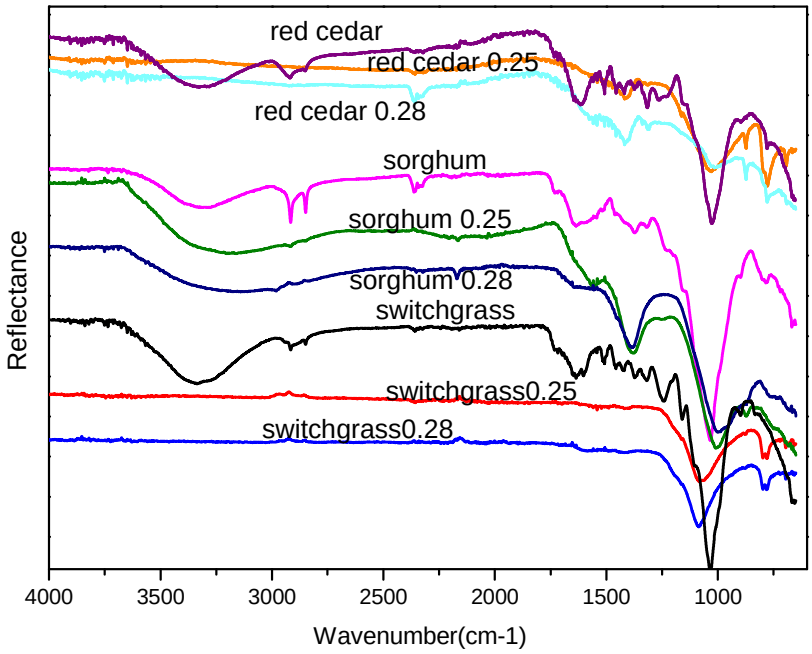

Figure 2.4. FT-IR spectra of raw biomass and biochar obtained at equivalent ratios of 0.25 and 0.2

Table 2.5. ATR FT-IR characteristic absorption of feedstocks and biochar

Functional Group	Characteristic Absorption (cm-1)	Feedstocks and biochars
Alkyl C-H Stretch [28]	2950 - 2850	Red cedar, switch grass, sorghum straw, biochar with 0.2 ER
Aromatic C-H Bending [28]	860 - 680	Red cedar, switch grass, sorghum straw and respective biochars
Aromatic C=C Bending [28]	1600 - 1500	Red cedar, switch grass, sorghum straw
aromatic C, indicative of lignin C=C [29]	1440, 1510	Red cedar, switchgrass, sorghum straw and sorghum biochar
Alcohol/Phenol O-H Stretch [28]	3550 - 3200	Red cedar, sorghum, sorghum biochar, switchgrass
Aldehyde, Ketone, Ester, Carboxylic Acid [10]	1780 -1700	Red cedar, switch grass, sorghum straw
Phenol O-H bending [28]	1375	Raw biomass, switchgrass(s) and sorghum biochar(w*)
C-O stretching C-O-C groups and aryl ethers; phenolic C-O associated with lignin [29]	1270-1250	Red cedar, switch grass, sorghum straw, switchgrass and sorghum biochar of ER 0.2,
Phosphines and phosphine oxides, Silican oxide [10, 30]	1100–950	All (s)

*S and W represent strong and weak peaks, respectively.

2.4. Conclusions

The effects of three biomass types (switchgrass, sorghum and red cedar) and three equivalence ratios (0.20, 0.25, and 0.28) on properties of char obtained through gasification were studied. The char moisture and fixed carbon contents decreased while ash content increased with increase in equivalence ratio. Surface areas of most of the char samples were 1 to 10 m^2/g. The red cedar-derived char had the highest BET surface area of 60.8 m^2/g at an equivalence ratio of 0.25. An increase in equivalence ratio increased BET surface area. Ash contents of all char samples were much higher (more than 40 wt.%) that those of the corresponding biomass feedstock ks (less than 5.05 wt%). The low surface areas and high ash contents of biomass gasification chars may present challenges in their utilization as precursors for activated carbon or as fuel for combustion. The FT-IR spectra showed that during gasification biomass feedstocks lose aliphatic C-H bonds but retain aromatic C-H bonds in the char. In addition, the C-O-C bond of char was weaker than that of biomass, indicating decomposition of cellulose and hemicellulose.

Acknowledgements

This project was funded, in part, by the Oklahoma Agricultural Experiment Station and the South Central Sun Grant Program through USDA-NIFA Award No. 2010-38502-21836.

2.5. References

[1] A. Zhang, R. Bian, G. Pan, L. Cui, Q. Hussain, L. Li, J. Zheng, J. Zheng, X. Zhang, X. Han, X. Yu, Effects of biochar amendment on soil quality, crop yield and greenhouse gas emission in a Chinese rice paddy: A field study of 2 consecutive rice growing cycles, Field Crop Res, 127 (2012) 153-160.

[2] S. Meyer, B. Glaser, P. Quicker, Technical, Economical, and Climate-Related Aspects of Biochar Production Technologies: A Literature Review, Environ. Sci. Technol., 45 (2011) 9473-9483.

[3] J. Lehmann, M.C. Rillig, J. Thies, C.A. Masiello, W.C. Hockaday, D. Crowley, Biochar effects on soil biota – A review, Soil Biology & Biochemistry, 43 (2011) 1812-1836.

[4] P. Oleszczuk, S.E. Hale, J. Lehmann, G. Cornelissen, Activated carbon and biochar amendments decrease pore-water concentrations of polycyclic aromatic hydrocarbons (PAHs) in sewage sludge, Bioresource Technol, 111 (2012) 84-91.

[5] R. Azargohar, A.K. Dalai, Steam and KOH activation of biochar: Experimental and modeling studies, Micropor Mesopor Mat, 110 (2008) 413-421.

[6] I.M. Lima, W.E. Marshall, Adsorption of selected environmentally important metals by poultry manure-based granular activated carbons, J Chem Technol Biot, 80 (2005) 1054-1061.

[7] D. Wang, W. Yuan, W. Ji, Char and char-supported nickel catalysts for secondary syngas cleanup and conditioning, Appl. Energy, 88 (2011) 1656-1663.

[8] Z. Abu El-Rub, E.A. Bramer, G. Brem, Experimental comparison of biomass chars with other catalysts for tar reduction, Fuel, 87 (2008) 2243-2252.

[9] J.J. Manyà, Pyrolysis for Biochar Purposes: A Review to Establish Current Knowledge Gaps and Research Needs, Environ. Sci. Technol., 46 (2012) 7939-7954.

[10] K.B. Cantrell, P.G. Hunt, M. Uchimiya, J.M. Novak, K.S. Ro, Impact of pyrolysis temperature and manure source on physicochemical characteristics of biochar, Bioresource Technol, 107 (2012) 419-428.

[11] A. Kumar, D. Jones, M. Hanna, Thermochemical Biomass Gasification: A Review of the Current Status of the Technology, Energies, 2 (2009) 556-581.

[12] A. Dąbrowski, P. Podkościelny, Z. Hubicki, M. Barczak, Adsorption of phenolic compounds by activated carbon—a critical review, Chemosphere, 58 (2005) 1049-1070.

[13] C.E. Brewer, K. Schmidt-Rohr, J.A. Satrio, R.C. Brown, Characterization of biochar from fast pyrolysis and gasification systems, Environ Prog Sustain, 28 (2009) 386-396.

[14] F. Melligan, R. Auccaise, E.H. Novotny, J.J. Leahy, M.H.B. Hayes, W. Kwapinski, Pressurised pyrolysis of Miscanthus using a fixed bed reactor, Bioresource technology, 102 (2011) 3466-3470.

[15] A. Sharma, A. Kumar, K. Patil, R. Huhnke, Performance evaluation of a lab-scale fluidized bed gasifier using switchgrass as feedstock, Transactions of the ASABE, 54 (2011) 2259-2266.

[16] ASTM Standard D3175-11 "Standard Test Method for Volatile Matter in the Analysis Sample of Coal and Coke", in, ASTM International, West Conshohocken, PA, 2011.

[17] ASTM Standard D4442-07 "Standard Test Methods for Direct Moisture Content Measurement of Wood and Wood-Base Materials", in, ASTM International, West Conshohocken, PA, 2007.

[18] ASTM Standard E1755-01(2007) "Standard Test Method for Ash in Biomass", in, ASTM International, West Conshohocken, PA, 2007.

[19] ASTM Standard D3172- 07a "Standard Practice for Proximate Analysis of Coal and Coke", in, ASTM International, West Conshohocken, PA, 2007.

[20] E.W. Bruun, Application of fast pyrolysis biochar to a loamy soil-effects on carbon and nitrogen dynamics and potential for carbon sequestration, in: Information Service

Department Risø National Laboratory for Sustainable Energy, Technical University of Denmark, Denmark, 2011.

[21] J. Lehmann, S. Joseph, Biochar for environmental management: science and technology, Earthscan, London, UK, 2009.

[22] C. Gai, Y.P. Dong, Experimental study on non-woody biomass gasification in a downdraft gasifier, Int J Hydrogen Energ, 37 (2012) 4935-4944.

[23] M.M. Maroto-Valer, G.D. Love, C.E. Snape, Relationship between carbon aromaticities and HC ratios for bituminous coals, Fuel, 73 (1994) 1926-1928.

[24] T.A.J. Kuhlbusch, P.J. Crutzen, Toward a global estimate of black carbon in residues of vegetation fires representing a sink of atmospheric CO2 and a source of O2, Global Biogeochemical Cycles, 9 (1995) 491-501.

[25] K.H. Kim, J.-Y. Kim, T.-S. Cho, J.W. Choi, Influence of pyrolysis temperature on physicochemical properties of biochar obtained from the fast pyrolysis of pitch pine (Pinus rigida), Bioresource Technol, 118 (2012) 158-162.

[26] B.V. Tangahu, S. Abdullah, S. Rozaimah, H. Basri, M. Idris, N. Anuar, M. Mukhlisin, A Review on heavy metals (As, Pb, and Hg) uptake by plants through phytoremediation, International Journal of Chemical Engineering, 2011 (2011).

[27] T. Okuno, N. Sonoyama, J. Hayashi, C.Z. Li, C. Sathe, T. Chiba, Primary release of alkali and alkaline earth metallic species during the pyrolysis of pulverized biomass, Energy Fuels, 19 (2005) 2164-2171.

[28] R.M. Silverstein, F.X. Webster, D. Kiemle, Spectrometric Identification of Organic Compounds, 7th ed., Wiley, 2005.

[29] M. Keiluweit, P.S. Nico, M.G. Johnson, M. Kleber, Dynamic Molecular Structure of Plant Biomass-Derived Black Carbon (Biochar), Environ. Sci. Technol., 44 (2010) 1247-1253.

[30] B. Shokri, M.A. Firouzjah, S.I. Hosseini, FTIR analysis of silicon dioxide thin film deposited by Metal organic-based PECVD, in: International plasma chemistry socierty, 2010.

.

CHAPTER III

CHARACTERIZATION OF CHAR OBTAINED FROM DOWNDRAFT BIOMASS GASIFICATION

This research paper was published as " K. Qian, A. Kumar, D. Bellmer, W. Yuan, D. Wang, M.A. Eastman, Physical properties and reactivity of char obtained from downdraft gasification of sorghum and eastern red cedar, Fuel, 143 (2015) 383-389."

Abstract: Downdraft gasification of forage sorghum and red cedar wood was studied with the aim of determining the characteristics of produced char for its further application, such as soil amendment, sorbent and solid fuel. Ultimate, proximate, XRD and NMR were used to investigate physical and chemical properties of char and thermo-analytic methods were used to determine kinetics of char gasification. The NMR results showed that red cedar and sorghum chars both contain aromatic carbon, but aliphatic carbon and o-alkyl carbon are more evident in red cedar char than in sorghum char. Char derived from downdraft gasification had higher heating values and lower ash contents than char derived from fluidized bed gasification, indicating char derived from downdraft gasification is more suitable for applications, such as soil amendment, than char from fluidized bed gasification. Micropores and mesopores were found in both red cedar and sorghum chars. The gasification reactivity of red cedar char was higher than that of sorghum char. Activation energies were found to be 163 and 167 kJ/mol based on shrinking core model and 147 and143 kJ/mol based on random pore model for sorghum char and red cedar char, respectively.
Keywords: downdraft gasification; sorghum char; red cedar char; CO_2 char gasification; NMR; surface mophorlogy

3.1. Introduction

Char has potential value as soil amendment material, activated carbon precursor and carbon based catalysts. Much attention has focused on how to make char more suitable for these applications [1-3]. The most common way to produce char is pyrolysis [4]. The adjustable pyrolysis conditions (pyrolysis temperature and resident time) for char production, together with diverse feedstock choices enable researchers to produce char with physical and chemical properties suitable for a given application. Char is also a product of gasification. The disadvantages of producing char through gasification are the low char yield (<15%) and difficulty in simultaneously optimizing the char quality and syngas quality. Although carbon retained in char produced from biomass gasification might be low, char carbon, if utilized effectively, can further increase carbon efficiency and environmental and economic sustainability of the gasification process. Co-combustion or co-gasification of char with coal or biomass is one method to utilize char. Therefore, it is critical to study the characteristics of char produced from gasification so that it can be effective utilized.

Solid-state ^{13}C NMR spectroscopy is a nondestructive and effective technique to study char structure at molecular level [5]. The other techniques, such as X-ray diffraction (XRD), Fourier transform infrared spectroscopy (FT-IR) only reveal the surface structure. Many studies [5-7] have applied ^{13}C cross-polarization magic angle spinning (CP/MAS) technique to analyze intrinsic carbon structure, in addition to the surface structure, of carbonaceous materials. ^{13}C CP/MAS has been used to determine structural changes of woody chars at different pyrolysis temperature [6].

The properties of char can be broadly categorized into physical and chemical properties. The relevant physical properties include bulk and particle densities, surface area, particle sizes, porosity and pore distribution. The relevant chemical properties include concentrations of C, N, minerals, bases and polycyclic aromatic hydrocarbon in char. Desired properties of char vary in different applications. High surface area is preferred in many applications. In terms of soil

amendment, high surface area is preferred because it is believed to improve the moisture retention and reduce the leach of nutrient components [8]. Higher surface area is also preferred for char-based electrolyte and char-based catalysts. High heating value of char is pivotal for application of solid fuel but may not be important for soil amendment. High alkali and alkaline metal content in char may be preferred for soil amendment [8] but not desired for application as solid fuel [9].

Earlier, we have studied properties of fluidized bed char including proximate analysis, ultimate analysis and BET surface area analysis [10]. We concluded that gasification conditions have significant effects on char properties. Reaction conditions, such as heat and mass transfer pathways and gasification temperature in downdraft gasifier are different from those in fluidized bed gasifier. However, detailed properties of char derived from downdraft gasification have not been yet reported. The objective of this study is to investigate chemical and physical properties of char derived from downdraft gasification in order to determine its suitability for value-added applications. Advanced analytical techniques such as NMR, XRD and N_2 physisorption were used to analyze char properties. Thermogravimetric analysis was used to study the reaction kinetics of char gasification under CO_2 atmosphere. The heterogeneous reaction kinetics of char gasification, obtained in this study, will enable effective reactor design, process simulation and optimization to utilize char.

3.2. Materials and methods

3.2.1. Material

The Kanlow variety of sorghum (*Panicum virgatum*) was obtained from the Oklahoma State University Agronomy Research Station. Large round bales of sorghum were chopped by a Haybuster tub grinder (H1000, Duratech Industries International, Inc., Jamestown, N.D.) with a screen size of 1.25 cm. Red cedar (eastern red cedar) was obtained locally and chopped with a screen size of 1.25 cm by a local company (Bliss Industries, Ponca City, Oklahoma). The loose-filled bulk densities of red cedar and sorghum were 0.14 g/cm^3 and 0.07 g/cm^3.

3.2.2. Char Preparation

Downdraft bed gasification

Char derived from gasification was produced by a unique downdraft gasifier at equilibrium ratio of 0.2. The unique downdraft gasifier [11] consists of a biomass feeding section, pyrolysis and tar cracking zone and the char gasification section. Test preparation started with loading 5 kg of wood charcoal onto the grate for initial firing. The pyrolysis and gasification sections were then completely filled with feedstocks. The hopper was also kept full with biomass. The gasifier was preheated using propane for about ten minutes. When the temperature of the pyrolysis and cracking zones reached to 600 °C, the desired air flow was introduced into the system. The biomass was fed through hopper and feeder and the fuel level in gasification area was maintained by adjusting the feeding system manually. The amount of biomass entering and exiting the gasifier and air flow were monitored in order to maintain the desired equivalence ratio. The temperature profile, pressure drop (monitored by Lab view™) were considered to monitor and prevent choking. The average gasification temperature was around 850 °C and the pressure was close to 1 atm. The biomass residence time was estimated to be around 9 s. Produced chars firstly fall into ash chamber located in bottom of the gasifier and was continuously transferred by a rotating screw conveyor from the bottom chamber to an ash drum to avoid overloading the bottom ash chamber. Char of small size entrained by syngas was trapped by a cyclone. After experiment, char was collected from ash drum, bottom ash chamber and cyclone. Char yield was obtained by weighing collected char and divided the char weight with feed biomass weight. However, due to practical difficulties faced in collecting all char and error occurred when measuring the input biomass mass, char yield may not be accurate but just estimation. Detailed description of the gasifier and process can be found in Patil et al. [11].

3.2.3. Determination of Physiochemical Properties

Biomass feedstocks and resultant char were analyzed for proximate and elemental analyses, NMR, surface and pore characteristics.

3.2.3.1. Proximate and Ultimate Analyses

For proximate analysis, volatile content was determined using ASTM D3175-11 [12]. Moisture content was analyzed by drying the samples at 105°C according to ASTM D4442-07 [13]. Ash content was determined by combusting the char at 600°C, based on ASTM E1755 [14]. Fixed carbon content was determined using ASTM D3172 [15] as the difference between 100 and the sum of percentage contents of volatile matter, moisture and ash. Mineral content was determined using an inductively coupled plasma (ICP) analyzer (Spectro Ciros, Kleve, Germany).

3.2.3.2. Energy Content and Surface Area Analysis

Energy content or higher heating value (HHV) was determined using a bomb calorimeter (Parr 6300, Parr Instrument Co, Moline, Illinois). Loose-filled bulk density was measured by loading biomass or char in a given volume container and calculated as the ratio of the mass to the bulk volume [11]. Surface areas and pore properties were measured via N_2 adsorption using a surface area analyzer (Autosorb-1C, Quantachrome, Boynton Beach, FL). Adsorption data were analyzed using the Brunauer–Emmett–Teller (BET) theory. Samples were degassed at 300 °C for 12 hours. The micropore volume was estimated by applying non-linear density functional theory (NLDFT) method. The total pore volume was calculated from the gas amount adsorbed at relative pressure of 0.98.

3.2.4. NMR Analysis

^{13}C NMR analysis was performed using a Chemagnetics 300 spectrometer (CMX-II, Varian/Chemagnetics, USA) at 75.69 MHz (300 MHz ^{1}H frequency). Qualitative compositional information was obtained with adequate sensitivity using the ^{13}C CP/MAS NMR technique with magic angle spinning (MAS) [16] speed of 6 kHz, cross-polarizarion (CP) time of 1 ms, and ^{1}H 90° pulse length of 5.5 μs. Four-pulse total suppression of sidebands (TOSS) [17] was employed

before detection, with two pulse phase-modulated (TPPM) proton decoupling applied during detection for improving resolution [18]. The number of scans taken was 100,000, with delay of 1 s between scans.

3.2.5. Thermogravimetric Experiments

Gasification and combustion of char were carried out in a thermogravimetric analyzer (TGA)(VersaTherm, Thermo Scientific, USA). In each gasification test, about 6 mg char was loaded in a platinum pan and heated at a rate of 50 ºC/min to temperature (850, 900, 950 ºC) under N_2 (99.999%) of 80 mL/min. After the desired gasification temperature was reached, the sample was held at that temperature for 5 min under the N_2 flow. Then, N_2 was switched to CO_2 (80 ml/min) to initiate the isothermal gasification. In each combustion experiment, 13 mg sample was loaded directly into the platinum crucible and the temperature was ramped up from 25 to 900 °C. The combustion was carried out under dynamic conditions at heating rates of 10, 20, and 40 °C/min using air as the reactive gas at a flow rate of 50 ml/min. The weight loss of the sample was continuously recorded by the TGA computer.

3.2.6. Determination of Kinetic Parameters

In order to evaluate the reactive behavior of char during the CO_2 gasification, two models, random pore model (RPM) and shrinking core model (SCM), were used to calculate kinetic parameters [19, 20]. RPM and SCM are the two most popular models used to study the gasification behavior in coal char and biomass char and have been successfully applied [20-22]. The RPM is based on assumption that the reaction occurs with the growth of pores. The reaction rate, using RPM, is expressed as [20]:

$$\frac{dX}{dt} = k_r(1-X)\sqrt{(1-\psi \ln(1-X)} \text{ or } X = 1 - \exp\left[-k_r t\left(1+\frac{\psi}{4}k_r t\right)\right] \quad \text{(Equation 3.1)}$$

Where, k_r is rate constant and X is carbon conversion ratio that is defined as the ratio of gasified char and initial char (on a dry ash-free basis) at any time, t (s). X can be expressed as follows:

$$X = \frac{m_0 - m}{m_0 - m_a} \quad \text{(Equation 3.2)}$$

Where, $m_{0,}$ m_a and m are masses of initial char, initial ash, and char at time t, respectively. ψ is a dimensionless structural parameter indicating the initial pore structure. ψ can be determined using empirical fitting or calculated as follows using pore length (Lo), porosity (ε_0) per unit volume of solid and initial specific surface area (S_0).

$$\psi = \frac{4\pi Lo(1-\varepsilon_0)}{S_0^2} \quad \textbf{(}\text{Equation 3.3}\textbf{)}$$

In this study, empirical fitting with least square regression method was used to determine ψ.

The shrinking core model (SCM), another kinetic model, is based on the assumption that the reaction initially occurs at the external surface of the char particles and gradually proceeds inside the pores. The SCM is expressed as [22]:

$$\frac{dX}{dt} = k_s(1-X)^{2/3} \text{ or } X = 1 - \left(1 - \frac{k_s t}{3}\right)^3 \quad \text{(Equation 3.4)}$$

Where, t represents the time (min) and k_s is the reaction rate constant.

The suitability of the RPM and SCM to represent gasification rate of chars was examined at 800, 900 and 1000 ℃. The fitting quality (FQ) was measured by following equation [20]:

$$FQ = 1 - \sqrt{\frac{1}{N}\sum_{i=1}^{N}\left(\frac{X_{model}-X_{exp}}{X_{exp}}\right)^2} \quad \text{(Equation 3.5)}$$

Where X_{model} and X_{exp} represent conversion obtained using the model and the experiment, respectively.

The relationship between reaction rate constants (k_r and k_s) and temperature was modeled using Arrhenius rate law.

3.3. Results and Discussion

3.3.1. Char Yield, Physical and Chemical Characteristics

Table 3.1 presents the proximate analysis and HHV of the biomass and char samples. Chars derived from fluidized bed gasification and pyrolysis are also listed for comparison. As shown in the table, heating values (HHVs) of both sorghum and red cedar char are higher than those of the respective biomass. The HHVs of red cedar and sorghum char were similar to that of pine wood

char derived from pyrolysis. The similar HHV could be results of their similar carbon contents. The ash content of red cedar char was lower than that of sorghum char, due to the lower ash content of red cedar as compared to sorghum. The ash contents of both sorghum and red cedar char (4–20%) were significantly lower than those of chars obtained from fluidized bed gasification (35–55%)[10]. The lower ash content and higher heating value of char derived from downdraft gasifier than those from fluidized bed gasifier imply that char derived from downdraft gasifier would be more suitable for applications such as soil amendment or solid fuel.

Table 3.1. Proximate analysis, ultimate analysis and HHV of biomass and char

Properties	Sorghum	Red cedar	Sorghum char	Red cedar char	Sorghum char (FB)	Pinewood char [38]
Moisture (w.b. %)	9.4	8.9	0.8	1.0	1.9	0.4
Volatile matter (w.b.%)	68.1	70.8	12.2	22.8	20.0	5.6
Ash (w.b. %)	5.1	1.8	20.2	4.5	45.9	3.5
Fixed carbon (w.b.%)	17.5	18.5	66.8	71.7	32.1	90.5
Nitrogen (d.b. %)	0.5	0.4	0.2	0.2	1.5	0.2
Hydrogen (d.b.%)	6.4	6.3	1.5	1.9	0.9	3.7
Sulfur (d.b.%)	0.2	1.1	0.4	0.5	0.1	0.1
Carbon (d.b.%)	40.7	47.5	67.9	66.4	40.1	75.5
HHV(MJ/Kg)	16.1	18.4	23.7	26.9	9.4	27.9

Notes: w.b represents wet basis and d.b represents dry basis., FB represents fluidized bed

The major minerals (>0.1%) of char and biomass include P, Ca, K, and Mg while the minor minerals (<0.1%) include Na, Fe, Zn, Cu and other heavy metals (Table 3.2). Sorghum char had higher concentrations of all mineral elements than red cedar char, which were due to its higher ash content (20% for sorghum char and 4% for red cedar char). Ca was the most abundant mineral in red cedar (0.65%), red cedar char (3.9%) and sorghum char (5.9%) but K was the most abundant in sorghum. The Ca to K content ratio of biomass (0.5 for sorghum and 5 for red cedar) was significantly higher than that of char (5 for sorghum char and 15 for red cedar char). This implies that Ca is more stable than K under gasification condition. The order of minor mineral

content in the biomass and chars were the same: Fe > Mn > Zn > Cu. Alkali and alkaline elements are necessary mineral for plant growth [8] but promote corrosion of reactor. High concentration of alkali and alkaline elements in sorghum char make it more suitable in soil amendment but less suitable as solid fuel than red cedar char.

Table 3.2. Mineral content of biomass and char obtained from downdraft gasifier

	P (%)	Ca (%)	K (%)	Mg (%)	Na (%)	S (%)	Fe (ppm)	Zn (ppm)	Cu (ppm)	Mn (ppm)
Sorghum	0.04	0.22	0.42	0.09	0.04	0.05	640	10	2	38
Sorghum char	0.18	5.96	1.30	0.48	0.27	0.14	4307	76	45	302
Red cedar	0.02	0.65	0.12	0.04	0.002	0.03	294	9	1	87
Red cedar char	0.04	3.91	0.23	0.14	0.14	0.08	1597	23	17	216

The loose bulk density red cedar char and sorghum char were 0.17 and 0.12 g/cm^3 with average particle sizes of 0.59 and 0.38 cm respectively. The char yield (amount of char produced per unit of biomass on weight basis) of downdraft gasification were estimated to be around 15%. The typical char yields of fluidized bed gasification were 5 to 10% [5, 10], while the char yields of pyrolysis varied from 20 to 50% [4]. Char yield is also dependent on production method, feedstock type, pyrolysis or gasification temperature, atmosphere, residence time and heating rate [23, 24]. High temperature and short residence time lead to high char yields [24, 25]. The char yield of downdraft gasification is generally lower than that of pyrolysis but higher than that of fluidized gasification. The higher char yield of downdraft gasification than fluidized gasification can be attributed to better heat and mass transfers using sand in fluidized-bed gasification. The high heat and mass transfers enhance gasification efficiency and reaction of solid carbon with gas resulting in lower char yield.

The X-ray diffraction patterns of the sorghum and red cedar chars are presented in Figure 3.1. XRD pattern of sorghum char and redcedar char, showing intensity of the diffracted beam as a function of the Bragg angle (2θ, in degrees). Sharp peaks indicate inorganic components. The

peaks at 26.7º and 29.5º correspond to SiO_2 and CaO, respectively. Broad peak at 23º correspond to hkl 200, crystallographic planes of completely ordered (i.e., crystalline) regions of cellulose [24]. Small broad peak of 43º correspond to graphite. The existence of broad peak at 23º in both red cedar char and sorghum char imply that the char was not fully carbonized and part of the biomass cellulose structure still remained in the char.

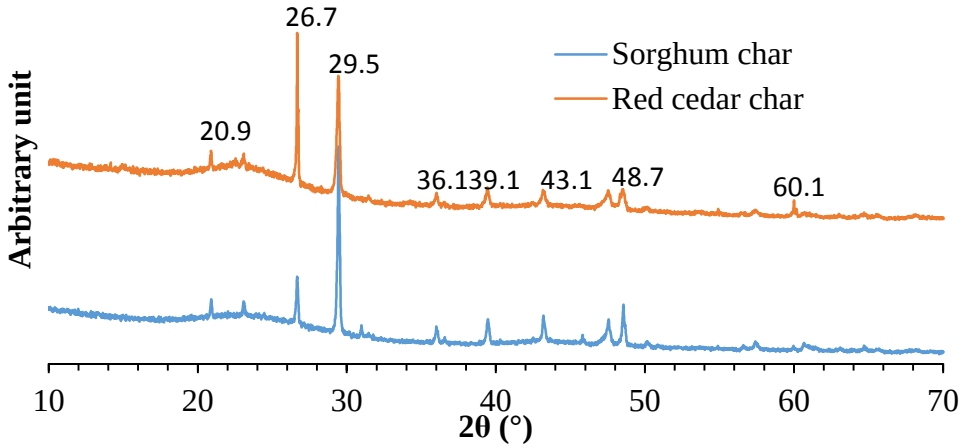

Figure 3.1. XRD pattern of sorghum char and redcedar char

The sorghum char appears to contain less carbon (at least less carbon with nearby H as detected by CP MAS), since the peak is smaller (Figure 3.2). The smaller peak of sorghum char can also be attributed to its higher ash content and lower carbon content, which are evident from its proximate and ultimate analyses. The carbon in both chars was primarily aromatic (corresponding to peak at about 130 ppm) but both chars seem to have some non-aromatic carbon as well. Both chars have intensity in the region of about 55 ppm, which corresponds to aliphatic C-H. Only red cedar char has some intensity in the regions of about 20 and 80 ppm corresponding to aliphatic carbon and C-OH, respectively. Cao et al. [6] also found that aliphatic and O-alkyl carbon decreased with increase in reaction temperature. However, they also found that 8% of O-alkyl carbon, 2.3% of CH_2 and 1.1% of CH_3 still existed in woody char treated at high temperature (700 °C) [6]. In addition, both chars had weak intensity at about 170-180 ppm,

indicating the presence of COOR functional groups. This finding was consistent with Cao's finding in woody char (4% of COOR).

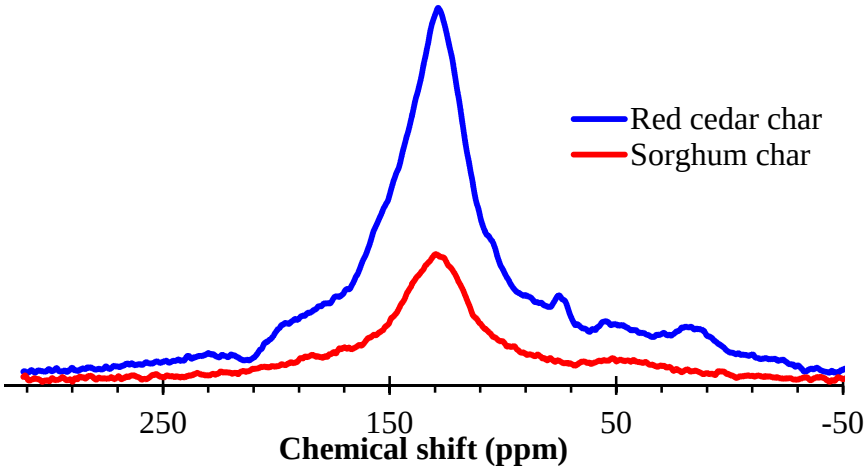

Figure 3.2. NMR spectrum of sorghum char and red cedar char

3.3.2. Pore Structure

Adsorption and desorption isotherms were obtained of char samples in nitrogen at 0.01-1 relative pressure range (Figure 3.3). All isotherms were found to be of type II, according to Brunauer classification, indicating wide distribution of pore sizes [26]. It was also found that classical BET relative pressure range (0.05-0.3) was not suitable to determining surface area of sorghum char and red cedar char samples because of negative C constant and unacceptable correlation coefficients. Hence, 0.02-0.1 relative pressure was used to estimate the specific surface area. Total surface area, total pore volume and micropore volume of sorghum char and red cedar char are listed in Table 3.3. The surface area of red cedar char (67 m^2/g) was higher than that of sorghum char (14 m^2/g). The percentage of total volume in micropore (< 2 nm) and mesopore (2-50 nm) range was high (90%) for both chars indicating that the char was mainly composed of micropores and mesopores rather than macropores (>50 nm). These results were consistent with results of char obtained from rice straw char [27] and coal [26]. Difficulty was encountered in achieving equilibrium under low relative pressure (10^{-5}) for the char samples indicating that ultramicropore (<0.7 nm) existed in char. Since ultramicropore and mineral particulates that may

exist on char surface are not easily accessible to nitrogen at low temperature [28, 29], the micropore volume in char samples may be larger than those estimated in this study. No closure of hysteresis loop for both char samples during adsorption/desorption isotherm can be observed below a relative pressure of 0.4, which can be attributed to the swelling of char during the adsorption [28].

Table 3.3. BET surface area and pore volume of char obtained using N_2 adsorption

	Surface area (m^2/g)	Micorpore volume (cm^3/g)	Mesopore volume (cm^3/g)	Total pore volume (cm^3/g)
Sorghum char	14.7	0.005	0.003	0.01
Red cedar char	68	0.018	0.022	0.042

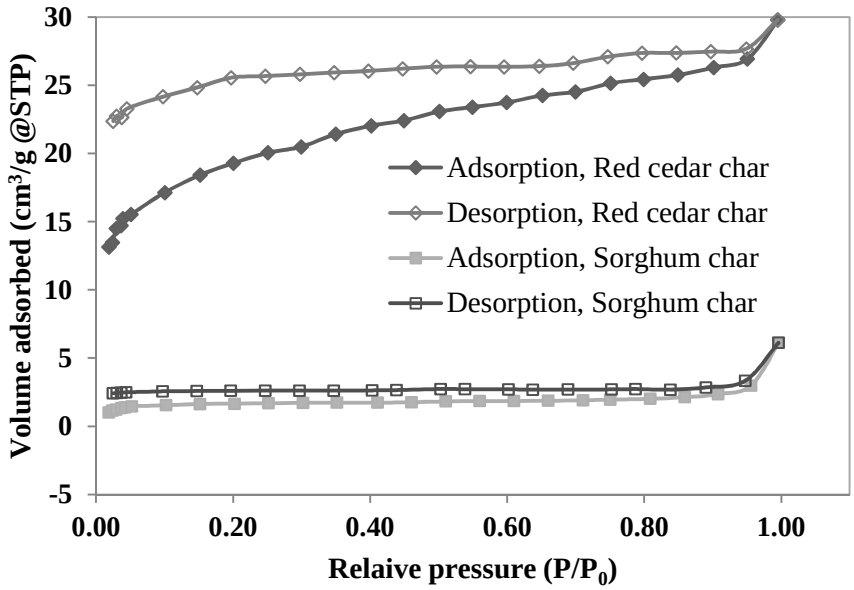

Figure 3.3. 77 K nitrogen isotherms of sorghum char and red cedar char

The surface area of char depends on release of volatiles during the pyrolysis because released vapors create pores and increase pore size [30] and the volatile release varies with conditions, such as heating rate, temperature and residence time. Generally, high temperature and longer residence time increase the surface area. By studying the effects of residence time on surface area of flax straw, Tushar et al. [31] found that surface area increased from 24 to 59 m^2/g with increase in residence time from 15 to 60 min. A review paper [30] summarized properties of

pyrolysis char derived from various biomass at temperature from 200 °C to 700 °C. They stated that surface areas of woody char can reach about 65 m^2/g and 300 m^2/g at 500 °C and 700°C, respectively, while surface areas of grass char can reach 14 m^2/g and 70 m^2/g at 500 °C and 700°C, respectively. The surface areas of sorghum char and red cedar char (14 and 55 m^2/g) obtained in this study were close to those of pyrolyzed at around 500 °C (14 and 65 m^2/g)) but much lower than those of grass and woody char pyrolyzed at temperature close to gasification temperature (700°C) [30]. Short residence time of downdraft gasification (<10 s) may have restricted pore development in the char. Volatile does not completely release in such short resident time, and thus the pore in char was not fully developed.

3.3.3. Gasification Kinetics

Results of the effect of gasification temperature (800, 900 and 1,000 °C) on the char conversion and mass loss are shown in Figure 3.4 and Figure 3.5. The char conversion was significantly affected by the reaction temperature and the time for complete carbon conversion decreased with increase in gasification temperature. The carbon conversions of both chars at 800 °C were quite low (about 20% after 50 minutes) while the carbon conversion at 1,000 °C reached 100% within 25 minutes.

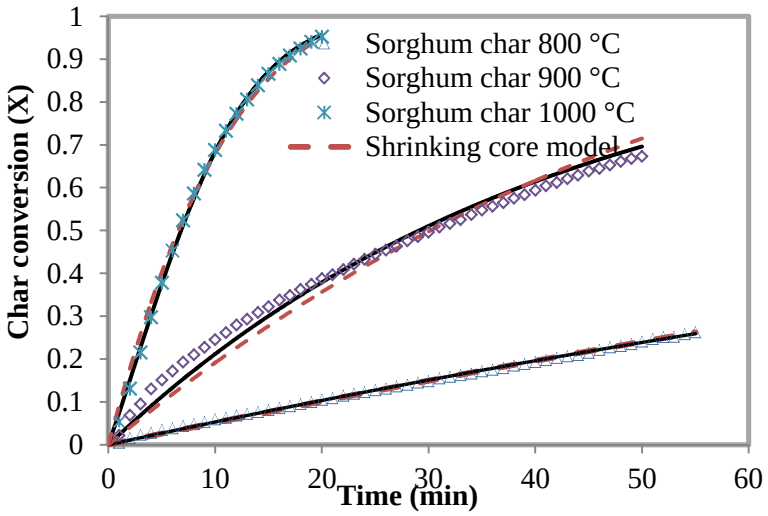

(a)

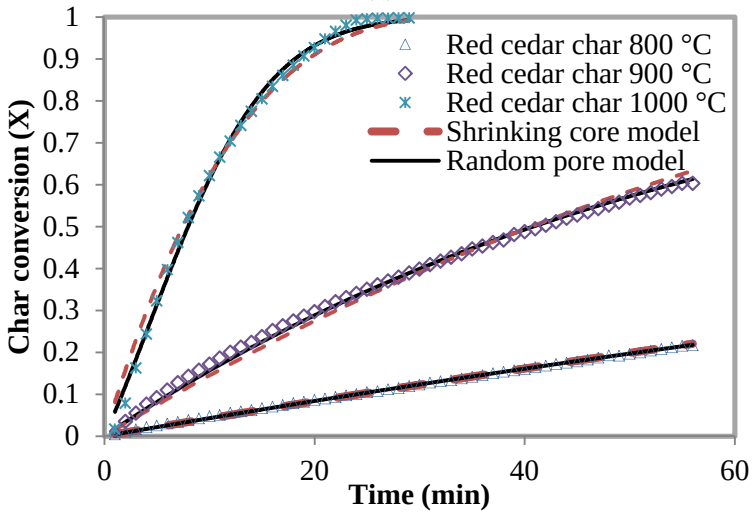

(b)

Figure 3.4. Experimental (markers) and model-predicted (lines) conversion histories of CO_2 gasification at three temperatures. (a) sorghum char and (b) redcedar char

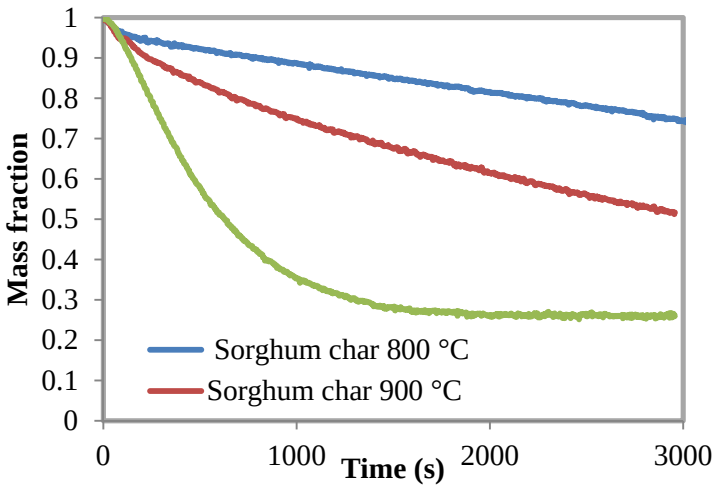

(a)

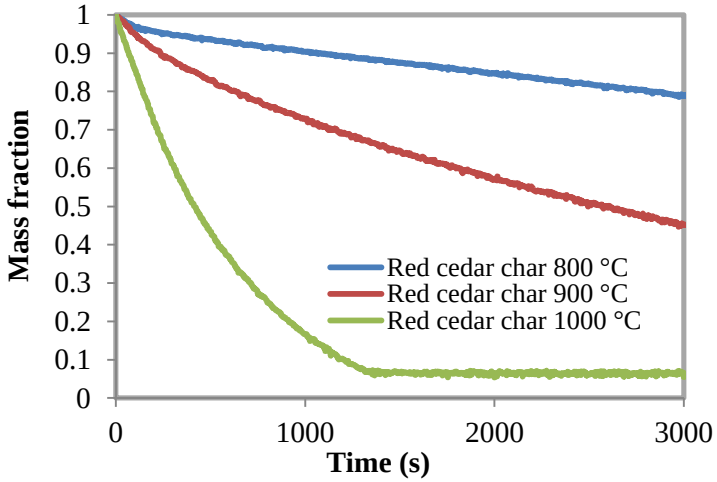

(b)

Figure 3.5. Mass loss profile of char during CO_2 gasification at three temperatures in TGA. (a) sorghum char, and (b) red cedar char

The gasification reactivity of char mainly depends on its morphological structure and inorganic content [32]. The inorganic contents of char primarily depend on inorganic contents of its precursor biomass. Hemicellulose, cellulose and lignin contents of biomass may also effect gasification rate of derived chars, but conclusive study is not available in literature [33]. Among char minerals, potassium (K) has been found to be the strongest catalyst, followed by sodium (Na) and calcium (Ca) [34]. Iron was also found to have high catalytic effect on gasification reactivity of char [22]. On the other hand, silicon content adversely affects char reactivity [34].

The activity of potassium catalyst was almost completely diminished during pretreatment when large amount of silicon existed in the char [34].

The morphological structure of char is influenced by reaction conditions, as discussed in section 3.3.2. Char with high porosity can provide more active sites for gasification [22]. The rate of char gasification depends on accessibility of CO_2 to the active sites located in internal surface. The reactivity of char is expected to be proportional to the surface area developed by mesopores and macropores rather than the total surface area, since only mesopores and macropores (not micropore) are accessible to reactant gas [33, 35]. The average CO_2 gasification reactivity of red cedar char (0.005, 0.014, 0.04 min^{-1} at 800, 900 and 1,000 °C respectively) was slightly higher than that of sorghum char (0.004, 0.011, 0.038 min^{-1} at 800, 900 and 1,000 °C respectively). The average gasification rate of char in this study was higher than that of the petroleum coke char and Zun-yi anthracite char [36] but lower than that of pistachio nut shell [19]. The higher gasification reactivity of red cedar char may be due to its higher surface area and lower ash content, although red cedar char contains lower potassium and iron contents as compared to sorghum char (as shown in Table 3.2). The adverse effect of high silicon content in sorghum char may have nulled the catalytic effect of potassium on sorghum char reactivity. We observed that the ash residues (primarily composed of silicon) of sorghum chars always contained some black carbon, instead of the pure ash residue found in red cedar char. The unreacted black carbon found in sorghum char implies that high silicon content of sorghum char may have adversely affected the reaction of CO_2 on carbon surface. This is possibly due to the blockage created by silicon content that affect diffusion of CO_2 into the carbon surface [32]. However, the catalytic activity of mineral also depends on dispersion rate of metal and the form of occurrence (dispersive metal, salts or organically bound compounds). The low reactivity of sorghum char can also be attributed to low availability of metal active cites as follows. Nishiyama[37] hypothesized that for metal to have catalytic effect, it must approach oxygenated groups on char to form active site [22]. However, to

further studies are needed to test the hypothesis that silicon content prevent char from gasification.

High R-squared obtained for linear fitting of carbon conversion (Figure 3.4) showed that the gasification was chemically controlled over the entire range and was not influenced by pore diffusion. The selected kinetic models were suitable to represent the gasification reaction [38]. The maximum reaction temperature (1,000 ℃) was still under chemical control region, which was consistent with findings of Yuan et al. (2011) that gasification reactions are chemical controlled at temperatures below 1,000 ℃ [27]. Transition from chemical to diffusion control region varies with sample properties and conditions [19, 27]. For most chars derived from lignocellulosic biomass, the transition temperature was found to be 900 -1000 ℃ in such as in studies of Wang et al. [39] and Lahijani et al. [19]. For coal char, transition temperature was above 1,000 ℃ [40]. With random pore model (RPM), structural parameter ψ that provided best fitting quality were 0, 0, 5.1 for red cedar char and 0, 0, 3.4 for sorghum char at 800, 900 and 1,000 ℃, respectively. A wide range of ψ has been reported for various chars (0 to 50) [20, 41]. Our calculated ψ were close to the values reported for the pine char [20]. The RPM assumes that the reaction surface changes due to competing processes: the effect of pore growth and the destruction of pores due to coalescence of neighboring pores [42]. Low value of ψ (< 2) was an indication of reaction with negligible pore growth and dominated by pore coalescence [21]. The average ψ values of red cedar char and sorghum char were 1.7 and 1.1 respectively, indicating that the reaction surface of redcedar and sorghum char changes mainly due to coalescence of neighboring pores rather than pore growth.

Table 3.4. Fitting quality of models at various temperatures

Temperature (°C)	Quality of fit			
	Red cedar char		Sorghum char	
	SCM	RPM	SCM	RPM
800	0.93	0.94	0.89	0.90
900	0.90	0.92	0.85	0.89
1000	0.81	0.94	0.81	0.90

The fitting qualities of the two models are presented in Table 3.4. RPM and SCM had good agreement with all experiment data and their fitting qualities were all higher than 0.8. However, the RPM model fitted better than the SCM at all temperature, especially at 1000℃. The pre-exponential factor, A, and the activation energy, Ea, are listed in Table 3.5. The activation energy based on RPM (143-147 MJ/kg) was lower than that based on SCM (163-167 MJ/kg), which was consistent with the findings of Sircar et al. [20]that activation energy calculated using RPM is normally lower than that calculated using SCM [20]. The activation energy values of redecedar and sorghum char were consistent with those reported in literatures (see Table 5). Sircar et al. [20] and Seo et al. [41] reported activation energy values of 125 ± 30 and 125-206 MJ/kg for pine char and various coal char, respectively [20]. However, activation energy of 204 MJ/kg for pistachio nut shell gasification was reported to be higher than our results [19].

Table 3.5. CO_2 gasification kinetic parameters of char

	Reaction Model	Ea (KJ/mol)	A (min^{-1})	R^2	References
Sorghum char	SCM	163.1	4.5E+05	0.993	This study
	RPM	147.4	8.6E+04	0.999	This study
Red cedar char	SCM	167.2	5.5E+05	0.992	This study
	RPM	143.8	5.5E+05	0.998	This study
Pistachio nut shell	RPM	204	-	-	[14]
Pine char	RPM	125±30	8.9E+3	-	[15]
Various coal chars	SCM	125-206	2.6E+4 - 4.7E+7	-	[35]

3.4. Conclusions

Physical and chemical properties of sorghum and red cedar char derived from a downdraft gasifier were investigated. Char derived from downdraft gasification had higher heating values and lower ash contents than char derived from fluidized bed gasification, indicating char derived from downdraft gasification is more suitable for further applications, such as soil amendment, than char derived from fluidized bed gasification. Micropores and mesopores dominated in both sorghum and red cedar chars. Red cedar char contained more micropores and mesopores than Sorghum char. XRD results indicated that the char was not completely carbonized. NMR showed that, while both chars have significant aromatic carbon, red cedar char also has some intensity in the regions corresponding to aliphatic carbon and C-OH. The gasification reactivity of red cedar char was higher than that of sorghum char. RPM and SCM had good agreement with all experiment data, but the RPM model fitted better than the SCM model at all temperatures.

Acknowledgements

Authors acknowledge the support of South Central Sun Grant Program and Oklahoma Agricultural Experiment Station for this study

3.5. References

[1] A.S. González, M.G. Plaza, F. Rubiera, C. Pevida, Sustainable biomass-based carbon adsorbents for post-combustion CO_2 capture, Chemical Engineering Journal, 230 (2013) 456-465.

[2] M. Li, Y. Zheng, Y. Chen, X. Zhu, Biodiesel production from waste cooking oil using a heterogeneous catalyst from pyrolyzed rice husk, Bioresour. Technol., 154 (2014) 345-348.

[3] W. Zheng, M. Guo, T. Chow, D.N. Bennett, N. Rajagopalan, Sorption properties of greenwaste biochar for two triazine pesticides, J Hazard Mater, 181 (2010) 121-126.

[4] J.J. Manyà, Pyrolysis for Biochar Purposes: A Review to Establish Current Knowledge Gaps and Research Needs, Environ. Sci. Technol., 46 (2012) 7939-7954.

[5] C.E. Brewer, K. Schmidt-Rohr, J.A. Satrio, R.C. Brown, Characterization of biochar from fast pyrolysis and gasification systems, Environ Prog Sustain, 28 (2009) 386-396.

[6] X. Cao, J.J. Pignatello, Y. Li, C. Lattao, M.A. Chappell, N. Chen, L.F. Miller, J. Mao, Characterization of wood chars produced at different temperatures using advanced solid-state ^{13}C NMR spectroscopic techniques, Energy Fuels, 26 (2012) 5983-5991.

[7] C. De Pasquale, V. Marsala, A.E. Berns, M. Valagussa, A. Pozzi, G. Alonzo, P. Conte, Fast field cycling NMR relaxometry characterization of biochars obtained from an industrial thermochemical process, J. Soils Sediments, 12 (2012) 1211-1221.

[8] J. Lehmann, M.C. Rillig, J. Thies, C.A. Masiello, W.C. Hockaday, D. Crowley, Biochar effects on soil biota – A review, Soil Biology & Biochemistry, 43 (2011) 1812-1836.

[9] S. Du, H. Yang, K. Qian, X. Wang, H. Chen, Fusion and transformation properties of the inorganic components in biomass ash, Fuel, 117, Part B (2014) 1281-1287.

[10] K. Qian, A. Kumar, K. Patil, D. Bellmer, D. Wang, W. Yuan, R. Huhnke, Effects of biomass feedstocks and gasification conditions on the physiochemical properties of char, Energies, 6 (2013) 3972-3986.

[11] K. Patil, P. Bhoi, R. Huhnke, D. Bellmer, Biomass downdraft gasifier with internal cyclonic combustion chamber: Design, construction, and experimental results, Bioresource Technol, 102 (2011) 6286-6290.

[12] ASTM Standard D3175-11 "Standard Test Method for Volatile Matter in the Analysis Sample of Coal and Coke", in, ASTM International, West Conshohocken, PA, 2011.

[13] ASTM Standard D4442-07 "Standard Test Methods for Direct Moisture Content Measurement of Wood and Wood-Base Materials", ASTM International, West Conshohocken, PA, 2007.

[14] ASTM Standard E1755-01(2007) "Standard Test Method for Ash in Biomass", in, ASTM International, West Conshohocken, PA, 2007.

[15] ASTM Standard D3172- 07a "Standard Practice for Proximate Analysis of Coal and Coke", in, ASTM International, West Conshohocken, PA, 2007.

[16] E.O. Stejskal, J. Schaefer, J.S. Waugh, Magic-angle spinning and polarization transfer in proton-enhanced NMR, Journal of Magnetic Resonance (1969), 28 (1977) 105-112.

[17] W.T. Dixon, J. Schaefer, M.D. Sefcik, E.O. Stejskal, R.A. McKay, Total suppression of sidebands in CPMAS C-13 NMR, Journal of Magnetic Resonance (1969), 49 (1982) 341-345.

[18] A.E. Bennett, C.M. Rienstra, M. Auger, K.V. Lakshmi, R.G. Griffin, Heteronuclear decoupling in rotating solids, The Journal of Chemical Physics, 103 (1995) 6951-6958.

[19] P. Lahijani, Z.A. Zainal, A.R. Mohamed, M. Mohammadi, CO_2 gasification reactivity of biomass char: Catalytic influence of alkali, alkaline earth and transition metal salts, Bioresour. Technol., 144 (2013) 288-295.

[20] I. Sircar, A. Sane, W. Wang, J.P. Gore, Experimental and modeling study of pinewood char gasification with CO_2, Fuel, 119 (2014) 38-46.

[21] R.C. Everson, H.W.J.P. Neomagus, R. Kaitano, R. Falcon, V.M. du Cann, Properties of high ash coal-char particles derived from inertinite-rich coal: II. Gasification kinetics with carbon dioxide, Fuel, 87 (2008) 3403-3408.

[22] M.F. Irfan, M.R. Usman, K. Kusakabe, Coal gasification in CO_2 atmosphere and its kinetics since 1948: A brief review, Energy, 36 (2011) 12-40.

[23] M. Uchimiya, L.H. Wartelle, K.T. Klasson, C.A. Fortier, I.M. Lima, Influence of pyrolysis temperature on biochar property and function as a heavy metal sorbent in soil, J Agr Food Chem, 59 (2011) 2501-2510.

[24] M. Keiluweit, P.S. Nico, M.G. Johnson, M. Kleber, Dynamic Molecular Structure of Plant Biomass-Derived Black Carbon (Biochar), Environ. Sci. Technol., 44 (2010) 1247-1253.

[25] P. Fu, S. Hu, J. Xiang, W. Yi, X. Bai, L. Sun, S. Su, Evolution of char structure during steam gasification of the chars produced from rapid pyrolysis of rice husk, Bioresour. Technol., 114 (2012) 691-697.

[26] L. Qian, Y. Zhao, S. Sun, H. Che, H. Chen, D. Wang, Chemical/physical properties of char during devolatilization in inert and reducing conditions, Fuel Processing Technology, 118 (2014) 327-334.

[27] S. Yuan, X.-l. Chen, J. Li, F.-c. Wang, CO2 Gasification Kinetics of Biomass Char Derived from High-Temperature Rapid Pyrolysis, Energy Fuels, 25 (2011) 2314-2321.

[28] C.R. Clarkson, R.M. Bustin, The effect of pore structure and gas pressure upon the transport properties of coal: a laboratory and modeling study. 1. Isotherms and pore volume distributions, Fuel, 78 (1999) 1333-1344.

[29] E. Cetin, R. Gupta, B. Moghtaderi, Effect of pyrolysis pressure and heating rate on radiata pine char structure and apparent gasification reactivity, Fuel, 84 (2005) 1328-1334.

[30] M. Ahmad, A.U. Rajapaksha, J.E. Lim, M. Zhang, N. Bolan, D. Mohan, M. Vithanage, S.S. Lee, Y.S. Ok, Biochar as a sorbent for contaminant management in soil and water: A review, Chemosphere, 99 (2014) 19-33.

[31] M.S. Hasan Khan Tushar, N. Mahinpey, A. Khan, H. Ibrahim, P. Kumar, R. Idem, Production, characterization and reactivity studies of chars produced by the isothermal pyrolysis of flax straw, Biomass and Bioenergy, 37 (2012) 97-105.

[32] L. Lin, M. Strand, Investigation of the intrinsic CO_2 gasification kinetics of biomass char at medium to high temperatures, Applied Energy, 109 (2013) 220-228.

[33] C. Di Blasi, Combustion and gasification rates of lignocellulosic chars, Progress in Energy and Combustion Science, 35 (2009) 121-140.

[34] Y. Zhang, M. Ashizawa, S. Kajitani, K. Miura, Proposal of a semi-empirical kinetic model to reconcile with gasification reactivity profiles of biomass chars, Fuel, 87 (2008) 475-481.

[35] B. Feng, S.K. Bhatia, Variation of the pore structure of coal chars during gasification, Carbon, 41 (2003) 507-523.

[36] W. Huo, Z. Zhou, F. Wang, G. Yu, Mechanism analysis and experimental verification of pore diffusion on coke and coal char gasification with CO_2, Chemical Engineering Journal, 244 (2014) 227-233.

[37] Y. Nishiyama, Catalytic behaviour of iron and nickel in coal gasification, Fuel, 65 (1986) 1404-1409.

[38] D.G. Roberts, E.M. Hodge, D.J. Harris, J.F. Stubington, Kinetics of Char Gasification with CO2 under Regime II Conditions: Effects of Temperature, Reactant, and Total Pressure, Energ Fuel, 24 (2010) 5300-5308.

[39] L. Wang, J. Sandquist, G. Varhegyi, B. Matas Güell, CO2 Gasification of Chars Prepared from Wood and Forest Residue: A Kinetic Study, Energy Fuels, 27 (2013) 6098-6107.

[40] Y.T. Kim, D.K. Seo, J. Hwang, Study of the Effect of Coal Type and Particle Size on Char–CO2 Gasification via Gas Analysis, Energy Fuels, 25 (2011) 5044-5054.

[41] D.K. Seo, S.K. Lee, M.W. Kang, J. Hwang, T.-U. Yu, Gasification reactivity of biomass chars with CO_2, Biomass and Bioenergy, 34 (2010) 1946-1953.

[42] S.K. Bhatia, D.D. Perlmutter, A random pore model for fluid-solid reactions: I. Isothermal, kinetic control, AIChE Journal, 26 (1980) 379-386.

CHAPTER IV

CATALYTIC REFORMING OF TOLUENE (MODEL TAR) BY CHAR SUPPORTED NICKEL CATALYST

Abstract: Char and tar are two byproducts of biomass gasification. Tars in biomass-generated syngas must be removed prior to utilization to prevent clogging in downstream facilities while char is traditionally considered as low value byproduct. The purpose of this study was to utilize gasification derived char as a catalyst for tar removal. Red cedar char collected from downdraft bed gasification was chemically activated into activated carbon and impregnated with nickel acetate and nickel nitrate. The effects of nickel salts precursor, nitric acid treatment of support and reduction of nickel in hydrazine medium on catalyst performance were studied. The catalysts were characterized by N_2 physisorption, TPD, TEM, and XRD, and tested in the steam reforming of toluene. The activated char support was dominated by mesopores and mesoopores. It was found nickel nitrate was a better nickel precursor than nickel acetate for preparation of char supported nickel catalyst. The catalyst impregnated with nickel nitrate was found more active in steam reforming of toluene than catalyst impregnated with nickel acetate. The TEM results indicated that the nickel particle size of catalyst impregnated with nickel nitrate was much smaller than that of catalyst impregnated with nickel acetate. The particle size of catalyst impregnated with nickel acetate was decreased by hydrazine reduction but was still larger than catalyst impregnated with nickel nitrate. The primary gas product of steam reforming of toluene was H_2 followed by CO and CO_2. The H_2 content and CO_2 decreased as the temperature increased from 600 to 700 °C while the CO content increased with decrease in temperature.

Keywords: char; catalyst, toluene reforming, gasification

4.1. Introduction

Gasification, a biomass thermochemical conversion technology, converts biomass into synthesis gas (syngas), a mixture of primarily carbon monoxide, carbon dioxide and hydrogen. The produced syngas can be further used as a feedstock for hydrocarbon fuels production through the Fischer–Tropsch synthesis (FTS) process, which produces hydrocarbons of different lengths. Syngas can also be used as an alternative to natural gas fuel for hydrogen or power production. However, biomass-generated syngas cannot be used directly because it contains high concentration of tars, a mixture of several aromatic compounds that must be removed prior to utilization of syngas [1, 2] because tars cause a lot of equipment problems such as condensation on facility leading to fouling [2]. The environmental legislation also requires removal of toxic aromatic compounds from syngas.

Wet scrubbing, catalytic conditioning and high temperature thermal cracking were three major syngas conditioning methods. Catalytic conditioning is of the most promising because of its high conditioning efficiency. However, catalytic conditioning of tar in syngas can increase H_2/CO in sygans [3-5]. The typical H_2/CO ratio of biomass-generated syngas is lower than 1, which is significantly lower than the desired hydrogen to carbon monoxide ratio for the FTS (about 2.0) [6].

Recently, biochar, one of the byproducts of biomass gasification, was reported as a potential catalyst for tar removal [7]. The catalytic activity of char for tar elimination can be related to its pore size, surface area, and ash or mineral content of the char. Char also can be activated into activated carbon and used as a support for preparing metal catalysts [8, 9]. When activated carbon is used as a catalyst support, it has unique properties, such as its stability in both acidic and basic media, the possibility of easy recovery of precious metals supported on it and the possibility of tailoring both its textural and surface chemical properties according to the targeted aims of the catalyst producers [10, 11].

Pretreatments to the carbon support can significantly affect the properties and performance of the carbon-based catalysts. High surface area, acid group and oxygen-containing functional groups on the surface play an important role in catalyst reactivity of biochar. The metal dispersion ratio and metal–carbon interactions also affect the reactivity of carbon supported metal catalysts. Several studies have confirmed that pre-treatments of activated carbon increase metal dispersion ratio, support surface area and surface functional group, thus, influence its reactivity [12, 13]. Pre-treatment of the catalyst includes acid treatment of carbon with various types of acid (H_2SO_4, HNO_3) and treatment with various reducing agent, such as hydrazine or $NaBH_4$. Acid treatment can increase surface oxygenated groups on the activated carbon, and thus increase its catalytic activity [12, 14-16]. Aksoylu et al. (2001) [12] studied the effect of HNO_3 treatment on Pt/carbon catalyst performance in the benzene hydrogenation reaction. The results showed that HNO_3 treatments not only led to increase in oxygen bearing groups on the exterior and interior surfaces of the activated carbon, but also enhanced dispersion of Pt. The catalyst activity test showed that the treated catalyst exhibited higher efficiency as compared to the untreated catalyst [14]. Besides acid treatment, hydrazine treatment has also widely been used for catalyst preparation as a reducing agent of metallic catalyst. Treating the catalyst with reducing agent produces nanoparticle metal catalyst with small average particle size and high dispersive ratio [13, 17, 18]. Wojcieszak et al. [13] compared the properties of hydrazine treated catalysts (reduction of nickel by aqueous hydrazine) and classically prepared catalysts (without the hydrazine treatment) and found that the hydrazine reduction process improved metal dispersion and catalyst efficiency.

Nickel based catalysts have been widely used in tar reforming [19-22]. Swierczynski et al. [23] found that the nickel based catalyst was very effective in reforming of tars. Michel et al. [20] compared performances of olivine-based catalysts for steam reforming of methylnaphthalene (MNP) as a model tar compound. The results showed that conversion efficiency of MNP to CO/H_2 with olivine alone (4%) was much lower than that with Ni/olivine (30%).

The objective of this study was to develop a novel char based catalyst. Red cedar-derived char was used as a support material for nickel. The pretreatment method and the precursor effect on the catalytic performances were studied: the first type of catalyst was prepared by mild oxidation of activated carbon (support) with nitric acid and reduction of impregnated nickel acetate or nickel nitrate with hydrogen; the second type of catalyst was prepared by reduction of nickel acetate with hydrazine. The properties of char based catalysts were evaluated using TEM, XRD and N_2 isotherms, and the catalysts' performances were tested in steam reforming of toluene (a model tar compound).

4.2. Materials and Methods

4.2.1. Materials

The char for making catalysts in this study was produced from gasification of eastern red cedar in a unique downdraft gasifier as described in chapter 3 [24]. The red cedar was obtained locally in Stillwater, OK, USA. The gasification temperature was around 900 °C [24]. $Ni(NO_3)_2 \cdot 6H_2O$, $Ni(CH_3COO)_2 \cdot 4H_2O$ (≥99.0%) and hydrazine anhydrate (50-60%) were purchased from Sigma Aldrich (St. Louis, MO, USA). The KOH was purchased from Fisher Scientific (Pittsburgh, PA, USA).

4.2.2. Activated Carbon Preparation

Chemical activation is a widely used activation method for making activated carbon [25, 26]. This method uses chemicals such as KOH and NaOH as an activator to develop pores. In our study, biochar was mixed with KOH and soaked for 2 h. The mixture was dried in an oven overnight at 105 °C. The dried mixture was then placed in a fixed-bed tubular reactor and activated. The reactor was first heated to 300 °C and held at this temperature for 2 h to prevent carbon loss from biochar. For carbonization, the temperature was then raised to 800 °C and biochar was activated at this temperature for 1.5 h under nitrogen flow of 200 ml/min. After carbonization, the biochar was washed with deionized water until the pH of leaching water reached 7.

4.2.3. Catalyst Synthesis

The activated carbon was treated with 30% HNO_3 before loading nickel. Activated carbon was loaded a round bottom flask equipped with a thermometer and reflux condenser. The flask was immersed in a water bath at 70 °C. The activated carbon suspension was stirred continuously using a magnetic stirrer bar. After 1.5 h acid treatment, activated carbon was filtered from the suspension into a funnel and washed with deionized water until pH of the filtered solution reached neutral. The acid soaked biochar was then dried in an oven at 105 °C overnight. The dried acid treated activated carbon was wet impregnated in a solution of nickel acetate or nickel nitrate. The concentration of the nickel acetate solution was calculated before impregnation in order to achieve 10 wt. % nickel loading. The mixture was ultrasonicated for 3 h and kept in a vacuum desiccator for 16 h. The soaked samples were then dried in the oven at 105 °C and denoted as Ni-AC-N (activated carbon loaded with nickel nitrate) and Ni-AC-A (activated carbon loaded with nickel acetate).

To study the effect of hydrazine reduction on catalyst properties, Ni-AC-A was further treated with hydrazine using a method developed in literature [13]. The catalyst precursor was soaked in a 2.0 M hydrazine solution for reduction. The reduction of nickel catalyst precursor was performed in a 250 ml three necked flask that was immersed in a hot water bath. The reaction flask was fitted with a reflux condenser, a thermometer and a gas tubing for using helium to purge the air out of the flask. The mixture of nickel catalyst precursor and hydrazine solution was stirred at 80°C for 4 h. After reduction, the catalyst was filtered and the excess hydrazine left in catalyst was washed off with deionized water. The catalyst was then dried in an oven at 105 °C before test and denoted as Ni-AC-AH.

4.2.4. Catalyst Activity Test

The catalyst activity test was performed in a fixed bed reactor with a 1/2 inch diameter stainless steel tube at temperature of 600, 700 and 800 °C. Catalyst was loaded in the reactor with two layers of quartz wool. One layer of quartz wool was kept beneath catalyst for support and one

layer of quartz wool was kept above the catalyst to make gas uniformly mixed. The catalyst particle sizes of 0.3-0.6 mm and catalyst weight was 0.25 g. The catalyst was reduced by 200 ml/min mixed hydrogen flow (50% hydrogen mixed with 50% nitrogen) at 350 °C for 3 h. After reducing, the reactor temperature was increased to the desired reforming temperature for each catalyst test. During each test, 150 ml/min of nitrogen controlled by a mass flow controller (Burkert, Charlotte, NC, USA) was introduced into the reactor. 0.95 ml/hr water and 0.4 ml/hr toluene (steam to carbon ratio: 2) were injected continually into the gas feeding line using syringe pumps (model 200, KDS scientific, Hollistion, MA, USA). Samples were taken at 45-55 min.

The gas hourly space velocity (GHSV = gas flow rate/catalyst bed volume) was about 8000 h^{-1}. Concentration of reactor outlet gas (hydrogen, carbon monoxide, carbon dioxide and methane) was measured by a gas chromatograph with FID detector (Model CP-3800, Varian, Inc., Palo Alto, CA, US) and installed with a packed column (HayeSep DB). The toluene concentration was determined by a gas chromatograph installed with a capillary column (DB-5) and a mass spectroscopy detector (GC 7980A, MS 5975, Agilent, Santa Clara, CA, US).
The toluene conversion can be defined by Equation 4.1 [27]:

$$\text{Conversion } (\%) = \frac{C_{toluene}^{in} - C_{toluene}^{out}}{C_{toluene}^{in}} \times 100 \qquad \text{(Equation 4.1)}$$

Where $C_{toluene}^{in}$ and $C_{toluene}^{out}$ were the model tar (naphthalene or toluene) molar flow rates of the inlet and outlet gases. Benzene yield as Equation 4.2 [27]:

$$\text{Benzene yield}(\%) = \frac{6 \times C_{benzene}^{out}}{7 C_{toluene}^{in}} \times 100 \qquad \text{(Equation 4.2)}$$

Gas composition was calculated as Equation 4.3 [27]:

$$\text{Gas composition } (\%) = \frac{\text{mole of each gas product}}{\text{total mole of gas products } (H_2+CO+CO_2+CH_4)} \times 100 \qquad \text{(Equation 4.3)}$$

4.2.5. Catalyst Characterizations

4.2.5.1. XRD and TEM

The morphologies of activated carbon supported catalysts were characterized by X-ray diffraction (XRD) and transmission electron microscopy (TEM). Particle size and crystalline phase of Ni were determined using XRD (PANalytical, Westborough, MA, US). XRD experiments were performed using Cu Kα radiation at 40 kV and 100 mA. Diffraction data was recorded using continuous scanning at a step size of 0.02°, 0.5s per step. The average particle size of Ni was calculated according to the Scherrer–Warren equation. The Ni dispersion was examined using transmission electron microscopy (TEM) (JEOL JEM-2100, AKISHIMA-SHI, Tokyo, Japan). TEM images were obtained by dispersing catalysts on carbon grids in isopropanol under supersonic-wave shaking.

4.2.5.2. Surface Area and Temperature-Programmed Desorption (TPD)

Surface area and pore properties (pore distribution and average pore size) of catalysts and char were measured via N_2 adsorption at -198 °C using a surface area analyzer (Autosorb-1C, Quantachrome, Boynton Beach, FL,US). Surface area (S_{BET}) was analyzed using Brunauer–Emmett–Teller (BET) theory. Pore volumes and pore size distribution were estimated using Quenched Solid State Functional Theory (QSDFT).

TPD experiments of activated carbon supports were carried out in the same equipment with N_2 adsorption. Samples were first dried at 140 °C for 60 min to remove moisture under 40ml/min helium flow. The dried sample was cooled to 100 °C before test and then heated from 100 °C to 900 °C with heating rate of 20 °C/min. The evolved CO and CO_2 were detected by a thermal conductivity detector (TCD).

4.3. Results and Discussion

4.3.1. Catalyst Characterization

4.3.1.1. Nitrogen Adsorption

Specific surface areas (S_{BET}) and pore volumes were measured using a liquid nitrogen isothermal method and listed in Table 4.1. Based on the results, char surface area was significantly increased by chemical activation (increased from 60 m^2/g to 1570 m^2/g). Acid treatment did not significantly reduce the surface area of activated carbon. 10% nickel loading significantly decreased the surface area of activated carbon (reduced about 30-40%). The red cedar char was dominated by mesopores (52 vol.%), followed by micropores (42 vol.%) with total pore volume of 0.04 cm^3/g. After activation, the total pore volume of activated carbon increased and so did the volume percent of micropores. More detailed pore size information was obtained from pore distribution analysis (see Figure 4.1). Large quantities of micropores (<2 nm) and mesopores (2-50 nm) were detected. The mesopores were mostly composed of small mesopores (<8 nm).

Table 4.1. Texture properties of the different activate carbons and Ni catalyst.

	S_{BET}, (m^2/g)	V_{micro}, (cm^3/g)	V_{micro}, (%)	V_{meso}, (cm^3/g)	V_{meso}, (%)	Total pore volume (cm^3/g)	$D_{Ni, TEM}$ (nm)	$D_{Ni, XRD}$ (nm)
Raw char	68	0.02	42.85	0.02	52.38	0.04	NA	N.A.
AC	1570	0.50	62.50	0.30	37.50	0.80	NA	N.A.
Acid AC	1524	0.50	70.40	0.21	29.60	0.71	NA	N.A.
Ni-AC-N	965	0.31	73.80	0.11	26.20	0.42	7-13	N.A.
Ni-AC-A	945	0.30	75.00	0.10	25.00	0.40	15-39	18
Ni-AC-AH	1021	0.35	79.50	0.06	20.50	0.44	11-18	17

"NA" means not applicable

Compared with acid activated carbon, the volume percent of micropores of Ni-AC-N and Ni-AC-A increased while volume percent of mesopores of Ni-AC-N and Ni-AC-A decreased (see Table 4.1). Peak corresponding to mesopores with pore diameter 8-10nm (Figure 4.1) presented in activated carbon supports but disappeared on Ni-AC-N and Ni-AC-A. The decrease of mesopores was probably due to integration of nickel to mesopores. A similar finding was

discovered by Garcia et al. [9] on carbon based nickel catalyst. They found that nickel dispersion positively related to the mesopores and macropores volume of the carbon support, and concluded that only mesopores and macropores were accessible by nickel precursor.

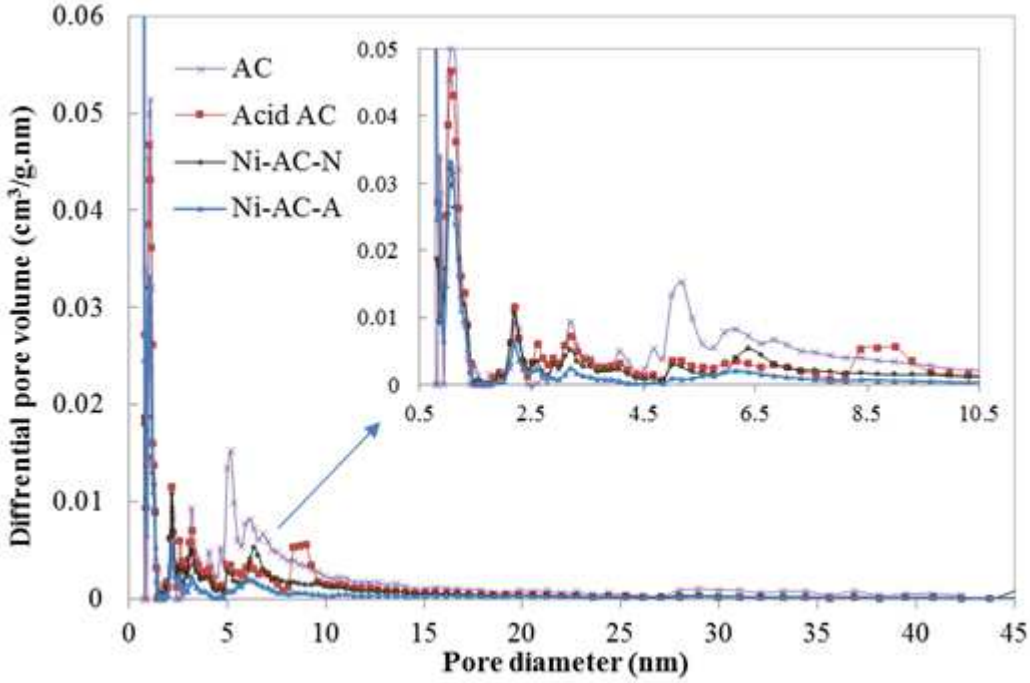

Figure 4.1. Pore distribution of activated carbons and char supported Ni catalysts.

4.3.1.2. TPD and FT-IR

Oxygenated functional groups on activated carbon were analyzed using TPD and FT-IR. Volatiles desorption occurred at different temperatures due to decomposition of various oxygenated functional groups over activated carbon surface. The decomposition temperatures of different oxygen bearing surface with TPD are well studied in literatures [12, 28]: the low temperature peak resulted from decomposition of carboxylic acids (200-300 °C); the medium temperature peaks were assigned to lactones (190-650 °C); higher temperature decompositions were associated with carboxylic anhydrides, carbonyl, phenols, ethers, carbonyls and quinone groups (700-1000 °C). As seen in Figure 4.2, peaks were observed in all temperature regions for both activated carbon and acid treated activated carbon, indicating that activated carbon and acid treated activated carbon contained multiple oxygen functional groups. The peaks of acid treated

activated carbon were higher than peaks of raw activated carbon, indicating that acid treatment increased the quantity of surface oxygen functional groups on activated carbon.

Small bands observed on region 1140-1000 cm^{-1}, 1620-1450 cm^{-1} and 1700 cm^{-1} FTIR spectra (Figure 4.3) were assigned to ether, quinone and lactonic groups [28]. Those three bands on the spectrum of acid treated activated carbon were more intense than activated carbon, suggesting that the acid treated activated carbon contained larger amounts of ether, quinone and lactonic groups than activated carbon. The observation of greater quinone groups was consistent with results from TPD.

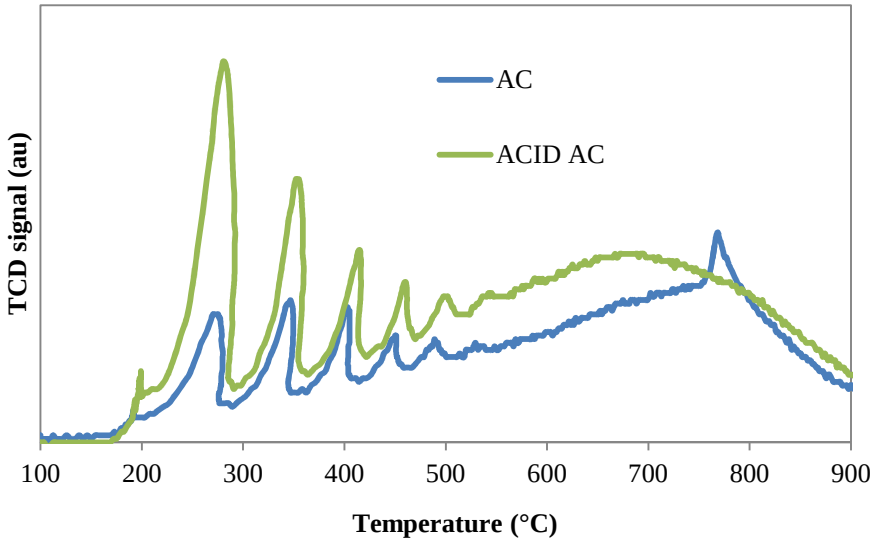

Figure 4.2. TPD profiles of raw activated carbon and acid treated activated carbon

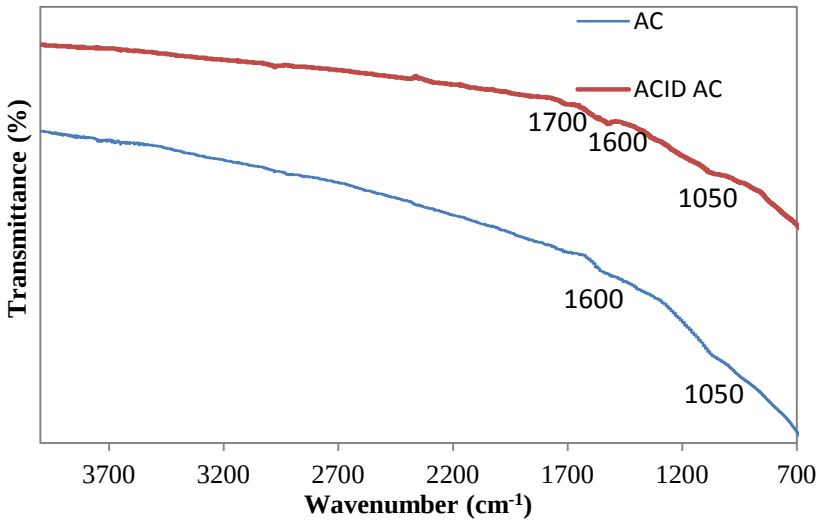

Figure 4.3. FTIR spectra of raw activated carbon and acid treated activated carbon

4.3.1.3. X-ray Diffraction (XRD)

One broad peak at 23° and one weak peak at around 43° were observed on activated carbon (Figure 4.4). The peak at 23° was attributed to the (002) reflection of the graphitic-type lattice and the peak at 43° corresponded to a superposition of (100) and (101) reflections of the graphitic-type lattice. The broadness and weakness of two reflection peaks of activated carbon indicated a low degree of graphitization. The XRD patterns of the Ni-AC-A and Ni-AC-AH showed three reflection peaks (Figure 4.4) at 44.5° and 51.5° and 76.4°. Those peaks were assigned to crystal planes of 111, 200 and 220 of metallic nickel with a face-centered cubic structure [13]. The signals on spectrum of Ni-AC-AH were less intense than Ni-AC-A, suggesting a smaller nickel particle size and better metal dispersion on Ni-AC-AH. XRD pattern of Ni-AC-N only showed two peaks at 44.5° and 51.5°. Both peaks were less intense than XRD peaks of Ni-AC-AH and Ni-AC-A, suggesting that Ni-AC-N had the highest nickel dispersion and smallest nickel particle size. The nickel crystal sizes of Ni-AC-A and Ni-AC-AH were estimated (see Table 4.1) using the Scherrer equation by knowing line broadening at half the maximum intensity of the most intense peak. The estimation of nickel crystal size of Ni-AC-N

was not possible to difficulty in obtaining the line broadening at half the maximum intensity of the most intense peak.

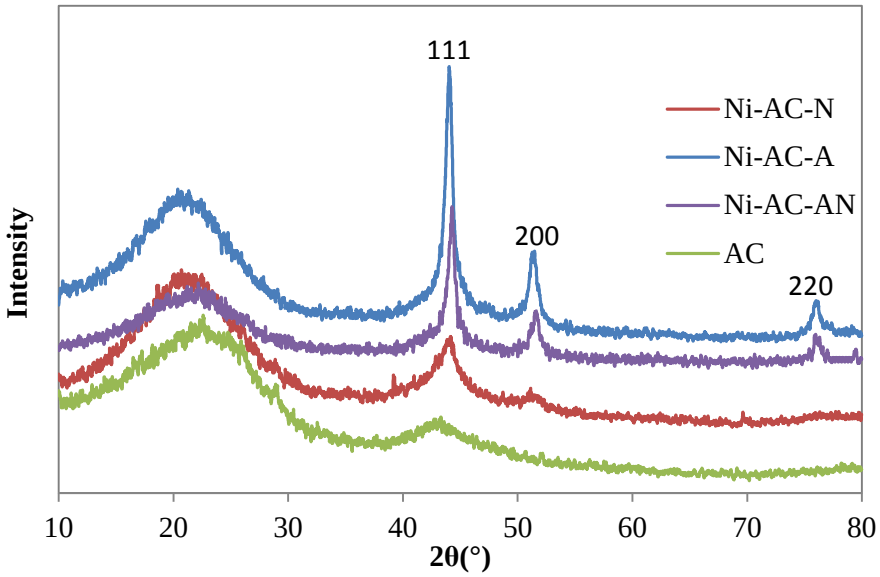

Figure 4.4. XRD pattern of activated carbon supports and nickel catalysts

4.3.1.4. TEM

As seen from Figure 4.5, the shape of the nickel particles on the three catalysts was essentially spherical. Ni-AC-N (Figure 4.5 (a)) showed the highest nickel dispersion and smallest particle sizes, which was consistent with the results obtained from XRD. The nickel particle size of Ni-AC-A (Figure 4.5 (b)) was larger and agglomeration of nickel particles was more severe, while the nickel particle of Ni-AC-AH (Figure 4.5 (c)) dispersed better and was smaller, indicating hydrazine treatment improved the metal dispersion on catalyst with nickel acetate precursor. The same phenomenon was also observed by Wojcieszak et al. [13]. When they prepared activated carbon supported nickel catalysts for benzene hydrogenation, they found that the nickel catalysts prepared by hydrazine chemical reduction had much smaller particle size (<5nm) than that prepared by hydrogen reduction methods (10-40 nm). The nickel particles sizes of Ni-AC-N, Ni-AC-A and Ni-AC-AH measured from TEM were 7-13, 11-18 and 15–30 nm respectively (Table 4.1).

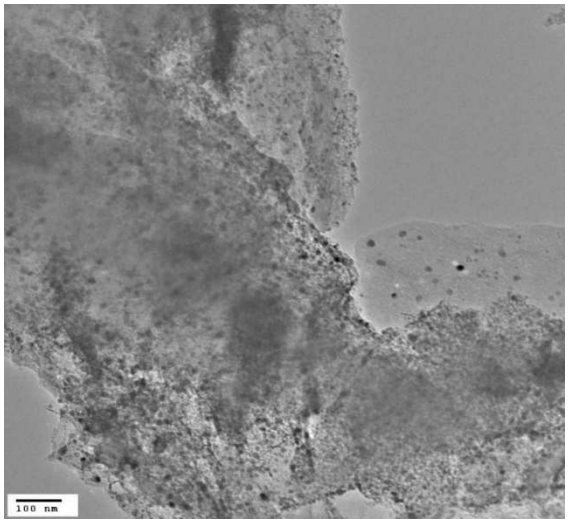

(a) Ni-AC-N

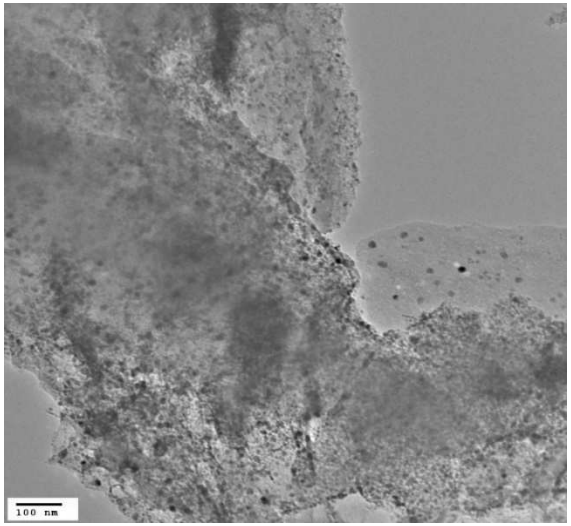

(b) Ni-AC-A

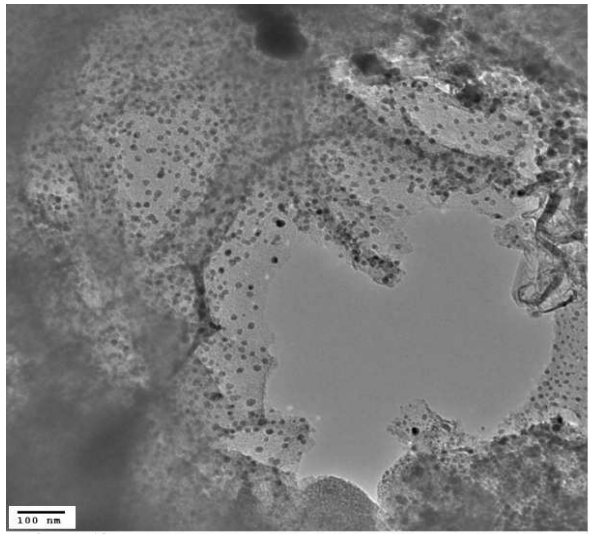

(c) Ni-AC-AH

Figure 4.5. TEM of activated carbon supported nickel catalysts. (a) Ni-AC-N, (b) Ni-AC-A, (c) Ni-AC-AH

4.3.2.Catalyst Activity

4.3.2.1. Influence of Reforming Temperature and Catalyst on Toluene Removal

It can be seen that the temperature significantly influence toluene conversion. Nickel precursor also greatly affected toluene conversion (see Figure 4.6). Catalyst prepared from nickel nitrate precursor (Ni-AC-N) showed the highest toluene conversion (72% and 80% at 600 and 700 °C respectively), whereas catalysts prepared from nickel acetate (Ni-AC-A and Ni-AC-AH) showed lower toluene conversion (58% and 65% for Ni-AC-A, 63% and 72% for Ni-AC-AH at 600 and 700 °C respectively). The lower activity of catalysts prepared from nickel acetate than catalyst prepared from nickel nitrate was probably due to lower dispersion and larger metal nickel particle sizes as seen from the results of XRD and TEM. The lower catalyst activity was also probably due to the incomplete reduction of nickel acetate. Wojcieszak et al. [29] found that catalyst with nickel acetate precursor was more difficult to be reduced than catalyst with nickel nitrate precursor. The nickel acetate precursor was not completely reduced by hydrogen at temperature below 733 K while the nickel nitrate catalyst could be easily reduced into metal nickel (Ni^0, 0 state) at 623 K [29]. The nickel nitrates precursor was able to reduce at such low temperature because nickel nitrates species could easily be calcined into NiO even at low temperature (500 K) [9].

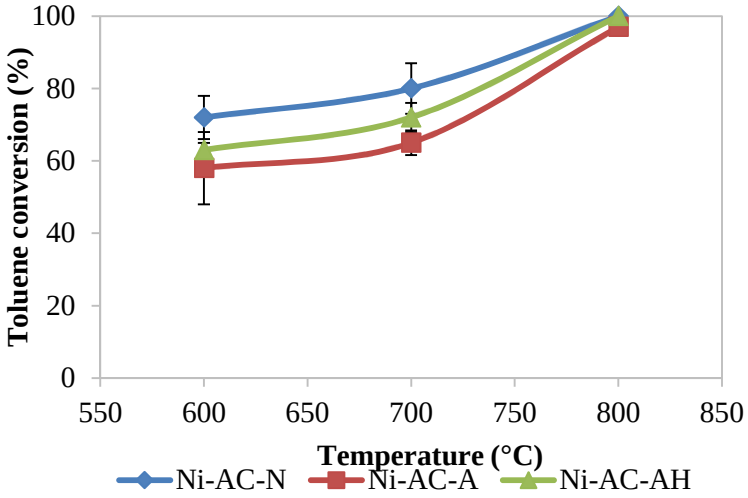

Figure 4.6. Toluene conversion at different temperature (600-800 °C)

Performances of various catalysts in steam reforming of toluene as model tar have been studied (Table 4.2) and different tar removing efficiencies have been reported. The efficiency of Ni-AC-N was close to other nickel catalysts reported in literature [23] and [30] and the efficiency of Ni-AC-A was lower than those catalysts. However, direct comparison of different catalysts in different studies may not be reasonable, because reforming conditions, such as steam to carbon ratio and space time, were different. Those conditions were proven to affect catalyst performance. For instance, two space times were used to test activity of three commercial catalysts (Cerium zirconium platinum, Hifuel R110 and Reformax 250) by Mudinoor et al. [31] and the results showed that high space velocity heavily enhanced the catalysts' efficiency.

Table 4.2. Catalytic performance of different catalysts in literatures

Catalyst	Temperature (°C)	Space time (kg_{cat} h/m^3)	Toluene conversion (%)	Reference
Ni/Olivine	600-850	9[1]	74-100	[23]
Ni-CeO_2/SBA-15	700-850	16[1]	80-99	[30]
Cerium zirconium platinum	700	7.5E-4 - 1.26E-3[2]	70-95	[31]
Hifuel R110	700	7.5E-4 - 1.26E-3[2]	80-97	[31]
Reformax 250	700	7.5E-4 - 1.26E-3[2]	75-93	[31]

[1] defined as the catalyst weight over the volumetric flow rate of toluene vapor

[2] defined as the catalyst weight over the volumetric flow rate of total gas flow

4.3.2.2. Influence of Reforming Temperature and Catalyst on Gas Composition and Benzene Yield

Various reactions mechanisms have been hypothesized in literatures during toluene reforming and are summarized as follows [23, 32]:

Steam reforming: $C_7H_8 + 7H_2O \rightarrow 7CO+11H_2$ (Equation 4.4)

$C_7H_8 + 14H_2O \rightarrow 7CO_2 + 18H_2$ (Equation 4.5)

Water gas shift: $CO + H_2O \leftrightarrow CO_2 + H_2$ (Equation 4.6)

Dry reforming: $C_7H_8 + 7CO_2 \rightarrow 14CO + 4H_2$ (Equation 4.7)

Hydrodealkylation: $C_7H_8 + H_2 \rightarrow C_6H_6 + CH_4$ (Equation 4.8)

Methane steam reforming: $CH_4 + H_2O \leftrightarrow CO + 3H_2$ (Equation 4.9)

Water gas reaction: $C+H_2O \leftrightarrow CO+H_2$ (Equation 4.10)

Boudouard reaction: $C+CO_2 \leftrightarrow 2CO$ (Equation 4.11)

As shown in Figure 4.7, low benzene yield was observed at all conditions (0-2%), except for Ni-AC-A catalyst at 600 and 700 °C (4-9%). For all catalysts, benzene yield decreased as the reaction temperature increased from 600 to 800 °C. The decrease in benzene yield was probably because high temperature promoted the decomposition of benzene into permanent gases. Benzene is more thermally stable than toluene and its decomposition requires more energy [33].

The primary gas product of steam reforming of toluene was H_2 followed by CO and CO_2 (see Figure 4.7). CH_4 was not detected in any experiments. The absence of methane in the final products indicated that methane, as an intermediate of hydrodealkylation reaction, was consumed by methane steam reforming. The H_2 content and CO_2 decreased as the temperature increased from 600 to 700 °C while the CO content increased with decrease in temperature. This might be caused by the improved endothermic reverse water gas shift reaction (Equation 4.6) at high temperature[30]. This trend was also reported by Tao et al. [30] during steam reforming of toluene over Ni/SBA-15 catalyst. The selectivity of product gas was not calculated in this study as carbon support was found to react with hydrogen when nickel was loaded on carbon [13].

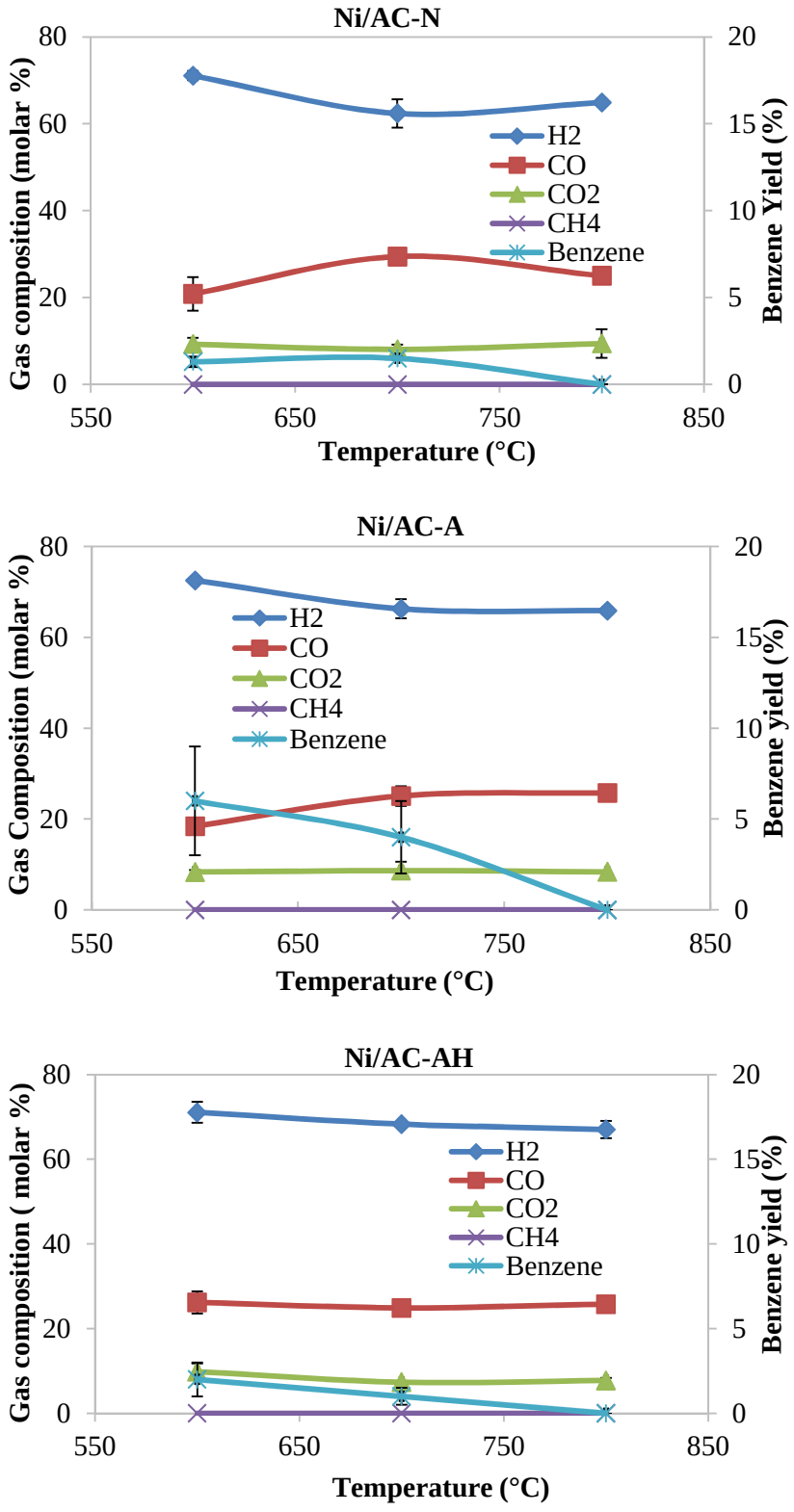

Figure 4.7. Gas composition in product gas of toluene steam reforming as a function of temperature (dry and nitrogen free basis).

4.4.Conclusions

Red cedar char produced from a downdraft bed gasification was chemically activated into activated carbon and used as a support for preparing char-nickel catalyst. The effects of nickel salts precursor, nitric acid treatment of support and reduction of nickel in hydrazine medium on catalyst performance were studied.

Nickel nitrate was found to be a better nickel precursor for preparing char supported nickel catalyst. The catalytic efficiency of toluene removal for the three catalysts was ranked from highest to lowest as Ni-AC-N > Ni-AC-AH > Ni-AC-A. Nickel particle size of the catalyst impregnated with nickel nitrate (Ni-AC-N) was smaller than that of catalyst impregnated with nickel acetate (Ni-AC-A and Ni-AC-AH). The particle size of catalyst impregnated with nickel acetate decreased with hydrazine reduction but was still larger than catalyst impregnated with nickel nitrate. The primary gas product of steam reforming of toluene was H_2 followed by CO and CO_2. The H_2 content and CO_2 decreased as the temperature increased from 600 to 700 °C while the CO content increased with decrease in temperature.

4.5. References

[1] T.A. Milne, R.J. Evans, Biomass Gasifier “Tars”:Their Nature, Formation, and Conversion, in, National Renewable energy laboratory, Golden Colorado, 1998.

[2] Z. Abu El-Rub, E.A. Bramer, G. Brem, Review of catalysts for tar elimination in Biomass gasification processes, Industrial & engineering chemistry research, 43 (2004) 6911-6919.

[3] L. Wang, D. Li, M. Koike, H. Watanabe, Y. Xu, Y. Nakagawa, K. Tomishige, Catalytic performance and characterization of Ni–Co catalysts for the steam reforming of biomass tar to synthesis gas, Fuel.

[4] S. Rapagnà, K. Gallucci, M. Di Marcello, M. Matt, M. Nacken, S. Heidenreich, P.U. Foscolo, Gas cleaning, gas conditioning and tar abatement by means of a catalytic filter candle in a biomass fluidized-bed gasifier, Bioresource Technology, 101 (2010) 7123-7130.

[5] S. Anis, Z.A. Zainal, Tar reduction in biomass producer gas via mechanical, catalytic and thermal methods: A review, Renewable and Sustainable Energy Reviews, 15 (2011) 2355-2377.

[6] G.P. Van Der Laan, A.A.C.M. Beenackers, Kinetics and Selectivity of the Fischer–Tropsch Synthesis: A Literature Review, Catalysis Reviews, 41 (1999) 255-318.

[7] Z. Abu El-Rub, E.A. Bramer, G. Brem, Experimental comparison of biomass chars with other catalysts for tar reduction, Fuel, 87 (2008) 2243-2252.

[8] X. Zheng, S. Zhang, J. Xu, K. Wei, Effect of thermal and oxidative treatments of activated carbon on its surface structure and suitability as a support for barium-promoted ruthenium in ammonia synthesis catalysts, Carbon, 40 (2002) 2597-2603.

[9] M. Domingogarcia, I. Fernandezmorales, F.J. Lopezgarzon, Activated Carbons as Supports for Nickel-Catalysts, Appl Catal a-Gen, 112 (1994) 75-85.

[10] G.M.K. Abotsi, A.W. Scaroni, A review of carbon-supported hydrodesulfurization catalysts, Fuel Processing Technology, 22 (1989) 107-133.

[11] M. Molina-Sabio, V. Pérez, F. Rodríguez-Reinoso, Impregnation of activated carbon with chromium and copper salts: Effect of porosity and metal content, Carbon, 32 (1994) 1259-1265.

[12] A.E. Aksoylu, M. Madalena, A. Freitas, M.F.R. Pereira, J.L. Figueiredo, The effects of different activated carbon supports and support modifications on the properties of Pt/AC catalysts, Carbon, 39 (2001) 175-185.

[13] R. Wojcieszak, M. Zieliński, S. Monteverdi, M.M. Bettahar, Study of nickel nanoparticles supported on activated carbon prepared by aqueous hydrazine reduction, J Colloid Interf Sci, 299 (2006) 238-248.

[14] H. Li, D. Yu, Y. Hu, P. Sun, J. Xia, H. Huang, Effect of preparation method on the structure and catalytic property of activated carbon supported nickel oxide catalysts, Carbon, 48 (2010) 4547-4555.

[15] J.-x. Guo, J. Liang, Y.-H. Chu, M.-C. Sun, H.-Q. Yin, J.-J. Li, Desulfurization activity of nickel supported on acid-treated activated carbons, Applied Catalysis A: General, 421–422 (2012) 142-147.

[16] Q. Xie, X.L. Zhang, Q.R. Chen, G.Z. Gong, Influence of surface modification by nitric acid on the dispersion of copper nitrate in activated carbon, New Carbon Mater., 18 (2003) 203-208.

[17] A.G. Boudjahem, S. Monteverdi, M. Mercy, M.M. Bettahar, Study of nickel catalysts supported on silica of low surface area and prepared by reduction of nickel acetate in aqueous hydrazine, Journal of Catalysis, 221 (2004) 325-334.

[18] M.M. Bettahar, R. Wojcieszak, S. Monteverdi, NiAg catalysts prepared by reduction of Ni2+ ions in aqueous hydrazine: II. Support effect, J Colloid Interf Sci, 332 (2009) 416-424.

[19] Y. Shen, K. Yoshikawa, Recent progresses in catalytic tar elimination during biomass gasification or pyrolysis—A review, Renewable and Sustainable Energy Reviews, 21 (2013) 371-392.

[20] R. Michel, A. Łamacz, A. Krzton, G. Djéga-Mariadassou, P. Burg, C. Courson, R. Gruber, Steam reforming of α-methylnaphthalene as a model tar compound over olivine and olivine supported nickel, Fuel, 109 (2013) 653-660.

[21] G. Guan, G. Chen, Y. Kasai, E.W.C. Lim, X. Hao, M. Kaewpanha, A. Abuliti, C. Fushimi, A. Tsutsumi, Catalytic steam reforming of biomass tar over iron- or nickel-based catalyst supported on calcined scallop shell, Applied Catalysis B: Environmental, 115–116 (2012) 159-168.

[22] H. Liu, T. Chen, X. Zhang, J. Li, D. Chang, L. Song, Effect of Additives on Catalytic Cracking of Biomass Gasification Tar over a Nickel-Based Catalyst, Chinese Journal of Catalysis, 31 (2010) 409-414.

[23] D. Świerczyński, S. Libs, C. Courson, A. Kiennemann, Steam reforming of tar from a biomass gasification process over Ni/olivine catalyst using toluene as a model compound, Applied Catalysis B: Environmental, 74 (2007) 211-222.

[24] K. Patil, P. Bhoi, R. Huhnke, D. Bellmer, Biomass downdraft gasifier with internal cyclonic combustion chamber: Design, construction, and experimental results, Bioresour. Technol., 102 (2011) 6286-6290.

[25] L.-Y. Hsu, H. Teng, Influence of different chemical reagents on the preparation of activated carbons from bituminous coal, Fuel Processing Technology, 64 (2000) 155-166.

[26] C. Moreno-Castilla, F. Carrasco-Marín, M.V. López-Ramón, M.A. Alvarez-Merino, Chemical and physical activation of olive-mill waste water to produce activated carbons, Carbon, 39 (2001) 1415-1420.

[27] F.M. Josuinkas, C.P.B. Quitete, N.F.P. Ribeiro, M.M.V.M. Souza, Steam reforming of model gasification tar compounds over nickel catalysts prepared from hydrotalcite precursors, Fuel Processing Technology, 121 (2014) 76-82.

[28] G. Lagos, R. García, A.L. Agudo, M. Yates, J.L.G. Fierro, F.J. Gil-Llambías, N. Escalona, Characterisation and reactivity of Re/carbon catalysts in hydrodesulphurisation of

dibenzothiophene: Effect of textural and chemical properties of support, Applied Catalysis A: General, 358 (2009) 26-31.

[29] R. Wojcieszak, M. Zielinski, S. Monteverdi, M.M. Bettahar, Study of nickel nanoparticles supported on activated carbon prepared by aqueous hydrazine reduction, J Colloid Interf Sci, 299 (2006) 238-248.

[30] J. Tao, L. Zhao, C. Dong, Q. Lu, X. Du, E. Dahlquist, Catalytic Steam Reforming of Toluene as a Model Compound of Biomass Gasification Tar Using Ni-CeO2/SBA-15 Catalysts, Energies, 6 (2013) 3284-3296.

[31] A. Mudinoor, D. Bellmer, L. Marin, A. Kumar, R. Huhnke, Conversion of Toluene(Model Tar) Using Selected Steam Reforming Catalysts, Transactions of the ASABE, 54 (2011) 1819-1827.

[32] P.N. Bhandari, A. Kumar, D.D. Bellmer, R.L. Huhnke, Synthesis and evaluation of biochar-derived catalysts for removal of toluene (model tar) from biomass-generated producer gas, Renew Energ, 66 (2014) 346-353.

[33] M. Kong, Q. Yang, J. Fei, X. Zheng, Experimental study of Ni/MgO catalyst in carbon dioxide reforming of toluene, a model compound of tar from biomass gasification, International Journal of Hydrogen Energy, 37 (2012) 13355-13364.

[34] L.S. Marin, Treatment of biomass-derived synthesis gas using commercial steam reforming catalysts and biochar, in: Biosystems engineering, Oklahoma state university, Stillwater, 2011.

[35] J. Delgado, M.P. Aznar, J. Corella, Biomass Gasification with Steam in Fluidized Bed: Effectiveness of CaO, MgO, and CaO−MgO for Hot Raw Gas Cleaning, Industrial & Engineering Chemistry Research, 36 (1997) 1535-1543.

[36] L. Devi, K.J. Ptasinski, F.J.J.G. Janssen, S.V.B. van Paasen, P.C.A. Bergman, J.H.A. Kiel, Catalytic decomposition of biomass tars: use of dolomite and untreated olivine, Renew Energ, 30 (2005) 565-587.

[37] J. Corella, J.M. Toledo, M.-P. Aznar, Improving the Modeling of the Kinetics of the Catalytic Tar Elimination in Biomass Gasification, Industrial & Engineering Chemistry Research, 41 (2002) 3351-3356.

CHAPTER V

NATHAPLENE REFORMING OVER CHAR BASED CATALYST

Abstract: Polyaromatic tar compounds, such as naphthalene, are difficult to crack and have not been studied extensively in the literature. In this study, a char based nickel catalyst was used for steam reforming of naphthalene and toluene. Effect of temperature on catalyst performance was studied. Results indicated that increase in temperature significantly increased the reforming efficiency of both toluene and naphthalene: the toluene conversion increased from 36% to 99% and the naphthalene conversion increased from 37% to 93% as temperature increased from 700 to 900 °C. H_2 was the main gas product followed by CO and CO_2. CH_4 was not found in product gas. Fresh and used catalysts were characterized by SEM and N_2 isotherm. SEM pictures showed that fresh catalyst maintained fibrous structure of red cedar. However, destruction of fibrous structure of catalyst was observed after the use. The surface area of the used catalyst (265 m^2/g) was significantly lower than that of the fresh catalyst (965 m^2/g). The fresh catalyst was primarily composed of micropores (74 %), followed by mesopores (26 %), while the used catalyst was primarily composed of mesopores (59%) followed by micropores (22%) and macropores (19%). The decrease in surface area of catalyst after use was caused by coking and destruction.
Keywords: naphthalene; steam reforming; char; catalyst

5.1. Introduction

Syngas derived from biomass gasification can be used for production of hydrocarbon- fuels, chemicals and power. However, unprocessed syngas cannot be used directly because it contains unacceptably high concentration of tar, which may deactivate downstream catalysts and condense on pipes and reactors. Biomass gasification tar is a complex mixture that contains hundreds of aromatic compounds. The components in biomass tar can be categorized tar into five classes (see Table 5.1): undetectable, heterocyclic, light aromatic hydrocarbons (LAH), light polyaromatic hydrocarbons (LPAH) and heavy polyaromatic hydrocarbons (HPAH) [1].

Table 5.1. Classification of tar components, adapted from reference [1]

Tar class	Class name	Property	Representative compounds
1	GC-undetectable	Very heavy tars, cannot be detected by GC	Determined by subtracting the GC-detectable tar fraction from the total gravimetric tar
2	Heterocyclic	Tars containing hetero atoms; highly water soluble compounds	Pyridine, phenol, cresols, quinoline, isoquinoline, dibenzophenol
3	Light aromatic (1 ring)	Usually light hydrocarbons with single ring; do not pose a problem regarding condensability and solubility	Toluene, ethylbenzene, xylenes, styrene
4	Light PAH compounds (2–3 rings)	2 and 3 rings compounds; condense at low temperature even at very low concentration	Indene, naphthalene, methylnaphthalene, biphenyl, acenaphthalene, fluorene, phenanthrene, anthracene
5	Heavy PAH compounds (4–7 rings)	Larger than 3-ring, these components condense at high-temperatures at low concentrations	Fluoranthene, pyrene, chrysene, perylene, coronene

Many researchers have studied the tar reforming process using model tar compounds instead of real tar, because of the complexity in using real tar. The common tar model components used are toluene, benzene, phenol, naphthalene and pyrene. Toluene and benzene represent one-ring compounds. Naphthalene represents 2-ring compounds, which are major tar component produced in high temperature gasification. Phenol represents heterocyclic compounds produced primarily at gasification temperature lower than 800 °C [2]. Pyrene represents 3-ring and higher compounds.

Coll et al. [3] studied the reactivity of five model biomass gasification tars in the literature, during steam reforming. Their research showed the order of reactivity to be benzene > toluene >anthracene > pyrene > naphthalene. Most of the paper reported the steam reforming performance using one-ring compounds such as toluene and benzene [4-6], and only limited study is available on reforming of model compounds with multiple rings.

Char-based catalyst is a cost-effective alternative for other transition metal-based catalysts [5], such as Ni/Al catalyst. Many studies have successfully applied char-based catalysts in various applications including removal of tars [7-9]. In this study, steam reforming of naphthalene and toluene was studied using char-based nickel catalyst. Toluene was used as light monoaromatic model tar compound. Naphthalene was used as light polyaromatic model tar compound because high molecular weight compounds, such as naphthalene, are difficult to crack and have not been studied extensively.

5.2. Material and Method

5.2.1. Catalyst Preparation

The raw char, used as the precursor for catalyst support material, was produced through air gasification in a pilot scale downdraft gasifier using eastern redcedar (obtained locally in Stillwater, OK, USA) as the biomass. The biomass to air equilibrium ratio for gasification was 0.2 and the gasification temperature was approximately 900 °C. Char was then activated and impregnated with nickel nitrated (Ni-AC-N). The detailed preparation procedure of catalyst is described in chapter 4.

5.2.2. Catalyst Characterization

Surface areas and pore properties were measured via N_2 isothermal adsorption using a surface area analyzer (Autosorb-1C, Quantachrome, Boynton Beach, FL, USA). Data were analyzed using the Brunauer–Emmett–Teller (BET) theory. The morphologies of the activated carbon, fresh and used catalyst (used in reforming for 2 h) were examined by Scanning Electron Microscopy (SEM) (FEI Quanta 600, FEI Company, Hillsboro, OR, USA).

5.2.3. Catalyst Tests

The catalytic reforming tests were performed in a fixed bed reactor with a 1/2 inch inner diameter. All pipes were heated at 230 °C to prevent tar condensation. The catalyst was reduced in 200 ml/min hydrogen (50% hydrogen, 50% nitrogen) flow at 350 °C for 3 h before testing. Conditioning temperatures were 700, 800 and 900 °C. Naphthalene was used in a solution with toluene as solvent (10 wt. % of naphthalene). During testing, 150 ml/min flow rate of nitrogen controlled by mass flow controller (Burkert, Charlotte, NC, USA) was introduced into the reactor. The water and naphthalene/ toluene mixture were injected into evaporator by syringe pumps (KDS scientific, model 200, Holliston, MA, USA) and then carried by nitrogen gas into reactor. The feeding rates of water and naphthalene/toluene mixture were adjusted to achieve steam to carbon ratio of 2. The gas hourly space velocities (GHSV) were about 8,000 h^{-1}. Sample was injected at about 50 min.

All product gases (hydrogen, carbon monoxide, carbon dioxide and methane) were collected in a 1 liter gas bag and analyzed by a Varian gas chromatograph with FID detector (Model CP-3800, Varian, Inc., Palo Alto, CA, USA) and installed with a packed column (HayeSep DB). The toluene and naphthalene was measured by an Agilent gas chromatograph installed with a capillary column (DB-5) and a mass spectroscopy detector (GC 7980A, MS 5975, Agilent, Santa Clara, CA, USA).

The tar conversion can be defined by Equation 5.1 [10]:

$$\text{Conversion}\ (\%) = \frac{C_{tar}^{in} - C_{tar}^{out}}{C_{tar}^{in}} \times 100 \qquad \text{(Equation 5.1)}$$

Where C_{tar}^{in} and C_{tar}^{out} were the model tar (naphthalene or toluene) molar flow rates of the inlet and outlet gases. Benzene yield as Equation 5.2 [10]:

$$\text{Benzene yield}(\%) = \frac{6 \times C_{benzene}^{out}}{7C_{toluene}^{in} + 10C_{naphthalene}^{in}} \times 100 \qquad \text{(Equation 5.2)}$$

Gas composition was calculated as Equation 5.3 [10]:

$$\text{Gas composition (\%)} = \frac{\text{mole of each gas product}}{\text{total mole of gas products } (H_2+CO+CO_2+CH_4)} \times 100 \quad \text{(Equation 5.3)}$$

5.3. Results and Discussion

5.3.1. Catalyst Activity for Naphthalene/Toluene Steam Reforming

The results of toluene and naphthalene steam reforming are shown in Figure 5.1. When temperature was below 900 °C, the conversions of toluene and naphthalene were similar. At 900 °C, the conversion of toluene was significantly higher than that of naphthalene. Increase in temperature significantly increased reforming efficiencies of both toluene and naphthalene: the toluene conversion increased from 36% to 99% and naphthalene conversion increased from 37% to 92% as temperature increased from 700 to 900 °C.

The conversion of toluene alone (no naphthalene addition in toluene) was presented in chapter 4. Compared to the data presented in chapter 4, the conversion of toluene alone (without naphthalene) was significantly higher than that of naphthalene/toluene done in this chapter. The conversion of toluene alone in chapter 4 was 87% at 700 °C, while conversion was only 36% for naphthalene/toluene reforming. This indicated that steam reforming of toluene in naphthalene/toluene was more difficult than steam reforming of toluene alone. This phenomena was also found by Jess [11] during catalytic reforming of naphthalene and benzene in the presence of hydrogen and steam. Jess found that the conversion of benzene during catalytic reforming of benzene/naphthalene was significantly lower than conversion of benzene only (with no naphthalene). The decrease of benzene removal efficiency in the presence of naphthalene was explained as follows: the adsorption of naphthalene on the surface of the catalyst occurred strongly, thereby decreasing the conversion of benzene. Benzene adsorbed only weakly and thus did not influence the catalytic conversion. For this study, temperature below 900 °C, naphthalene did not completely reform and the unconverted naphthalene strongly adsorbed on the surface of

the catalyst. As a result, adsorbed naphthalene might have covered the active sites on catalyst and affected the reforming efficiency.

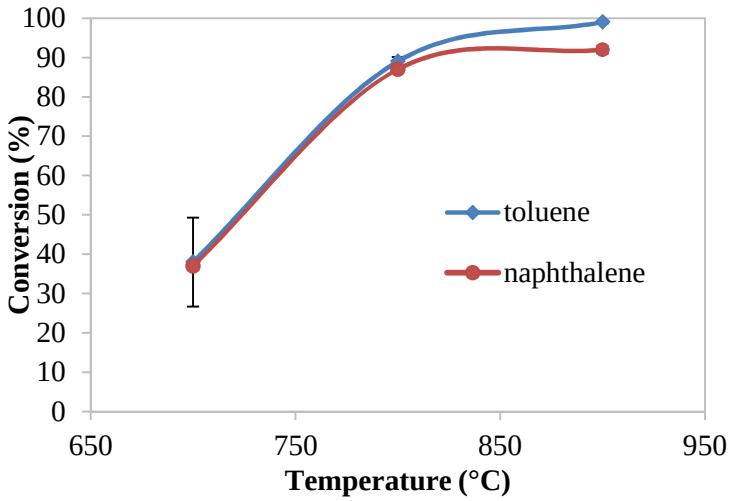

Figure 5.1. Naphthalene and toluene conversions of naphthalene/toluene steam reforming at different temperatures. Steam to carbon ratio: 2.0.

Benzene yield and product gas composition are presented in Figure 5.3 and Figure 5.3. The benzene yields were very low (less than 3% at three temperatures) and decreased with temperature. The benzene yields of toluene alone were presented in chapter 4. The benzene yield of naphthalene/toluene reforming was slightly higher than that of toluene alone (0-1 % at 600-800 °C).

In the product gas, H_2 was the main component at all temperatures followed by CO and CO_2. The amount of CH_4 was unnoticeable at all temperatures. H_2 molar composition was highest at 700 °C and kept nearly constant at 800-900 °C (65% for 800 °C and 66% for 900 °C). Similar to H_2, the composition of CO_2 was highest at 700 °C and held nearly constant at 800-900 °C. The CO composition showed a different trend with respect to temperature as compared to H_2 and CO_2. CO composition was the lowest (13%) at 700°C and the highest at 800 °C (28%).

Zhao et al. [12] performed thermodynamic analysis on steam reforming of toluene with different steam to carbon ratios (1.0-4.0) and temperatures (650-1500 °C). Their calculation was based on equivalent reaction described in literature [10, 12]. Trends of H_2, CO_2 and CO with respect to temperature based on thermodynamic equilibrium was different from the trends we obtained in this study's experimental data. H_2 held almost constant at all temperatures based on the thermodynamic equilibrium while it was the highest at 700 °C in our experimental results. CO composition almost linearly increased with temperature based on thermodynamic equilibrium while it was first increased then decreased with temperature. CO_2 decreased with temperature and was highest at 700 °C. Similar to the absence of methane in this study, methane was absent in thermodynamic equilibrium results. The difference in gas composition between thermodynamic equilibrium and this experiment indicates that steam reforming of naphthalene/toluene over a char based catalyst is more complicated than the equivalent reaction described in literature [10, 12].

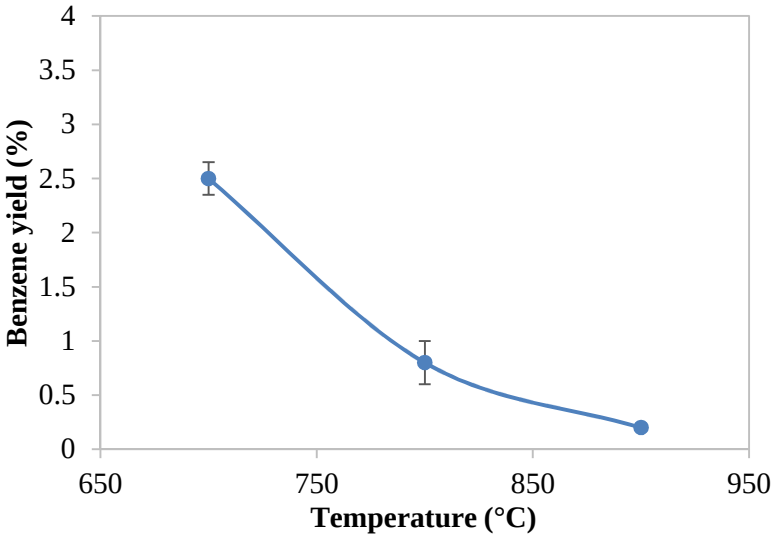

Figure 5.2. Benzene yields of naphthalene/toluene steam reforming at 700-900 °C. Steam to carbon ratio: 2.0.

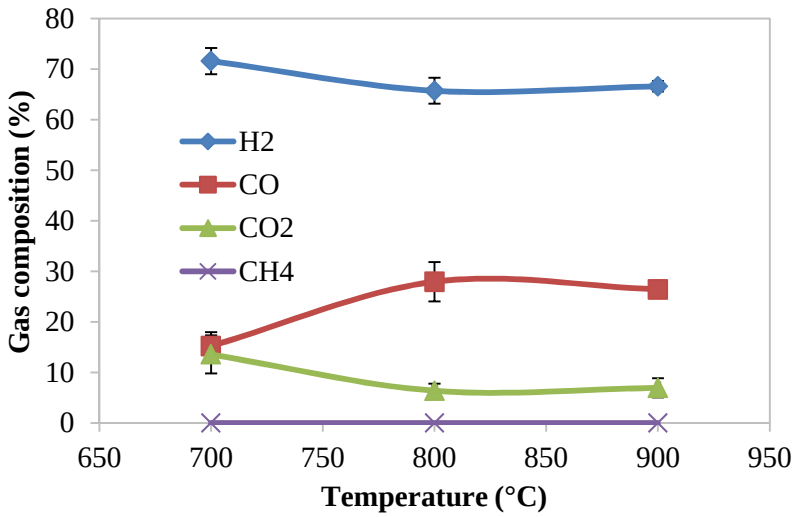

Figure 5.3. Compositions of gas resulted from naphthalene/toluene steam reforming at 700-900 °C.

5.3.2. Catalyst Characterization

Adsorption and desorption isotherms of fresh catalyst and used catalyst are presented in Figure 5.4. Detailed properties of fresh catalyst can be found in chapter 4. Pore volumes were estimated using Quenched Solid State Functional Theory (QSDFT). As discussed in chapter 3, since ultramicropore and mineral particulates that may exist on activated surfaces are not easily accessible to nitrogen at low temperature [13, 14], the micropore volume may be larger than that estimated in this study. The observed adsorption isotherm had features from type I as well as type IV isotherm, indicating that both catalysts contained pore over a wide range of pore sizes, including micropores and mesopores [15]. The significant increase in adsorbing volume at relative pressure of 1.0 on used catalyst indicated existence of macropore. Both catalysts exhibited type H4 loops which were associated with slit pores or micropore [15]. Total surface area, total pore volume and micropore volume of fresh catalyst and used catalyst were listed in Table 5.2. The surface area of used catalyst (265 m^2/g) was significantly lower than that of fresh catalyst (965m^2/g). The high percentage of total volume in micropores (< 2 nm) on fresh catalyst (74 %) indicated that the fresh catalyst was mainly composed of micropores. The used catalyst

was primarily composed of mesopores (59%) followed by micropores (22%) and macropores (19%).

Table 5.2. BET surface area and pore volume of catalysts obtained using N_2 adsorption

	Surface area (m^2/g)	V_{micro}, (cm^3/g)	V_{micro}, (%)	V_{meso}, (cm^3/g)	V_{meso}, (%)	Total pore volume (cm^3/g)
Fresh catalyst	965	0.31	73.80	0.11	26.20	0.42
Used catalyst	265	0.07	21.80	0.19	59.37	0.32

V_{micro} and V_{meso} represents micropore and mesopore volume respectively.

S_{BET} represents BET surface area.

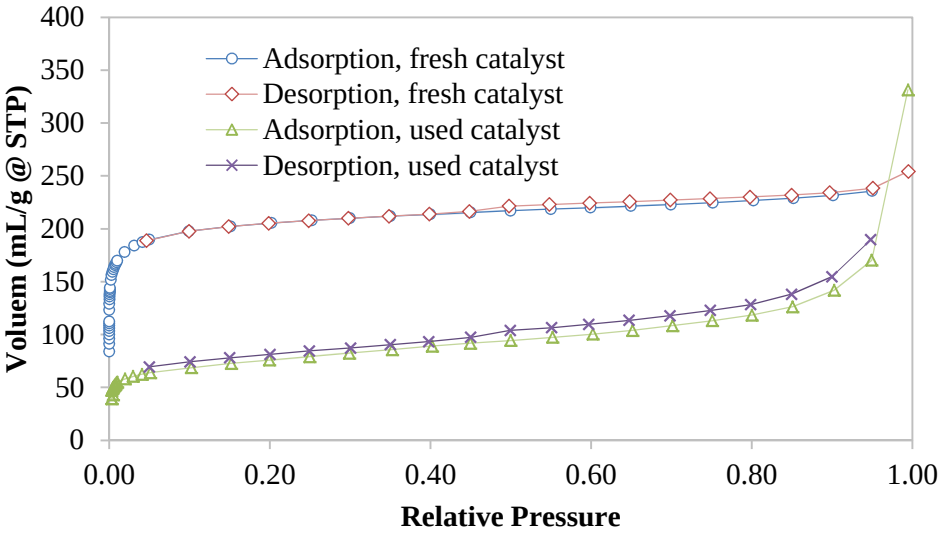

Figure 5.4. N_2 isotherm adsorption on fresh and used catalyst

The morphologies of the activated carbon, fresh and used catalyst were examined by Scanning Electron Microscopy (SEM). As shown in SEM images of activated carbon and the fresh catalysts (Figure 5.5 (a) and (b)), we can still see the basic fibrous structure of the red cedar. The micropores (< 2 nm) on activated carbon was too small to be seen due to limitation on SEM resolution. On the images of the used catalyst (Figure 5.5(c)), structural damage seemed to occur on the activated carbon support. This resulted from coking [16] and thermal degradation of the catalysts. As discussed in chapter 4, the carbon support was also found to participate in the toluene steam reforming reaction when nickel was present in the catalyst, resulting in thermal

degradation and structural damage to the carbon support. The structural destruction of the used catalyst may have caused destruction of micropore structure of the activated carbon and thus leading to significant decreases in surface area and pore volume of micropores (see Table 5.2).

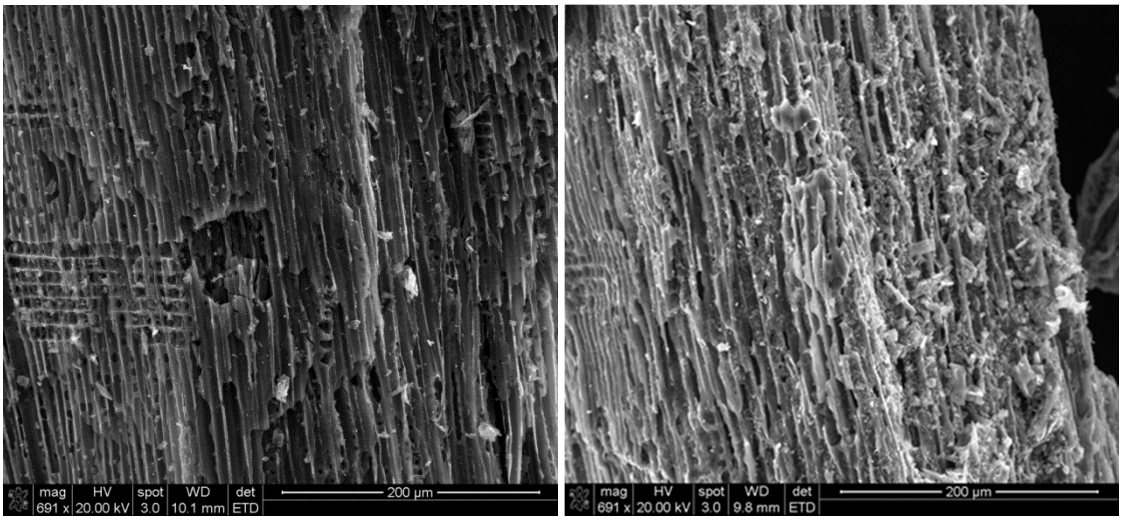

(a) (b)

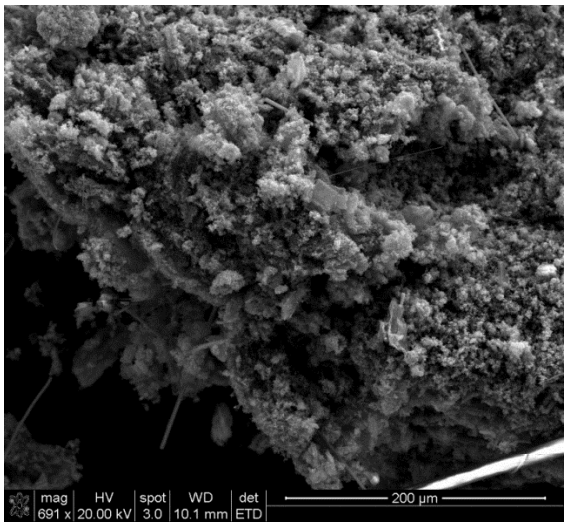

(c)

Figure 5.5. Scanning electron microscopy (SEM) images of (a) activated carbon, (b) fresh catalyst and (c) used catalyst.

Figure 5.6 shows the backscattered image of fresh catalyst and used catalyst. Only a very small amount of supported nickel appeared to scatter on the surface of fresh catalyst, since most of the nickel was impregnated in the pores of activated carbon. In comparison, a large portion of nickel particles appeared to disperse on the surface of the used catalyst. This was probably

because the impregnated nickel was exposed due to the structural destruction of the activated carbon during reforming.

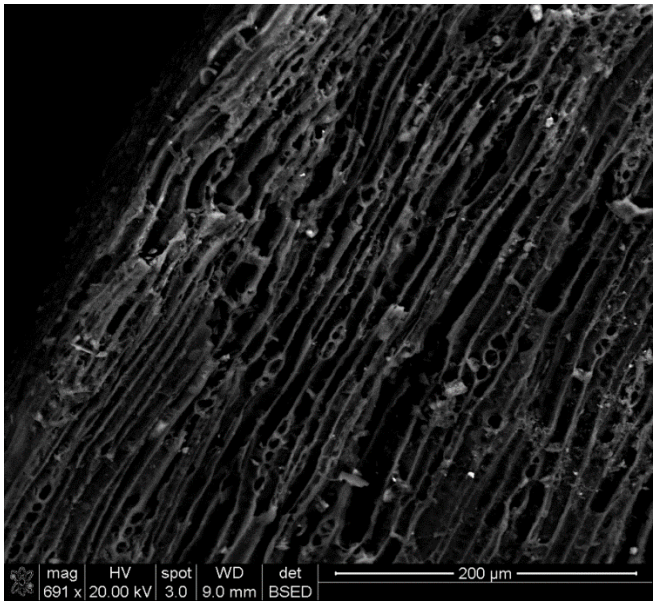

(a)

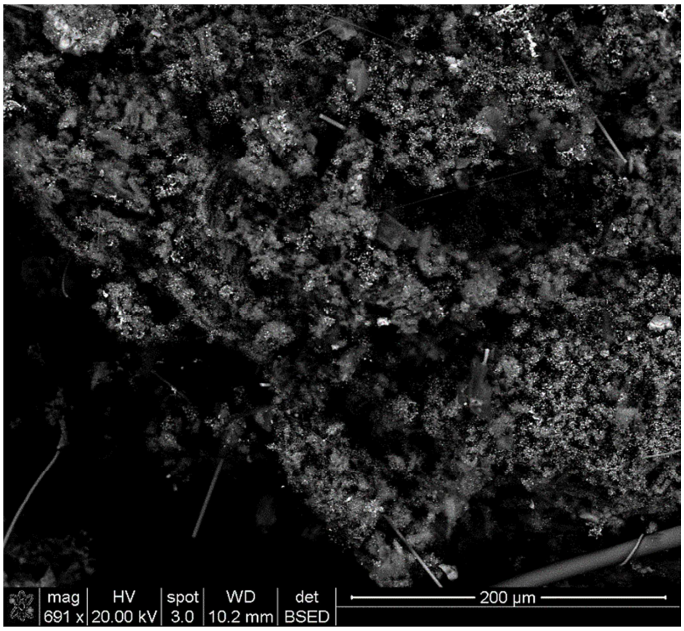

(b)

Figure 5.6. Scanning electron microscopy (SEM) backscattered images of (a) fresh catalyst and (b) used catalyst

5.4. Conclusions

A char based nickel catalyst was used for steam reforming of naphthalene/toluene. Effect of temperature on catalyst performance was studied. Results indicated that increase in temperature significantly increased the reforming efficiency of both toluene and naphthalene: the toluene conversion increased from 36% to 99% and the naphthalene conversion increased from 37% to 93% as temperature increased from 700 to 900 °C. H_2 was the main gas product followed by CO and CO_2. CH_4 was not found in product gas. Fresh and used catalysts were characterized by SEM and N_2 isotherm. The surface area of the used catalyst (265 m^2/g) was significantly lower than that of the fresh catalyst (965m^2/g). The fresh catalyst was mainly composed of micropores (74%), followed by mesopores (26%), while the used catalyst was primarily composed of mesopores (59%) followed by micropores (22%) and macropores (19%). The decrease in surface area of the catalyst after use was caused by coking and destruction.

5.5. References

[1] S. Anis, Z.A. Zainal, Tar reduction in biomass producer gas via mechanical, catalytic and thermal methods: A review, Renewable and Sustainable Energy Reviews, 15 (2011) 2355-2377.

[2] Z. Abu El-Rub, E.A. Bramer, G. Brem, Experimental comparison of biomass chars with other catalysts for tar reduction, Fuel, 87 (2008) 2243-2252.

[3] R. Coll, J. Salvadó, X. Farriol, D. Montané, Steam reforming model compounds of biomass gasification tars: conversion at different operating conditions and tendency towards coke formation, Fuel Processing Technology, 74 (2001) 19-31.

[4] D. Świerczyński, S. Libs, C. Courson, A. Kiennemann, Steam reforming of tar from a biomass gasification process over Ni/olivine catalyst using toluene as a model compound, Applied Catalysis B: Environmental, 74 (2007) 211-222.

[5] P.N. Bhandari, A. Kumar, R.L. Huhnke, Simultaneous Removal of Toluene (Model Tar), NH3, and H2S, from Biomass-Generated Producer Gas Using Biochar-Based and Mixed-Metal Oxide Catalysts, Energy & Fuels, 28 (2013) 1918-1925.

[6] T. Chen, H. Liu, P. Shi, D. Chen, L. Song, H. He, R.L. Frost, CO2 reforming of toluene as model compound of biomass tar on Ni/Palygorskite, Fuel, 107 (2013) 699-705.

[7] K. Qian, A. Kumar, H. Zhang, D. Bellmer, R. Huhnke, Recent advances in utilization of biochar, Renewable and Sustainable Energy Reviews, 42 (2015) 1055-1064.

[8] A.M. Dehkhoda, N. Ellis, Biochar-based catalyst for simultaneous reactions of esterification and transesterification, Catal. Today, 207 (2013) 86-92.

[9] W. Yuan, D. Wang, Char supported catalysts for syngas cleanup and conditioning, in, Kansas State University Research Foundation, USA, 2011.

[10] F.M. Josuinkas, C.P.B. Quitete, N.F.P. Ribeiro, M.M.V.M. Souza, Steam reforming of model gasification tar compounds over nickel catalysts prepared from hydrotalcite precursors, Fuel Processing Technology, 121 (2014) 76-82.

[11] A. Jess, Catalytic upgrading of tarry fuel gases: A kinetic study with model components, Chemical Engineering and Processing: Process Intensification, 35 (1996) 487-494.

[12] B. Zhao, X. Zhang, L. Chen, R. Qu, G. Meng, X. Yi, L. Sun, Steam reforming of toluene as model compound of biomass pyrolysis tar for hydrogen, Biomass and Bioenergy, 34 (2010) 140-144.

[13] C.R. Clarkson, R.M. Bustin, The effect of pore structure and gas pressure upon the transport properties of coal: a laboratory and modeling study. 1. Isotherms and pore volume distributions, Fuel, 78 (1999) 1333-1344.

[14] E. Cetin, R. Gupta, B. Moghtaderi, Effect of pyrolysis pressure and heating rate on radiata pine char structure and apparent gasification reactivity, Fuel, 84 (2005) 1328-1334.

[15] L. Qian, Y. Zhao, S. Sun, H. Che, H. Chen, D. Wang, Chemical/physical properties of char during devolatilization in inert and reducing conditions, Fuel Processing Technology, 118 (2014) 327-334.

[16] P.N. Bhandari, A. Kumar, D.D. Bellmer, R.L. Huhnke, Synthesis and evaluation of biochar-derived catalysts for removal of toluene (model tar) from biomass-generated producer gas, Renew Energ, 66 (2014) 346-353.

CHAPTER VI

REFORMING OF LIGNIN-DERIVED TARS OVER CHAR-BASED CATALYST USING PY-GC/MS

Abstracts: Tar removal is one of the major challenges in implementation of biomass gasification technology. Syngas tars causes formation of aerosols and soots, which plug filters, reactors and fuel lines. In this study, a char-derived catalyst was tested for removal of tar produced from pyrolysis of kraft lignin in a pyroprobe reactor. The effects of reaction temperature (700, 800 and 900 °C), water amount (5-10µl), pressure (0.1-2.2 MPa) and atmosphere (inert and hydrogen) on catalytic conditioning of tar components were assessed. The tar components were analyzed by GC/MS. Catechols were the most abundant tar components followed by phenols and guaiacols during non-catalytic kraft lignin pyrolysis. Results indicated that the char-based catalyst effectively decreased the contents of lignin tar. Reaction temperature, water loading and reaction pressure significantly affected the tar removal. An increase in reaction temperature led to an increase in removal efficiency of most tar components except naphthalene. Excessive water loading (10µl) decreased the tar removal efficiency of the char-based catalyst. High pressure promoted the catalytic conditioning of lignin tar. Tar contents decreased significantly when hydrogen was used as a gasification agent and thus promoted the conversion of lignin into non-condensable gas.

Keywords: lignin; char; catalyst; tar removal; Py-GC/MS

6.1. Introduction

Increase in global greenhouse gas emissions and concerns about global fossil fuels reserves have promoted the research in renewable energy. Biomass gasification is one type of efficient renewable energy technology converting lignocellulosic solid feedstocks into combustible gas. However, during gasification many contaminants are generated, such as NOx, SOx and tar. Particularly, the presence of considerable tar in syngas leads to formation of aerosols and soots due to repolymerization and plugs filters and fuel lines due to tar condensation [1]. Therefore, tar removal is one of the major challenges in implementation of biomass gasification technology at commercial scales for fuels, chemicals and power production.

Biomass is mainly composed of cellulose, hemicellulose and lignin. Many studies have showen that cellulose, hemicellulose and lignin produce different tar compounds [1, 2]. Primary tars produced from cellulose are furans and small molecule aldehydes [3]. Primary tars produced from hemicellulose are acetic acid [2] and those from lignin are furfurals and phenolics [4].

Table 6.1 shows the compositional analysis of switchgrass, wheat straw and eastern red cedar used in our laboratory [5]. Approximately 20-40 wt.% of biomass is composed of lignin. Lignin is a complex polymer of p-hydroxyphenyl, guaiacyl and syringyl alcohols. Three species of hydroxycinnamyl alcohols (p-coumaryl alcohol, coniferyl alcohol and sinapyl alcohol) are considered as monoligol monomers incorporated in lignin polymer structure in the form of p-hydroxyphenyl, guaiacyl, and syringyl phenylpropanoid [1, 6]. Since only the lignin fraction of the biomass is aromatic in nature, lignin represents a potential precursor for formation of polyaromatic hydrocarbon (PAH) in tar. The study of catalytic lignin-derived tar reforming is critical for understanding strategies to reduce syngas tar.

Table 6.1. Compositions of switchgrass, wheat straw and eastern redcedar. Adapted from reference [5]

Composition	Switchgrass	Wheat straw	Eastern redcedar
Glucan (% dry)	38.46 ± 0.69	39.18 ± 2.01	40.30 ± 1.50
Xylan (% dry)	26.34 ± 0.54	24.62 ± 1.36	8.50 ± 0.04
Galactan (% dry)	1.16 ± 0.18	0 ± 0	2.00 ± 0.60
Arabinan (% dry)	3.41 ± 0.32	1.68 ± 0.25	1.40 ± 1.00
Mannan (% dry)	0.13 ± 0.22	0 ± 0	6.00 ± 1.20
Lignin (% dry)	21.40 ± 0.24	17.17 ± 0.46	35.90 ± 0.70

Tar formation is affected by reaction conditions such as atmosphere and pressure. Gopakuma et al. [7] studied the hydrogen effect on formation of oxygenated compounds during pine wood pyrolysis. They found that the presence of hydrogen significantly enhanced hydrodeoxygenation, which rejected the bio-oil oxygen in the form of water [7]. As a result, yield of higher molecular weight oxygenated compounds for non-catalytic pyrolysis of pine wood under H_2 atmosphere was much lower than that under helium atmosphere [7]. The pressure will affect composition of syngas as well as tar. Knight et al. [8] studied the effect of pressure on the biomass gasification products and found that increasing pressure (from 0.8 to 2.2 MPa) decreased oxygenated species. Specifically, phenols were almost completely eliminated, but the PAH fractions increased. Research was also conducted on pressurized gasification of coal [9]. Pressurized operation not only reduced the volatile evolution during coal pyrolysis and increased char gasification rate by influencing the physical structure of pyrolysis char, but it also lowered the energy cost for compressing syngas prior to the gas turbine combustion chamber [9].

The objective of this study was to evaluate the effects of reacting pressure, temperature and atmosphere on non-catalytic and catalytic reforming of lignin tar. A char based catalyst was used in catalytic reforming. Since hydrogen is the primary component of syngas, hydrogen was used to investigate the effect of atmosphere on tar cracking.

6.2. Material and Methods

6.2.1. Chemicals and Catalyst

The potassium hydroxide was purchased from Fisher Scientific (Pittsburgh, PA, USA) and nickel nitrate was purchased from Sigma Aldrich (St. Louis, MO, USA). The lignin, named Indian AT, was provided by Mead Westvaco (Richmond, VA, USA). Indian AT is a purified form of kraft pine lignin. It is derived by hydrolysis of kraft lignin, removing the sodium and hemicellulose [10].

The char-based nickel catalyst was prepared by loading nickel on char-derived activated carbon. The activated carbon was produced using a chemical activation method from char. The char was produced from downdraft gasification of red cedar. The char was mixed with KOH and was then placed in a fixed-bed tubular reactor to activate. The reactor was heated to 300 °C and held at this temperature for 2 h to prevent carbon loss from char. For carbonization, the temperature was then raised to 800 °C and the char was activated at this temperature for 1.5 h under nitrogen flow of 200 ml/min. Activated carbon obtained was then wet impregnated with nickel nitrate solution. The catalyst precursor was dried at 105 °C for 3 h and reduced in 100 ml/min hydrogen flow at 350 °C for 3 h. Reduced catalyst was then kept in vacuum desiccator. The procedure of making this catalyst had been filed as a provisional patent with the US Patent Office.

6.2.2. Pyrolysis of Kraft Lignin in Py–GC/MS

Catalytic reforming of lignin-derived tars was performed using a commercial micro-pyrolyzer (Pyroprobe model 5200/high pressure, CDS Analytical Inc., Oxford, PA). The pyrolyzer was connected with a gas chromatograph/mass spectrometer (GC/MS, Agilent 7893). The pyrolyzer was composed of a probe and a tubular catalytic reactor. The probe was heated with a platinum heating coil, which can be heated up to 1400 ºC. The lignin powder and catalyst were packed in a quartz tube (approximately 25 mm long and 1.9 mm inner diameter), which was then held in the platinum heating coil. About 0.5 mg of lignin sample and 5 mg catalyst were

loaded in the quartz tube. To make sure all tar volatiles passed through the catalyst layer, two layers of catalysts were kept on both sides of the lignin powder. The catalyst layer and lignin layer were separated by quartz wool. In order to simulate steam gasification, 5 µl water was injected into lignin powder during non-catalytic pyrolysis. The sample was pyrolyzed at a heating rate of 1500 °C/s in presence of different gases (He, 100% and H_2 100%). To make sure the sample was completely pyrolyzed, the sample was held at pyrolysis temperature for 20 s. When helium was used as reactant gas, 40 ml/min helium was purged for about 1 min in the system before the experiment to remove air. After purging with helium, the experiment started immediately in the same helium flow. When H_2 was used as reactant gas, 40 ml/min helium was also purged for about 2 min to remove air and residual hydrogen before the gas was switched to reactant gas (H_2) with flow rate of 40 ml/min. The actual temperature inside the quartz tube (biomass temperature) was, typically, about 50-100 °C lower than the filament temperature [11, 12].

6.2.3. Tar Composition Analysis

The reactant gas carried the pyrolysis vapors (tars) from the probe to a trap (adsorbent). The trap adsorbed the condensed vapors. Non-condensable gases escaped from the trap and were not analyzed in this study. The adsorbed tar component was desorbed by heating the trap to 300 °C and purging with helium. The gaseous tar was then carried by helium gas and injected into the GC through a transfer line for compositional analysis. The transfer line was heated at 300 °C to prevent tar condensation. A gas chromatograph combined with mass spectrometer (GC/MS 7890A, 5975C, Agilent, Santa Clara, CA, USA) was used to analyze composition of tars. A capillary column (HP-5, 0.03mm OD, 3m length) was installed in GC for separating the tar components. The injector of the GC was held at 250 ºC. The column temperature was maintained at 40 ºC for 2 min and then increased to 280 ºC with a heating rate of 5 ºC /min. Helium of ultra-high purity (99.999%) was used as a carrier gas at a flowrate of 1.25 mL/min.

The mass spectrometer was configured for electron impact ionization at 70 eV, with an

interface temperature of 250 °C. Electron impact mass spectra were obtained by an Agilent 5975C mass spectrometer at the mass range from m/z 45 to 300. Tar compounds were identified by comparing the mass spectra with the NIST (National Institute of Standards and Technology) mass spectral library and the retention time of the standard compounds. The concentration of tar components were analyzed using an external standard method. 26 pyrolysis products were quantified using 24 external standards including 10 aromatic hydrocarbons, 8 phenols, 6 phenol-guaiacols, 1 furan and benzoic acid as listed in Table 6.2. 2-methyl-phenol and 4-ethylcatechol were quantified using corresponding standard from similar structure compounds [13] (P-cresol for 2-methyl-phenol and methylcatechol 4-ethylcatechol).

6.2.4. Experimental Design and Data Analysis

For non-catalytic pyrolysis of lignin, a full factorial design was performed at five pressures of 0, 0.5, 0.8, 1.1 and 2.2 MPa (0, 50, 100, 150 and 300 psig) and three temperatures of 700, 800 and 900 ºC. For catalytic pyrolysis of lignin, a full factorial design was performed at three pressures of 0.1, 0.5 and 1.1 MPa (0, 50 and 150 psig) and three temperatures of 700, 800 and 900 ºC. To study the effect of water loading on catalytic performance, the lignin was gasified with 5 or 10 µl at the three temperatures (700, 800 and 900 ºC). The lignin was also gasified under hydrogen atmosphere at 800 ºC to study the hydrogen effect on catalyst performance.

The statistical analysis was performed using JMP software (SAS Institute Inc. Cary, NC, USA). Results were analyzed at α=0.05 significance level. Polynomial surfaces were plotted using MATLAB (Mathworks, Natick, MA, USA) for total content of monoaromatic and polyaromatic hydrocarbons. The surfaces were generated approximating the tar contents to a quadratic polynomial of temperature and pressure. The coefficients for the respective surfaces are given in Figure 6.3.

6.3. Results and Discussions

The composition of tar produced from pyrolysis of lignin is complex. Tar compounds range from simple single-ring aromatics to polycyclic aromatics. This paper, however, only

analyzed and discussed compounds with boiling point below 250 °C which is detectable by GC/MS. Based on the GC/MS data collected from lignin catalytic and non-catalytic pyrolysis at 700-900 °C, around 60 tar compounds were found. Around 46 out of 60 were major compounds with relative area larger than 0.5%. The remaining 15 were minor compounds with relative percent area of less than 0.5%. The 46 major components are listed in Table 6.2 with name, retention time and family group. Out of 46 listed, 26 compounds were quantified using external standards and identified with quantification method. In the discussion that follows, the tar content for a compound was defined as

$$\mathrm{T} = \frac{\text{mass of compound in tar}}{\text{mass of lignin}} \left(\frac{\text{ng}}{\text{mg}}\right) \qquad \text{(Equation 6.1)}$$

The removal percentage was defined as

$$\text{Removal percentage (\%)} = \frac{\mathrm{T_0} - \mathrm{T}}{\mathrm{T_0}} \times 100 \qquad \text{(Equation 6.2)}$$

Where $\mathrm{T_0}$ represents content of tar produced from lignin pyrolysis with no catalyst at a certain reaction temperature; and T represents content of tar produced from lignin pyrolysis with catalyst at a specific reaction temperature.

Table 6.2. Major products from catalytic and non-catalytic pyrolysis of Kraft Lignin by GC-MS

No.	Name	CAS	Family	Chemical used for quantification
1	Benzene	071-43-2	Monoaromatic	Benzene
2	Toluene	108-88-3	Monoaromatic	Toluene
3	Ethylbenzene	100-41-4	Monoaromatic	Ethylbenzene
4	p-Xylene	106-42-3	Monoaromatic	p-Xylene
5	o-Xylene	95-47-6	Monoaromatic	o-Xylene
6	Styrene	100-42-5	Monoaromatic	Styrene
7	Phenol	108-95-2	Phenol	Phenol
8	Benzofuran	271-89-6	Furan	Benzofuran
9	Benzaldehyde, 2-hydroxy-	090-02-8	Phenol	N.A.
10	Phenol, 2-methyl-	095-48-7	Phenol	P-cresol
11	P-cresol	106-44-5	Phenol	P-cresol
12	Phenol, 2-methoxy-	090-05-1	Phenol-guaiacol	Phenol, 2-methoxy-
13	Phenol, 2,6-dimethyl-	576-26-1	Phenol	Phenol, 2,6-dimethyl-

14	Phenol, 2-ethyl-	090-00-6	Phenol	N.A.
15	Phenol, 2,4-dimethyl-	105-67-9	Phenol	Phenol, 2,4-dimethyl-
16	2-Hydroxy-5-methylbenzaldehyde	613-84-3	Phenol	N.A.
17	Phenol, 4-ethyl-	123-07-9	Phenol	N.A.
18	Phenol, 3,5-dimethyl-	108-68-9	Phenol	N.A.
19	Phenol, 2-methoxy-3-methyl-	18102-31-3	Phenol-guaiacol	N.A.
20	Indene	095-13-6	Polyaromatic	Indene
21	Naphthalene	091-20-3	Polyaromatic	Naphthalene
22	Creosol	093-51-6	Phenol-guaiacol	Creosol
23	Catechol	120-80-9	Phenol	Catechol
24	Catechol, 4-methyl	452-86-8	Phenol	Catechol, 4-methyl
25	Benzofuran, 2,3-dihydro-	496-16-2	Phenol	N.A.
26	Phenol, 3-ethyl-5-methyl-	698-71-5	Phenol	N.A.
27	Benzene, 1-ethyl-4-methoxy-	1515-95-3	Phenol	N.A.
28	2-Hydroxy-4-methylbenzoic acid	050-85-1	Phenol-guaiacol	N.A.
29	1,2-Benzenediol, 3-methyl-	488-17-5	Phenol	N.A.
30	Phenol, 4-ethyl-2-methoxy-	2785-89-9	Phenol-guaiacol	N.A.
31	1,2-Benzenediol, 4-methyl-	452-86-8	Phenol	N.A.
32	2-Methylnaphthalene	90-12-0	Polyaromatic	2-Methylnaphthalene
33	2-Methoxy-4-vinylphenol	7786-61-0	Phenol-guaiacol	2-Methoxy-4-vinylphenol
34	1,4-Benzenedicarboxaldehyde, 2-methyl-	27587-17-3	Phenol	N.A.
35	1,3-Benzenediol, 4,5-dimethyl-	527-55-9	Phenol	N.A.
36	Eugenol	097-53-0	Phenol-guaiacol	Eugenol
37	4-Ethylcatechol	1124-39-6	Phenol	Catechol
38	Vanillin	121-33-5	Phenol-guaiacol	Vanillin
39	Naphthalene, 1,5-dimethyl	571-61-9	Polyaromatic	Naphthalene, 1,5-dimethyl
40	Phenol, 4-ethyl-2-methoxy-	2785-89-9	Phenol-guaiacol	N.A.
41	Trans-Isoeugenol	5932-68-3	Phenol-guaiacol	Trans-Isoeugenol
42	Homovanillyl alcohol	2380-78-1	Phenol-guaiacol	N.A.
43	Benzoic acid, 3,5-dimethyl-	499-06-9	Carboxylic acid	Benzoic acid, 3,5-dimethyl-
44	Homovanillic acid	306-08-1	Phenol-guaiacol	N.A.
45	Phenanthrene	085-01-8	Polyaromatic	N.A.
46	Fluoranthene	0206-44-0	Polyaromatic	N.A.

N.A. represents tar component was not quantified.

6.3.1. Non-catalytic Lignin Pyrolysis

Corresponding contents of aromatic and phenolic tar compounds obtained at 700-900 °C pyroprobe temperature and 0.1 MPa (0 psig) are presented in Figure 6.1. The height of bars and the error bar presented average value and standard deviation of two replications respectively. As seen from Figure 6.1, the most abundant tar components were phenols, such as catechol, 4-methylcatechol and phenol. The second most abundant tar components were guaiacols, including creosol, 2-methoxyphenol and 2-methoxy-4-vinylphenols. Polyaromatic hydrocarbons were the least abundant in tar. Syringol groups derived from sinapyl alcohol monomers were not detected in kraft lignin tar. Large fractions of phenols and guaiacols in kraft lignin tar originated from large quantities of phenolic monomers present in the lignin polymer. Temperature significantly affected the tar composition. Most of the phenolic components in tar decreased when temperature increased from 700 to 900 °C, while the aromatic hydrocarbons increased with increasing temperature. The decrease of phenolic components with increasing temperature was consistent with data from lignin pyrolysis obtained by Zhang and Zhou [14, 15]. In their studies, the contents of phenolics in tar reached to maximum at 600 °C followed by a decrease when temperature was further increased to 700 °C.

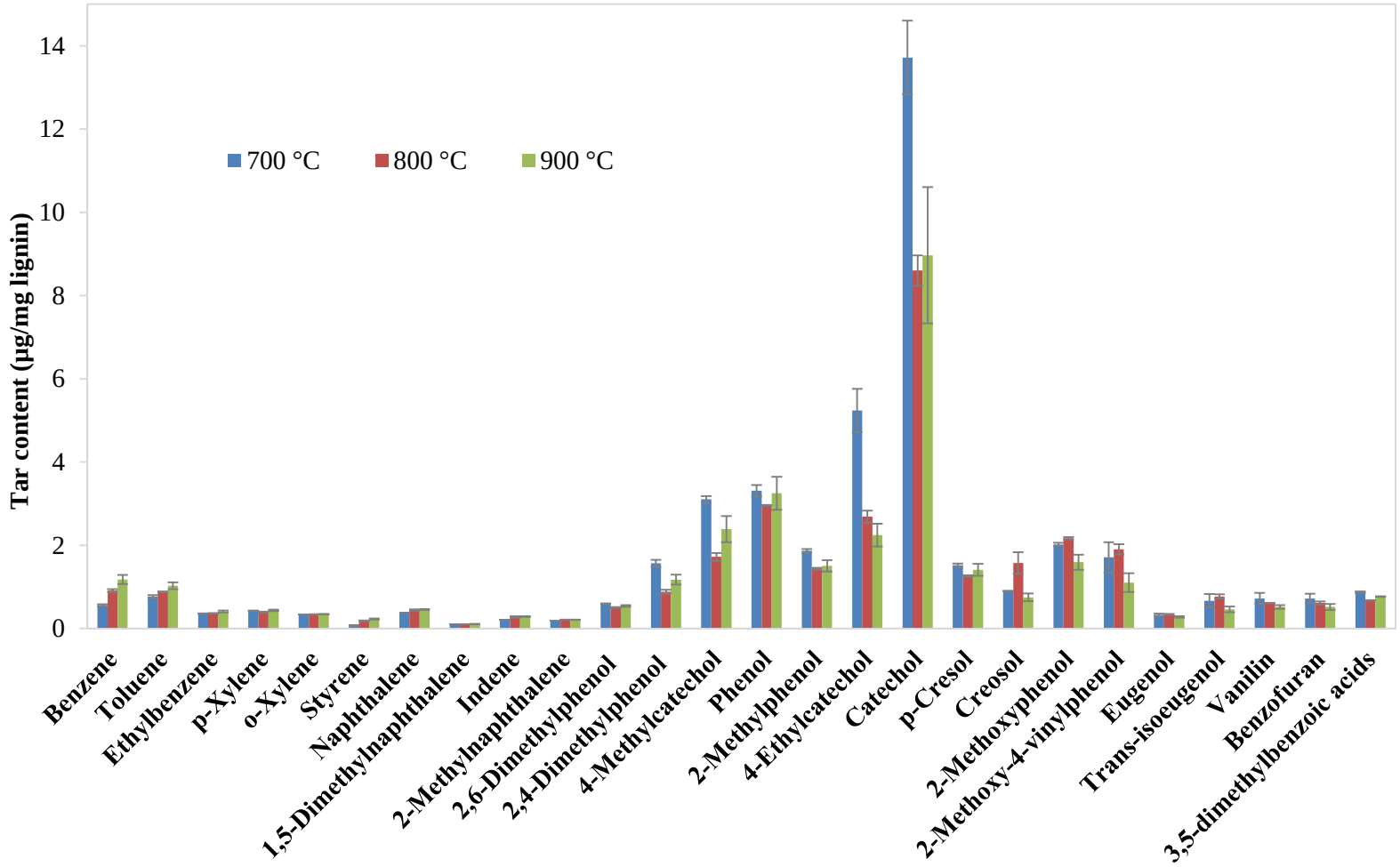

Figure 6.1. Composition of tar produced from kraft lignin pyrolysis with no catalyst at atmospheric pressure and pyrolysis temperature of 700, 800 and 900 °C.

The composition of tar obtained from kraft lignin pyrolysis in this study was different from that obtained from pyrolysis of lignin reported in literatures [16, 17]. In literatures [16, 17], syringols and guaiacols were the most abundant components followed by phenols. Catechols, one of the subspecies of phenols, were scarcely detected. In this study, tars were dominated by phenols, especially catechols. This may be caused by higher reaction temperature (700-900 °C in this study compared to 400-600 °C in literature) used in this study and presence of water. Hu et al. [6] and Jiang et al. [18] found that high temperature (>600 °C) promoted the demethoxylation and demethylation reactions on methoxyl groups, resulting in aromatic C-OCH_3 and aromatic C-O-CH_3 cracking and subsequent generation of phenols, such as phenol, cresol and catechols (see Figure 6.2). The temperature (700-900 °C) applied in this study may have favored the demethoxylation of guaiacols into phenol. On other hand, H· donor provided by water could be stabilized by aromatic O· radical generated from hemolytic cracking of aromatic O-CH_3 resulting in catechols formation (see Figure 6.2). The lack of syringols in tar may be related to the source of lignin. The syringols were not observed in the tar produced from pyrolysis and hydrogenolysis of pine lignin either [4, 19]. Thangalazhy [20] attributed the absence of syringols in tars to the missing sinapyl alcohol structures in pine wood.

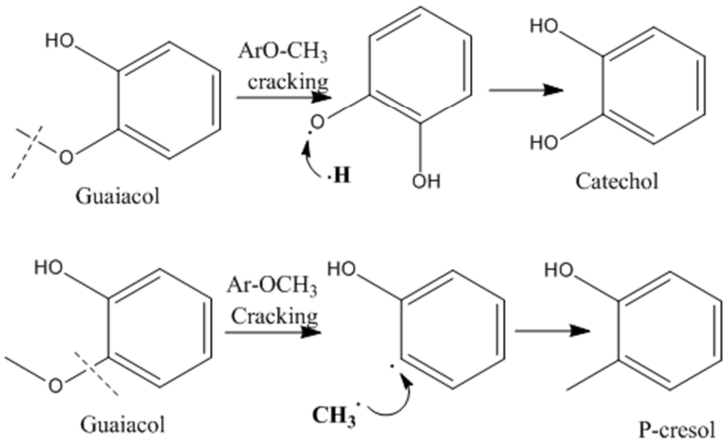

Figure 6.2. Possible cleavage mechanisms of the methoxyl group during pyrolysis. Adapted from Hu et al. [6].

The variations in total contents of monoaromatic hydrocarbons, polyaromatic hydrocarbons, phenols, and guaiacols with respect to reaction temperature and pressure are depicted in Figure 6.3 and Figure 6.4. Statistical analysis showed that temperature ($p < 0.05$) and pressure ($p < 0.05$) significantly affected production of monoaromatic hydrocarbons, polyaromatic hydrocarbons and phenols. However, guaiacols was statistically significantly affected only by pressure ($p < 0.05$) but not by temperature ($p>0.05$). The interaction of temperature and pressure was significant on phenols ($p < 0.05$) but not statistically significant on monoaromatic hydrocarbons, polyaromatic hydrocarbons and guaiacols ($p >0.05$).

Second order polynomial regression was applied to generate response surfaces of monocyclic aromatic hydrocarbons and polycyclic aromatic hydrocarbons as functions of temperature and pressure (Figure 6.3). Similar shapes of surface plots of monoaromatic hydrocarbons and polyaromatic hydrocarbons showed that these products have similar trends with respect to pressure and temperature. At a given temperature both the contents of monoaromatic and polyaromatic hydrocarbons reached a peak at 1.1 MPa (150 psig) and with increasing temperature the total contents further increased. The highest contents of monoaromatic hydrocarbons (7.2 μg/mg lignin) and polyaromatic hydrocarbons (2 μg/mg lignin) were observed at 900 °C and 1.1 MPa (150 psig).

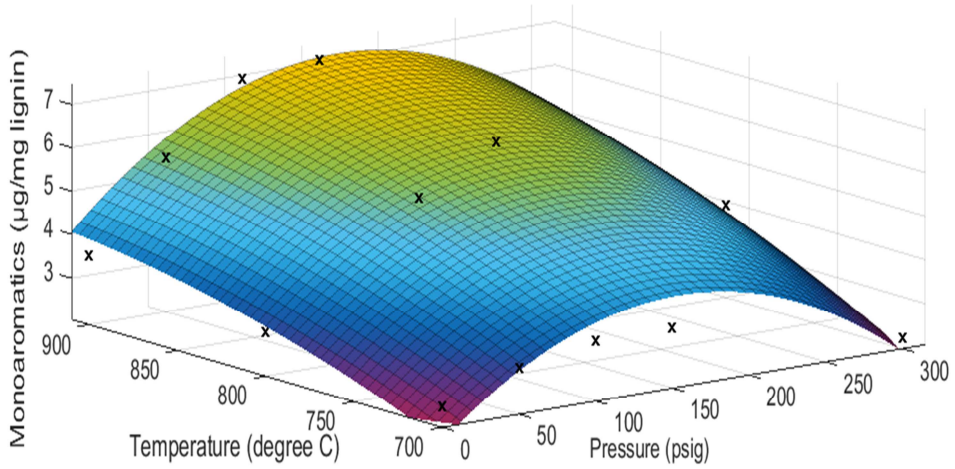

The polymonial for response surface: $f(x,y) = 5725 + 936.7x + 1148y - 1164x^2 + 162.9xy - 231.1y^2$; x is pressure and y is temperature.
R-square: 0.9139; Adjusted R-square: 0.8661
(a)

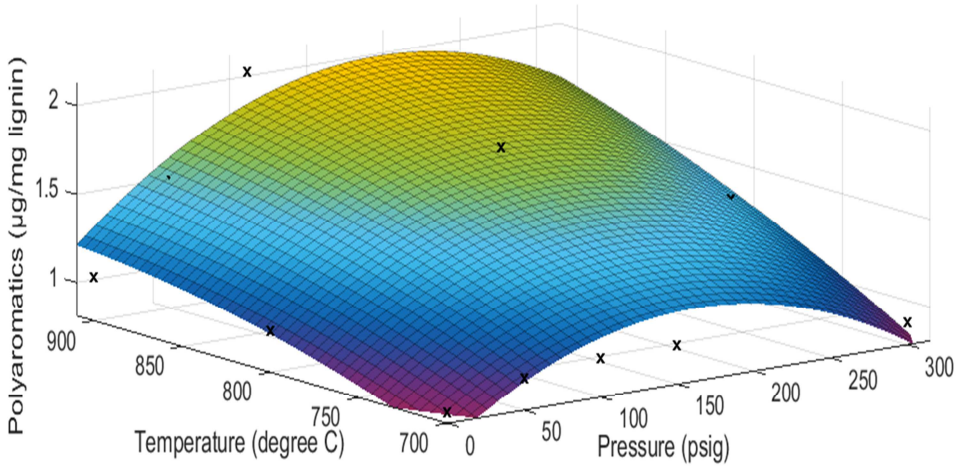

The polymonial for response surface: $f(x,y) = 1596 + 249.4x + 283.1y - 230.1x^2 + 59.51xy - 54.7y^2$; x is pressure and y is temperature.
R-square: 0.8714; Adjusted R-square: 0.8
(b)

Figure 6.3. Aromatic hydrocarbon content of tar produced from kraft lignin pyrolysis at different temperatures and pressures (a) total content of monocyclic aromatic hydrocarbon (benzene, toluene, ethylbenzene, xylene and styrene) (b) total content of polyaromatic hydrocarbon (naphthalene, 1,5-dimethynaphthalene, 2-methylnaphthalene and indene)

The optimum pressure for maximum polyaromatic hydrocarbon yield at each temperature was 1.1 MPa (150 psig). The effects of pressure on the polyaromatic hydrocarbon was explained by Mayerhofer et al. [20]. On one hand, increase in system pressure caused the reaction equilibrium to shift to fewer molecules based on equilibrium law. In order to have fewer molecules in the whole system, polyaromatics were favored at high pressure as they have the higher aromaticity. On the other hand, high pressure suppressed the evaporation of tar and extended tar residence time, which promoted the polymerization reactions forming polyaromatic hydrocarbons. However, after the pressure reached a certain value (1.1 MPa in our study) leading to the maximum residence time needed for polymerization reactions, further pressure increase may have enhanced steam reforming of polyaromatic hydrocarbons with the catalytic effect of pyrolysis-derived lignin char. In summary, moderate pressure increase (0.1-1.1 MPa) promoted the formation of polyaromatic hydrocarbons; however, further increase in pressure (up to 2.2 MPa) led to a decrease in polyaromatic hydrocarbons due to consumption in the steam reforming reaction.

Second order polynomial regression failed to generate response surfaces of phenols and guaiacols (R^2 obtained were low). Data was plotted without quadratic fitting. The trends of phenols and guaiacols with respect to reaction pressure and temperature (Figure 6.4) differed from the trends of aromatic hydrocarbons (Figure 6.3). At 0.1-1.1 MPa (0-150 psig), phenols (Figure 6.4 (a)) decreased with increase in pressure as well as temperature. Up to 2.2 MPa (300 psig), the content of phenols further decreased but hardly changed with temperature. The highest phenol content (2 μg/mg lignin) was observed at 700 °C and 0 psig, and the lowest content (2.4 μg /mg lignin) was observed at 700 °C and 2.2 MPa (300 psig). Similar to aromatic hydrocarbons and phenols, pressure significantly affected contents of guaiacols. The plot of guaiacols (Figure 6.3 (a)) showed that content of guaiacols reached a maximum at 1.1 MPa (50 psig) and decreased with further increase in pressure from 0.5 to 2.2 MPa (50 to 300 psig). No clear trend was found

for the effect of temperature on total guaiacols content. The highest guaiacol content (7.8 μg /mg lignin) was observed at 900 °C and 0.5 MPa (50 psig).

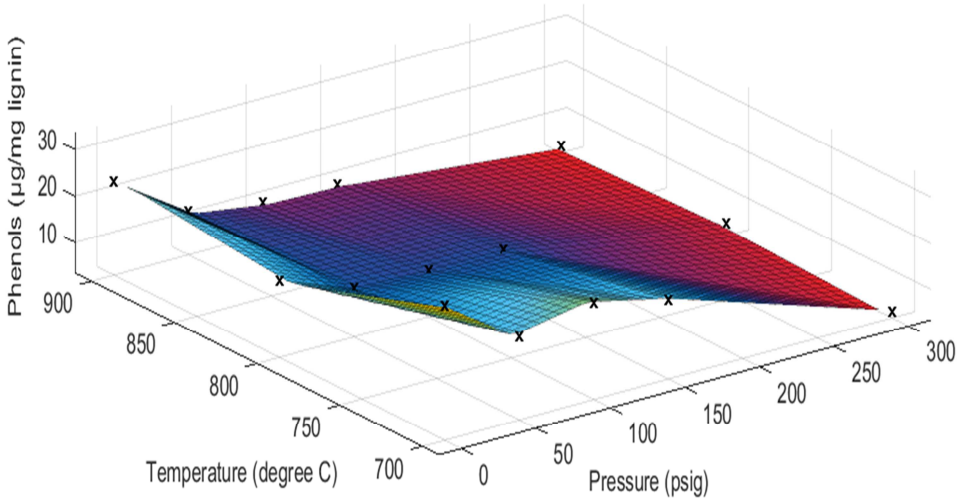

(a)

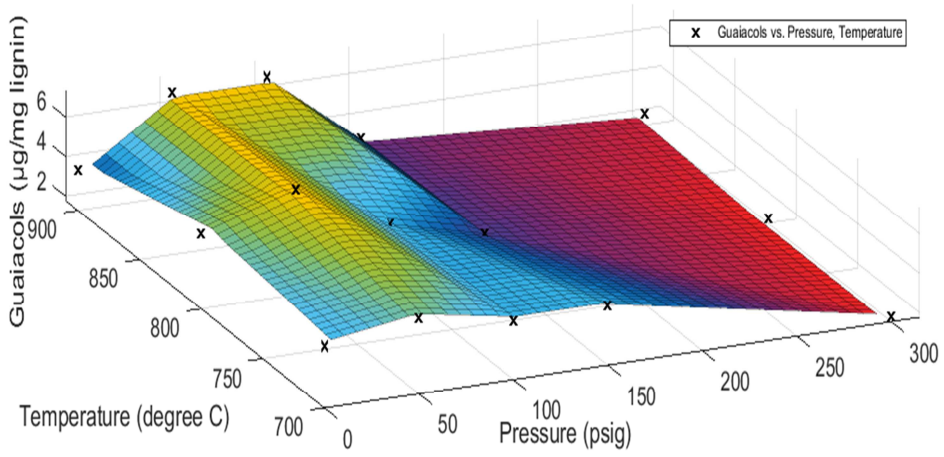

(b)

Figure 6.4. Phenolic contents of tar produced from kraft lignin pyrolysis at different temperature and pressure. (a) total content of phenols (2,6-dimethylphenol, 2,4-dimethylphenol, 4-methylcatechol, phenol, 2-methyl phenol, 4-ethylcatechol, catechol and p-cresol), (b) total content of guaiacols (Creosol, 2-methoxyphenol, 2-methoxy-4-vinylphenol, eugenol, trans-isoeugenol and Vanilin)

In literature, most of pressurized pyrolysis and gasification were conducted below 150 psig and limited data are available at higher pressure [8, 20, 21]. At reaction pressure below 150 psig, our observations on the effect of temperature on tar contents were consistent with literature. Mayerhofer et al. [20] reported that tar composition varied with temperature . Phenolic species (phenol and cresols) greatly decreased with increasing temperature whereas naphthalene increased with increasing temperature. Mastral et al. [21] reported an increase in polyaromatic compounds with increasing temperature during pyrolysis of polyethylene in a free-fall reactor at 800 to 1000 °C. However, effect of pressure on tar composition was inconclusive. Mayerhofer [20] found phenols and cresols were not affected by increasing pressure (from 0.1 to 0.3 MPa) but polyaromatics substantially increased by almost 200%. Knight et al.[8] found that increasing pressure (from 0.8 to 2.1 MPa) resulted in decrease of oxygenated species. Phenols were almost completely eliminated, while polyaromatic fraction increased. Berrueco et al. [22] performed pressurized gasification of torrefied woody biomass in a lab-scale fluidized bed at 0.1, 0.5 and 1 MPa. Their data showed an increase in tar content as pressure increased.

6.3.2. Catalytic Conditioning of Tar Produced from Lignin Pyrolysis

6.3.2.1. Effects of Temperature and Water Loading

Effects of temperature and the water loading on the catalyst performance were studied. Aromatic hydrocarbons, phenolics and total contents of lignin tar with and without char based catalyst are illustrated in Figure 6.5, Figure 6.6 and Figure 6.7, respectively. The temperatures were set at 700, 800 or 900 °C and volume of water injected on lignin was 5µl (same as non-catalytic lignin pyrolysis) or 10µl.

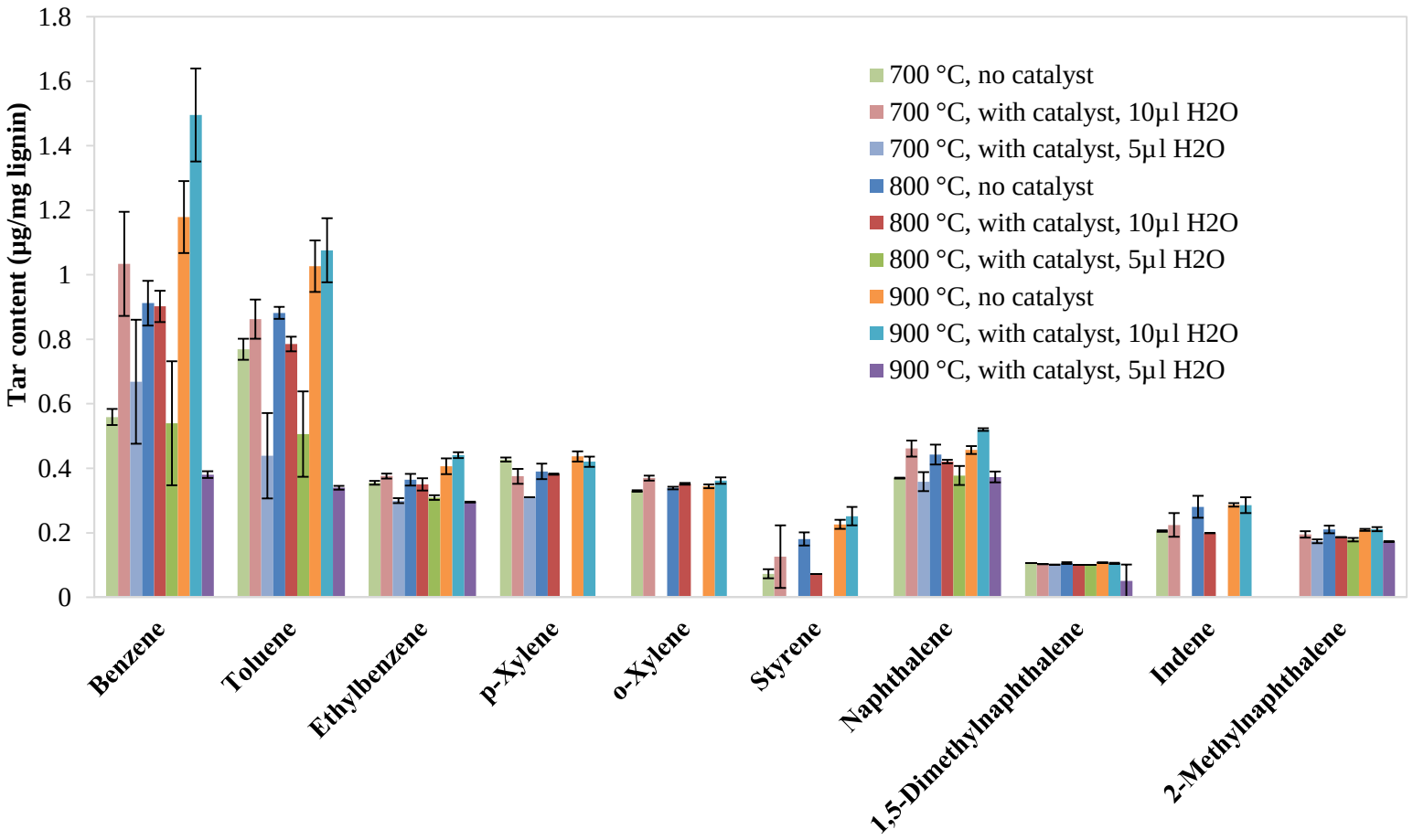

Figure 6.5. Effects of temperature and water loading on aromatic hyrocarbons in kraft lignin tar. Reaction temperature: 700, 800 and 900 °C, pressure: 0 psig, water amount: 5 or 10 µL.

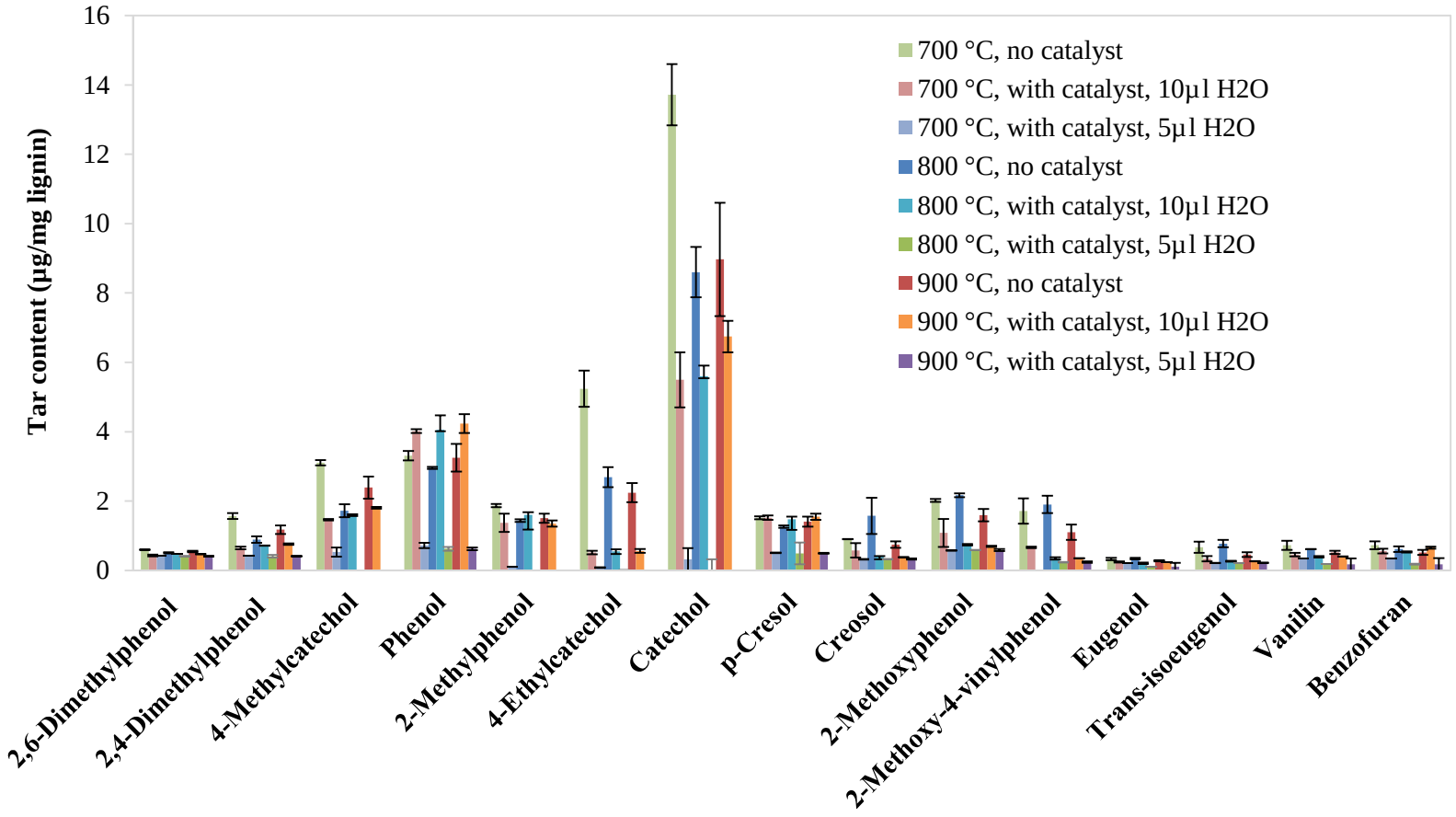

Figure 6.6. Effects of temperature and water loading on phenolics in kraft lignin tar. Reaction temperature: 700, 800 and 900 °C, pressure: 0 psig, water amount: 5 or 10 µL.

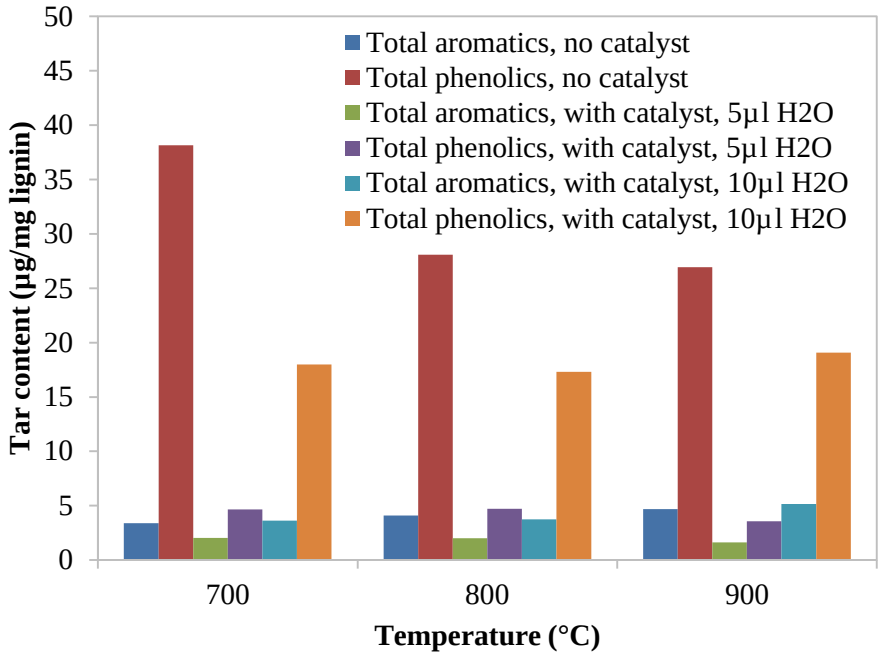

Figure 6.7. Effects of temperature and water loading on total tar contents produced from kraft lignin. Reaction temperature: 700, 800 and 900 °C, pressure: 0 psig, water amount: 5 or 10 µL.

As observed from Figure 6.5 and Figure 6.6 and Figure 6.7, the amount of water loading significantly affected catalyst performance. With 10 µl water, the total phenolics contents were only reduced by 50% at 700 °C and by 30% at 800-900 °C, while with 5µl water, total phenolics' contents were reduced by more than 90% at all temperature (see Figure 6.7). The total aromatic hydrocarbons were hardly reduced in catalytic conditioning of lignin tar with 10 µl water, while these were greatly reduced (50% on average) in presence of 5 µl water. As shown in Figure 6.5 and Figure 6.6, the contents of most phenolics were reduced by less than 30% with 10µl water; only 4-ethylcatechols, 2-methoxyphenol and 2-methoxy-4-vinylphenol were reduced by more than 50%. Decrease in tar content was not observed for most of the aromatic hydrocarbons with 10µl water. For individual tar components with 5µlwater, most of the phenols had been significantly removed and the maximum removal rate was found for catechol and 4-ethyl catechol with average of 96 % and 94%, respectively. An average removal of 70-80% for guaiacols was observed at 700-900 °C and the maximum removal rate was found for 2-methoxy-4-vinylphenol

with an average of 80-90%. For aromatic hydrocarbons in the presence of 5µl water, the highest removal rate (100%) was found for xylenes, styrene and indene, as their contents were below the GC/MS detection limit and thus considered as zero. The lowest removal rate was found for naphthalene, for which no decrease was observed. Overall, the catalyst performed better with 5 µl water than with 10 µl water. This can be attributed to the excess water (10 µl) that may have clogged the char pore and prevented tar vapor from accessing active sites on the catalyst. The effect of temperature on lignin tar removal was moderate. Increase in temperature only increased removal of benzene, toluene, catechols and benzofuran for catalytic conditioning with 5µl water.

Overall, char-derived catalysts were the most effective in removing phenolics, lesser effective in removing monoaromatic hydrocarbons and the least effective in removing polyaromatics. At the lowest pyroprobe temperature (700 °C), the average removal of phenolics was about 50%. Catechols were removed more than 85%, which was the highest among all individual phenolics. However, almost no aromatic hydrocarbons were removed at 700 °C. When the pyroprobe temperature was raised to 900 °C, more than 90% of phenolics and 60% of monoaromatic hydrocarbons were removed while removal percentages of naphthalene. 1,5-dimethylnaphthalene and 2-methylnaphthalene were still less than 30%. The removal efficiencies of the char-derived catalysts on individual tar compounds can be attributed to reactivity and stability of each compound. According to literature, the reactivity of tar compounds in catalytic conditioning from the highest to lowest are phenolics, monoaromatic hydrocarbons and polyaromatic hydrocarbons [23-25]. Coll et al. [25] studied steam reforming on five model tar compounds, including benzene, toluene, pyrene, anthrathene and naphthalene, and found that naphthalene was the toughest and benzene was the easiest to reform. By reviewing steam reforming of phenol and benzene at similar reaction conditions (similar nickel/aluminum catalyst and similar reactor) [24, 26, 27], it can be observed that that phenol was easier to reform than benzene or toluene. High phenols conversion (more than 90%) can be achieved even at low temperature (450 °C) by steam reforming over Ni/aluminum catalyst [24]. However, catalytic

conditioning of benzene or toluene require at least 600 °C over Ni/aluminum in order to achieve conversion/removal above 60% [26, 27].

As shown in Figure 6.5, benzene content in the catalytic reforming was higher than that in non-catalytic pyrolysis. The increased benzene content was probably because of conversion of phenols into benzene with catalyst or oligomerization of hydrocarbon monomer. However, benzene was more likely converted from oligomerization of hydrocarbon monomer than phenols based on the study of Ben et al. [28] and Garbarino et al. [24]. Ben et al.[28] found that $NiCl_2$ and ZSM-5 zeolite catalysts hardly improved decomposition of phenolic hydroxyl groups of lignin but significantly improved the decomposition of aliphatic hydroxyl groups, carboxyl and aromatic-methoxyl groups. However, by studying steam reforming of phenol using in-situ FT-IR, Garbarino et al. [24] found that phenol steam reforming reaction occurred at the expense of surface phenate species adsorbed on Ni centers. These surface phenate species were active above 400 °C and directly reformed with steam into CO and hydrogen with no intermediates or by-products.

6.3.2.2. Effect of Pressure

The effect of pressure on catalysts performance was studied with 10 µl water loading. Contents of aromatic hydrocarbons and phenolics at three pressure of 0.1, 0.5 and 1.1 MPa (0, 50 and 150 psig) and a pyroprobe temperature of 900 °C are illustrated in Figure 6.8 and Figure 6.9. The pressure significantly affected the catalytic reforming of lignin tar over char-based catalyst. When pressure increased from 0.1 to 0.5 MPa (0 to 50 psig), the removal of most aromatic hydrocarbons increased from nearly 0 to 30% except o-xylene and the removal of most phenolics increased from 30% to 50 % except p-creosol. When the pressure further increased to 1.1 MPa (150 psig), the removal of most aromatic hydrocarbons and phenolics increased to more than 70%. The absence of catechol, 2-methoxyvinylphenol, 4-methylcatechol and o-xylene at 1.1 MPa (150 psig) indicated their nearly 100% removal.

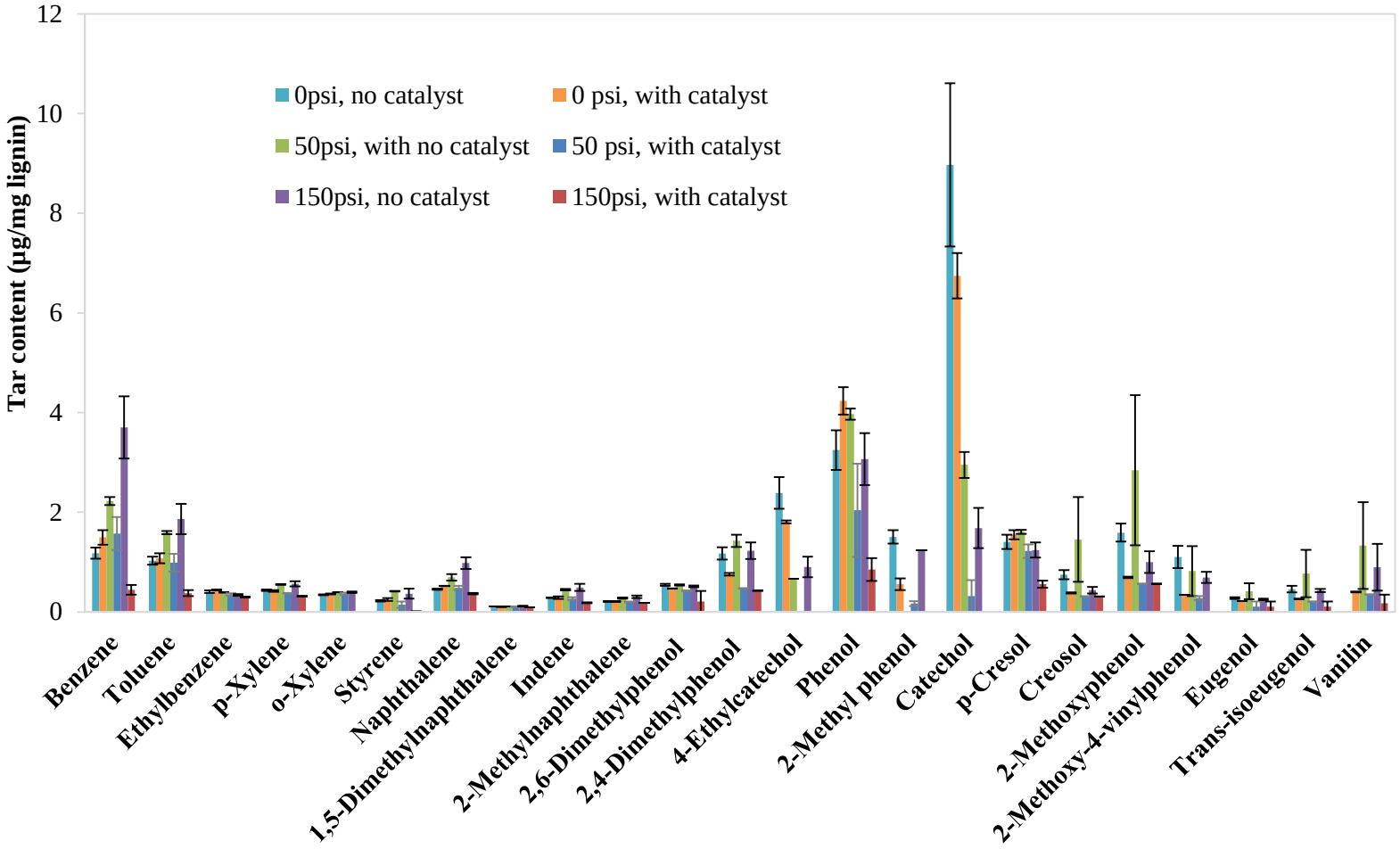

Figure 6.8. Effect of pressure on tars produced from kraft lignin. Reaction temperature: 900 °C, pressure: 0, 5 and 150 psig, water amount: 10 µL.

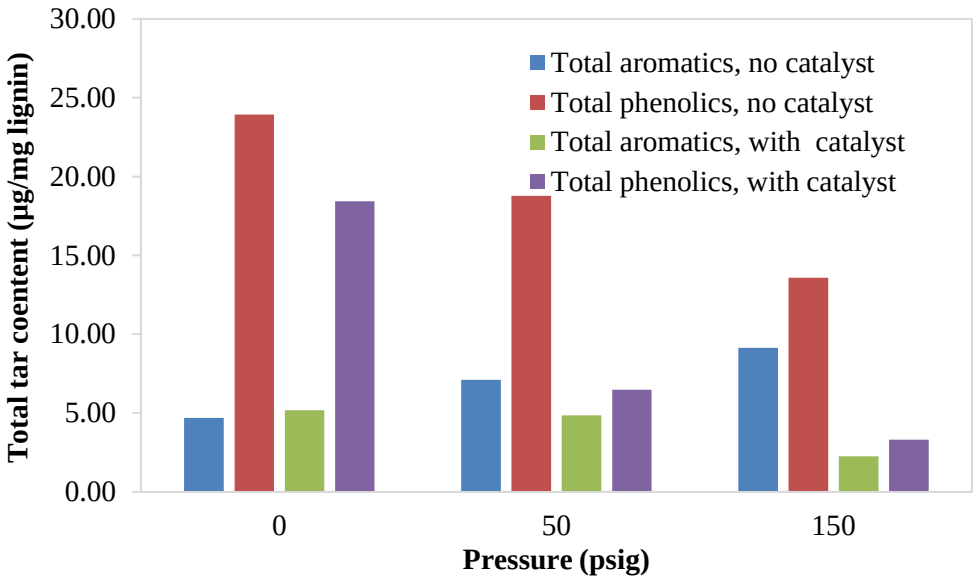

Figure 6.9. Effect of pressure on total tar contents produced from kraft lignin. Reaction temperature: 900 °C, pressure: 0, 5 and 150 psig, water amount: 10 µL.

The total contents of aromatic hydrocarbons and phenolics from kraft lignin pyrolysis with and without catalyst are illustrated in Figure 6.9. Increase in pressure improved removal of total aromatic hydrocarbons and phenolics contents. The removal efficiency of aromatic hydrocarbons and phenolics increased from 0% to 75% and from 20% to 75%, respectively, when pressure increased from 0.1 MPa (0 psig) to 1.1 MPa (150 psig). The effects of pressure on removal efficiency could be related to prolonged residence (reaction) time. As discussed in 6.3.1, rising pressure suppresses the release of tar through the catalytic layer and thus increases the reaction time of tar with the catalyst, which subsequently improves the tar reforming.

6.3.2.3.Effect of Atmosphere

Contents of aromatics hydrocarbons and phenolic substitutes obtained from lignin pyrolysis in the presence of H_2 are illustrated in Figure 6.10. It was obvious that the contents of most tar components in hydrogen atmosphere were lower than that in helium atmosphere. The major decreases (>50%) were observed in catechols, 2-methoxyphenol, 2-methoxy-4-vinylphenol and trans-isoeugenol and minor decreases (<20%) were observed in phenol, dimethylphenols and polyaromatic hydrocarbons. Monocyclic aromatic hydrocarbons such as benzene and toluene showed slight increase. Decrease in tar contents in the presence of hydrogen was possibly

because hydrogen acted as a gasification agent and thus promoted the conversion of lignin into non-condensable gas rather than tar.

When the char-based catalyst was used, tar contents were further reduced. The contents of dimethylphenols, 2-methoxyphenol, vanillin, ethylbenzene, methylnaphthalene, 1, 5-dimethylnaphthalene, trans-isoeugenol and xylenes were not been detected. Most of the remaining tar compounds was reduced by more than 50%. However, the removal of naphthalene was still only about 20%.

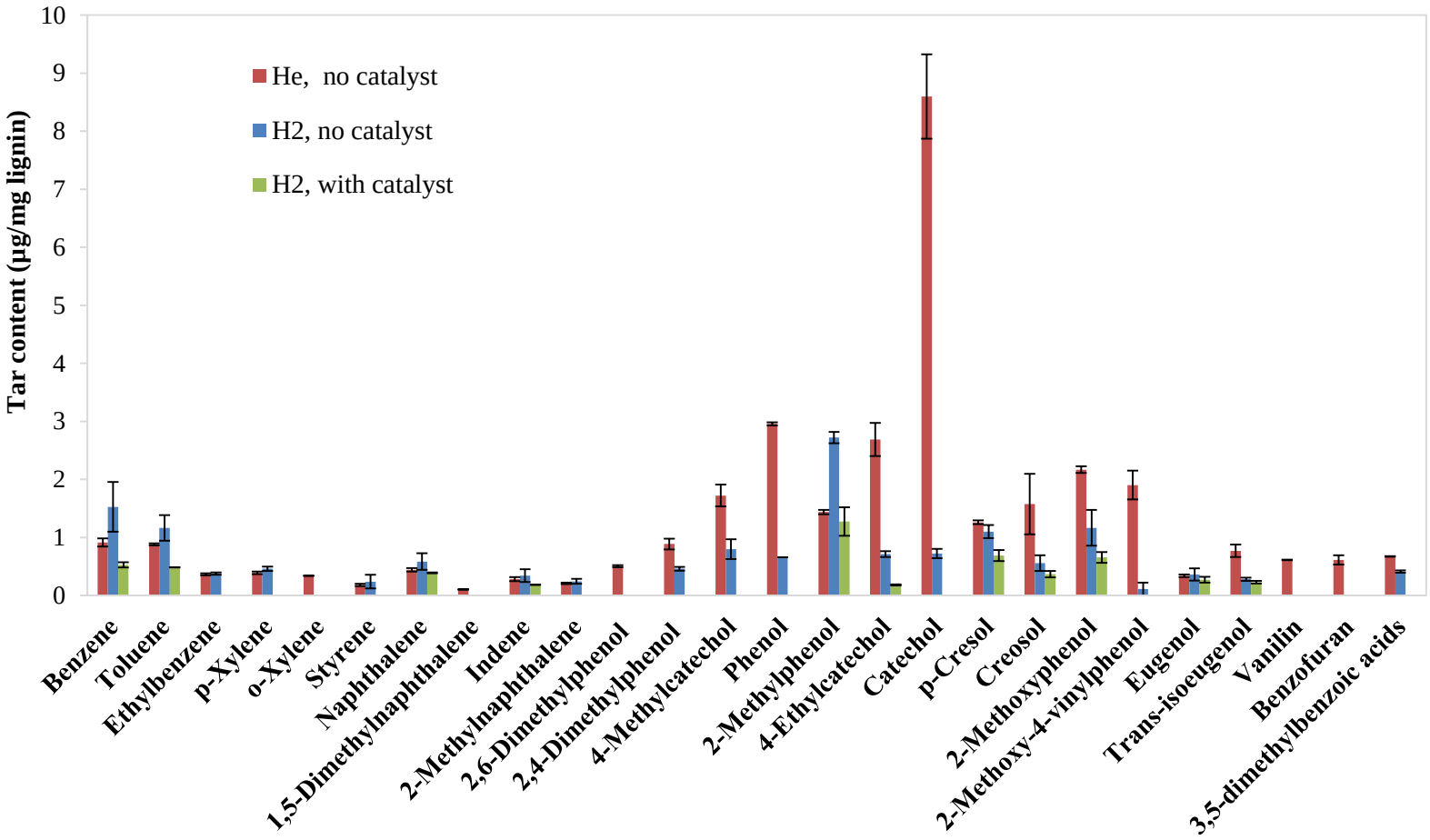

Figure 6.10. Effect of H_2 atmosphere on tars produced from kraft lignin at atmospheric pressure and 800 °C.

6.4. Conclusions

Pyrolysis of kraft lignin was performed in a pyroprobe reactor in presence of water with a novel char-based catalyst. The effects of reaction, temperature, water loading, pressure and atmosphere on tar were investigated by conducting quantitative analysis of tar. Catechols were found to be the most abundant tar components followed with phenol and guaiacols produced from lignin in absence of the catalyst. Increase in pressure from 0.1 to 1.1 MPa (0 to 150 psig) led to increase in aromatic hydrocarbons. High pressure may have caused increase in tar residence time in lignin and resulted in polymerization reactions forming polyaromatic hydrocarbons. Further increase in pressure to 2.2 MPa (300 psig) led to a reduction of polyaromatic hydrocarbons due to prolonged residence time during steam reforming reaction.

During catalytic reforming of lignin tar, the effect of temperature on lignin tar removal was moderate. Increase in temperature only increased removal of benzene, toluene, catechols and benzofuran for catalytic conditioning with 5µl water. High water loading (10µl) decreased the removal efficiency of char-based catalyst probably because the excess water clogged the char pore and prevented tar vapor from accessing active sites on the catalyst. Higher pressure promoted the catalytic decomposition of lignin tar. When pressure increased from 0.1 to 1.1 MPa (0 to 150 psig), the removal percentage of most aromatic hydrocarbons increased from nearly 0% to 70% and the removal percentage of phenols increased from 30% to 70%. Catechol, 2-methoxyvinylphenol, 4-methylcatechol and o-xylene at 1.1 MPa (150 psig) reached nearly 100% removal.

When pyrolysis was performed in hydrogen atmosphere, tar contents significantly decreased, as hydrogen acted as a gasification agent, promoting the conversion of lignin into non-condensable gas. In all cases, removal of phenolics was higher than that of aromatic hydrocarbons. Naphthalene, 1, 5-dimethylnaphthalene, 2-methylnaphthalene were the toughest tar component to be decomposed with the lowest removal efficiency.

Acknowledgements

Authors acknowledge the support of South Central Sun Grant Program and Oklahoma Agricultural Experiment Station for this study.

6.5. References

[1] Font Palma C. Modelling of tar formation and evolution for biomass gasification: A review. Applied Energy. 2013;111:129-41.

[2] Shen DK, Gu S, Bridgwater AV. Study on the pyrolytic behaviour of xylan-based hemicellulose using TG–FTIR and Py–GC–FTIR. J Anal Appl Pyrol. 2010;87:199-206.

[3] Lv G, Wu S. Analytical pyrolysis studies of corn stalk and its three main components by TG-MS and Py-GC/MS. J Anal Appl Pyrol. 2012;97:11-8.

[4] Faix O, Meier D. Pyrolytic and hydrogenolytic degradation studies on lignocellulosics, pulps and lignins. Holz als Roh-und Werkstoff. 1989;47:67-72.doi: 10.1007/BF02628617

[5] Pasangulapati V, Ramachandriya KD, Kumar A, Wilkins MR, Jones CL, Huhnke RL. Effects of cellulose, hemicellulose and lignin on thermochemical conversion characteristics of the selected biomass. Bioresour Technol. 2012;114:663-9.

[6] Hu J, Shen D, Xiao R, Wu S, Zhang H. Free-Radical Analysis on Thermochemical Transformation of Lignin to Phenolic Compounds. Energy Fuels. 2012;27:285-93.

[7] Thangalazhy-Gopakumar S, Adhikari S, Gupta RB, Tu M, Taylor S. Production of hydrocarbon fuels from biomass using catalytic pyrolysis under helium and hydrogen environments. Bioresour Technol. 2011;102:6742-9.

[8] Knight RA. Experience with raw gas analysis from pressurized gasification of biomass. Biomass and Bioenergy. 2000;18:67-77.

[9] Berrueco C, Montané D, Matas Güell B, del Alamo G. Effect of temperature and dolomite on tar formation during gasification of torrefied biomass in a pressurized fluidized bed. Energy. 2014;66:849-59.

[10] Schorr D, Diouf PN, Stevanovic T. Evaluation of industrial lignins for biocomposites production. Ind Crop Prod. 2014;52:65-73.

[11] Thangalazhy-Gopakumar S, Adhikari S, Gupta RB. Catalytic Pyrolysis of Biomass over H+ZSM-5 under Hydrogen Pressure. Energy Fuels. 2012;26:5300-6.doi: 10.1021/ef3008213

[12] Zhang M, Resende FLP, Moutsoglou A, Raynie DE. Pyrolysis of lignin extracted from prairie cordgrass, aspen, and Kraft lignin by Py-GC/MS and TGA/FTIR. J Anal Appl Pyrol. 2012;98:65-71.

[13] Zhang M, Resende FLP, Moutsoglou A. Catalytic fast pyrolysis of aspen lignin via Py-GC/MS. Fuel. 2014;116:358-69.

[14] Zhang M, Moutsoglou A. Catalytic Fast Pyrolysis of Prairie Cordgrass Lignin and Quantification of Products by Pyrolysis–Gas Chromatography–Mass Spectrometry. Energy Fuels. 2014;28:1066-73.

[15] Zhou S, Garcia-Perez M, Pecha B, Kersten SRA, McDonald AG, Westerhof RJM. Effect of the Fast Pyrolysis Temperature on the Primary and Secondary Products of Lignin. Energy Fuels. 2013;27:5867-77.

[16] Fahmi R, Bridgwater AV, Thain SC, Donnison IS, Morris PM, Yates N. Prediction of Klason lignin and lignin thermal degradation products by Py–GC/MS in a collection of Lolium and Festuca grasses. J Anal Appl Pyrol. 2007;80:16-23.

[17] Fu Y, Kato K, Ohtani H, Chen Y. Pyrolysis Products of Lignin in Open and Sealed Vessels Studied by Py-GC-MS. Journal of Wood Chemistry and Technology. 2013;34:1-7.

[18] Jiang GZ, Nowakowski DJ, Bridgwater AV. Effect of the Temperature on the Composition of Lignin Pyrolysis Products. Energy Fuels. 2010;24:4470-5.

[19] Thangalazhy-Gopakumar S, Adhikari S, Gupta RB, Fernando SD. Influence of Pyrolysis Operating Conditions on Bio-Oil Components: A Microscale Study in a Pyroprobe. Energy Fuels. 2011;25:1191-9.

[20] Mayerhofer M, Mitsakis P, Meng X, de Jong W, Spliethoff H, Gaderer M. Influence of pressure, temperature and steam on tar and gas in allothermal fluidized bed gasification. Fuel. 2012;99:204-9.

[21] Mastral JF, Berrueco C, Ceamanos J. Pyrolysis of High-Density Polyethylene in Free-Fall Reactors in Series. Energy Fuels. 2006;20:1365-71.

[22] Berrueco C, Recari J, Güell BM, Alamo Gd. Pressurized gasification of torrefied woody biomass in a lab scale fluidized bed. Energy. 2014;70:68-78.

[23] Abu El-Rub Z, Bramer EA, Brem G. Review of catalysts for tar elimination in Biomass gasification processes. Industrial & engineering chemistry research. 2004;43:6911-9.doi: Doi 10.1021/Ie0498403

[24] Garbarino G, Sanchez Escribano V, Finocchio E, Busca G. Steam reforming of phenol–ethanol mixture over 5% Ni/Al2O3. Applied Catalysis B: Environmental. 2012;113–114:281-9.

[25] Coll R, Salvadó J, Farriol X, Montané D. Steam reforming model compounds of biomass gasification tars: conversion at different operating conditions and tendency towards coke formation. Fuel Processing Technology. 2001;74:19-31.

[26] Mudinoor A, Bellmer D, Marin L, Kumar A, Huhnke R. Conversion of Toluene(Model Tar) Using Selected Steam Reforming Catalysts. Transactions of the ASABE. 2011;54:1819-27

[27] Tao J, Zhao L, Dong C, Lu Q, Du X, Dahlquist E. Catalytic Steam Reforming of Toluene as a Model Compound of Biomass Gasification Tar Using Ni-CeO2/SBA-15 Catalysts. Energies. 2013;6:3284-96

[28] Ben H, Ragauskas AJ. Pyrolysis of Kraft Lignin with Additives. Energy Fuels. 2011;25:4662-8.

VITA

KEZHEN QIAN

Candidate for the Degree of

Doctor of Philosophy

Dissertation: PROPERTIES OF GASIFICATION-DERIVED CHAR AND ITS UTILIZATION FOR CATALYTIC TAR REFORMING

Major Field: Biosystems and Agricultural Engineering

Biographical:

Education:

Completed the requirements for the Doctor of Philosophy in Biosystems Engineering at Oklahoma State University, Stillwater, Oklahoma in May, 2015.
Completed the requirements for the Masters of Engineering in Thermal and Power Engineering at Huazhong University of Science and Technology, Wuhan, China in July 2012.
Completed the requirements for the Bachelors of Engineering in Thermal and Power Engineering at Chongqing University, Chongqing, China in July, 2005.

Experience:

Research Assistant (Biomass Thermochemical Conversion), Oklahoma State University, Stillwater, Oklahoma, 2011 to Present.
Research Assistant (State key laboratory of coal combustion), Huazhong University of Science and Technology, Wuhan, China in 2009 - 2011.

Professional Memberships:
American Society of Agricultural and Biological Engineers (ASABE)